UNIVERSITÀ
DEGLI STUDI
DI PADOVA

Sede Amministrativa: Università degli Studi di Padova

Dipartimento di Geoscienze

SCUOLA DI DOTTORATO DI RICERCA IN : SCIENZE DELLA TERRA

INDIRIZZO: UNICO

CICLO: XXVI

VOLCANISM AND INTRUSIONS OF THE DECCAN TRAPS, INDIA: GEOCHEMISTRY AND GEOCHRONOLOGY OF THE MAGMATIC ROCKS AND PALEOENVIRONMENTAL CONSEQUENCES

Direttore della Scuola: Ch.mo Prof. Massimiliano Zattin

Supervisore: Ch.mo Prof. Andrea Marzoli

Dottorando : Laura Parisio

Table of contents

ABSTRACT

The Deccan Traps are one of the most important Large Igneous Provinces (LIP) in the world, they are mainly constituted by tholeiitic lava flows, now covering almost one sixth of the Indian continent, and reaching the maximum exposed thickness of 1300 m. The emplacement of such quantities of magma and its timing (ca. 66Ma) close to the Cretaceous-Paleogene (K-Pg) boundary, have led several authors to propose a causal link between the formation of the province and the K-Pg boundary mass extinction . Moreover, a distinctive feature of the province is the presence, beside the tholeiites, of several alkaline bodies, associated with the main fault zones of India.

These two important aspects of the Deccan Traps have been investigated in the northern portion of the province by sampling both alkaline and tholeiitic rocks, in order to provide precise timing of emplacement and to constrain the relationship between them through the definition of their mantle source.

$^{40}Ar/^{39}Ar$ step-heating analyses provided two different age peaks that straddle the K-Pg boundary, one with an age comparable with the main phase of Deccan volcanism (ca 66.5 Ma), the other slightly younger (ca. 65.2 Ma), thus confirming the synchrony between the emplacement of the province and the end-Cretaceous mass extinction. Therefore, the input in the atmosphere of huge quantities of gas, produced by the emplacement of the Deccan Traps, could have contributed to the extinction. In particular a crucial role may be provided in this sense by the alkaline magmas, which are likely enriched in volatile elements.

Whole rock analyses showed that the samples span a wide compositional range varying from little-evolved compositions such as picro-basalts to fairly evolved ones such as rhyolite; the large variation is observed in the total alkali content (Na_2O+K_2O) as well, ranging from the subalakaline basalt field, up to strongly alkaline samples like phonolites. Alkaline rocks appear enriched in the most incompatible elements and present higher La/Yb ratios (19.5-68.8). They are also characterized by negative K anomaly (possibly suggesting the presence of a K-rich residual mantle mineral), and Pb spikes; on average they present patterns similar to those displayed by other alkaline rocks of the Deccan Traps, thus suggesting analogous origin and source.

Sr-Nd isotopes define a large spectrum of compositions, departing from a similar depleted end-member (ε_{Ndt} ca. +3 and $^{87}Sr/^{86}Sr_t$ ca. 0.705) and trending towards low ε_{Ndt} and relatively low $^{87}Sr/^{86}Sr_t$ (-12.96 and 0.71061, respectively), and toward very high $^{87}Sr/^{86}Sr_t$ (0.72788) and low ε_{Ndt} (-12.50). The trend with higher $^{87}Sr/^{86}Sr_t$ has been interpreted as the result of Assimilation-Fractional Crystallization (AFC) process, starting from a magma similar to Réunion OIBs or

Central Indian Ridge basalts progressively contaminated by rocks from the Indian cratons (Dharwar and Aravalli cratons). The trend towards low ε_{Ndt} and relatively low $^{87}Sr/^{86}Sr_t$ is defined mainly by mafic sulbalkaline rocks from the Phenai Mata intrusion. These rocks are characterized also by very high $^{207}Pb/^{204}Pb_t$ and $^{208}Pb/^{204}Pb_t$ ratios. Given the preliminary $^{187}Os/^{188}Os_t$ compositions (0.1584 to 0.2457), mafic subalkaline rocks assimilated only negligible amounts of crust. Their enriched Sr-Nd-Pb isotopic composition is thus best interpreted as resulting from recycling of ancient sediments in their mantle source. On the contrary, alkaline samples present quite homogeneous isotopic compositions, slightly more enriched than that of nearby carbonatite complexes (e.g. Amba Dongar) and substantially more enriched than Reunion basalts. Therefore, the alkaline rocks are unlikey a product of the Reunion mantle plume, but more probably of the subcontinental lithospheric mantle, as is consistent also with their incompatible trace element contents and patterns.

RIASSUNTO

I Deccan Traps sono una delle più importanti grandi province magmatiche del mondo, sono principalmente costituiti da colate di lava tholeiitica, attualmente ricoprono circa un sesto del continente Indiano e raggiungono uno spessore massimo di 1300m. La messa in posto di queste grandi quantità di magma avvenuta al limite Cretaceo-Paleogene (K-Pg), ha portato diversi autori a proporre un rapporto di causalità tra la formazione di questa provincia e l'estinzione di massa al limite K-Pg.

Inoltre, una caratteristica dei Deccan Traps è la presenza, oltre alle tholeiiti, di diversi corpi alcalini associati con le principali zone di faglia indiane.

Questi due importanti aspetti dei Deccan traps sono stati studiati nella porzione nordoccidentale della provincia, campionando rocce alcaline e tholeiitiche, al fine di definire un preciso tempo di messa in posto e caratterizzare la relazione tra le diverse litologie, attraverso la determinazione della loro sorgente di mantello.

Le analisi $^{40}Ar/^{39}Ar$ step-heating hanno restituito due diversi picchi di età a cavallo del limite K-Pg, il primo con un'età comparabile a quella della fase principale del magmatismo Deccan (ca. 66.5Ma), il secondo più giovane (ca. 65.2 Ma), confermando quindi l'effettiva sincronia tra la formazione della provincia e l'estinzione di massa alla fine del Cretaceo. Quindi, l'immissione in atmosfera di grandi quantità di gas, prodotta dalla messa in posto dei Deccan Traps, può aver contribuito all'estinzione. In particolare un ruolo molto importante potrebbe essere stato quello dei magmi alcalini, che verosimilmente sono arricchiti in elementi volatili.

I campioni coprono un ampio range composizionale in termini di elementi maggiori, variando da composizioni poco evolute come i picro-basalti, a evolute come le rioliti; la variabilità è osservata anche nel contenuto di alcali (Na_2O+K_2O), variando dal campo subalcalino dei basalti a quello di campioni fortemente alcalini come le fonoliti. Le rocce alcaline sono arricchite negli elementi più incompatibili e presentano un rapporto La/Yb più alto (19.5-68.8). sono inoltre caratterizzate da una anomalia negativa in K, (probabilmente dovuta alla presenza di una fase residuale ricca in K nel mantello) e ad una positiva in Pb; in genere presentano pattern simili a quelli di altre rocce alcaline dei Deccan Traps, suggerendo quindi un'origine simile.

Anche i rapporti isotopici di Sr e Nd definiscono un ampio range composizionale, partendo da un end-member impoverito (ε_{Ndt} ca. +3 and $^{87}Sr/^{86}Sr_t$ ca. 0.705), verso composizioni a basso ε_{Ndt} e relativamente basso $^{87}Sr/^{86}Sr_t$ (-12.96 and 0.71061, rispettivamente), e verso composizioni a $^{87}Sr/^{86}Sr_t$ (0.72788) molto alto e basso ε_{Ndt} (-12.50). Il trend a più alto $^{87}Sr/^{86}Sr_t$ è stato interpretato come il risultato di un processo di assimilazione e cristallizzazione frazionata (AFC), a partire da un magma simile alle composizioni tipiche di Réunion o del Central Indian Ridge, progressivamente contaminato da rocce dei Cratoni indiani (Dharwar e Aravalli). Il trend verso composizioni a basso ε_{Ndt} e relativamente basso $^{87}Sr/^{86}Sr_t$ è definito principalmente da rocce mafiche subalcaline dell'intrusione di Phenai Mata, queste rocce sono anche caratterizzate da rapporti $^{207}Pb/^{204}Pb_t$ and $^{208}Pb/^{204}Pb_t$ molto alti. Date le prime composizioni isotopiche $^{187}Os/^{188}Os_t$ (da 0.1584 a 0.2457), queste rocce hanno assimilato porzioni trascurabili di crosta. Le loro composizioni Sr-Nd-Pb arricchite sono quindi meglio interpretate come il risultato del contributo nella sorgente di mantello di antichi sedimenti riciclati. Al contrario i campioni alcalini presentano composizioni isotopiche piuttosto omogene, leggermente più arricchite rispetto a quelle dei vicini complessi carbonatitici (p. es. Amba Dongar) e decisamente più arricchiti dei basalti di Réunion. Perciò le rocce alcaline sembrano non essere il prodotto del plume di Réunion, ma più probabilmente del mantello litosferico subcontinentale, come suggerito anche dai contenuti e dai pattern degli elementi in traccia.

CHAPTER 1.
INTRODUCTION: THE DECCAN TRAPS

The Deccan Traps are a large igneous province (LIP) emplaced in the western-central part of India; their present surface reaches about 500000 km^2, with an original covered surface of about $1.5x10^6$ km^2 (Raja Rao et al., 1978). They can be subdivided in four subprovinces: the Saurashtran Plateau in the northwestern portion of the province, the Malwa plateau on the north of the Narmada river, the Mandla lobe in the northeastern region, and the Main Deccan, south of the Narmada river (fig.1).

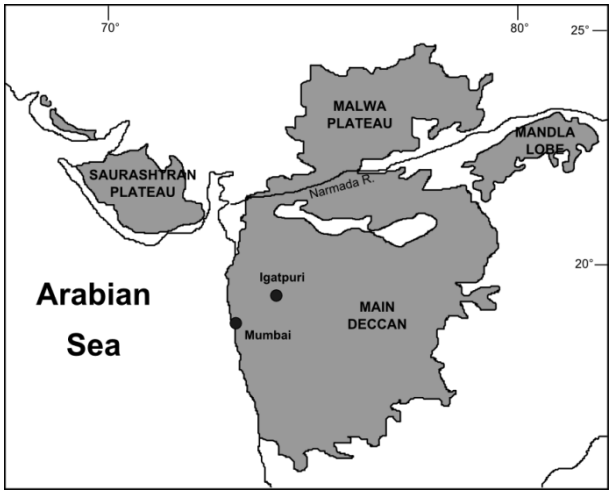

Fig.1.1. Map of northwest–central India showing extent of the Deccan Traps (shaded area).

The formation of the western coast of India began with the separation of India from Gondwana and that of Madagascar from India between 100 and 84 Ma, after a rifting phase at 88Ma (Storey et al., 1995). The emplacement of the Deccan Traps is connected with the subsequent northward migration of India above the Reunion hotspot (Morgan, 1981). After the emplacement of the province, the northern part of the western coast underwent rifting which brought to the formation of the Carlsberg Ridge, whose oldest magnetic anomaly is dated at about 62 Ma (Subrahmanya, 1998), thus confirming that the Deccan volcanism predated the rifting (Hooper, 1990). The rifting resulted in the separation of the Seychelles microcontinent, and the relative shift of the Reunion hotspot from the Indian subcontinent to offshore, where its trail is now represented by Mascarene plateau and Chagos Laccadive Ridge (Subrahmanya, 1998).

The province consists of a thick sequence of nearly horizontal tholeiitic lava flows which reach their maximum exposed thickness of 1700m in the Igatpuri area (Mahoney et al., 1982), in the

Western Ghats, the escarpment along the west coast, where the good exposure of the flows allows distinguishing, on the base of field observations and geochemical data, 11 formations, grouped in three Subgroups: the Kalsubai, Lonavala and Wai Subgroups, from the bottom to the top (Beane et al., 1986). The sequence is thinner in the E and thickens towards W, and in general shows a gentle dip between 0.5 and 2° (Cox and Hawkesworth, 1985), with the oldest and thicker formations outcropping mainly on the north, and thinning southward, where they are overlain by southward thickening younger formations, which become thinner further south (Beane et al., 1986). Lower formations are mainly constituted by compound flows (massive and amygdaloidal), whereas the upper ones are mostly highly jointed simple flows (Marathe et al., 1981).

The Kalsubai Supergroup is formed by the Jahwar, Igatpuri, Neral, Thakurvadi and Bimashankar formations, with picrites and picrite basalt frequently found throughout the sequence and often divided by giant plagioclase basalts (GPB) which separate different formations and represent the most evolved composition in the sequence; the Lonavala Supergroup represents the transition between lower and upper formations, with the uppermost of the lower formations (Khandala formation), and the first of the upper formations (Bushe formation); the Wai Supergroup consists of the last four formations: Poladpur, Ambenali, Mahabaleshwar and Panhala formations (fig. 2).

1.1. Geochemical compositions of the Deccan formations

Among lower formations, the Khandala one is generally characterized by higher Pb/Nb and La/Nb (0.35-0.52, and 1.5-2.25, respectively), and lower Ti/Y (250-400); the Thakurvadi formation shows similar values, but has higher Ti/Y; Jawhar and Igatpuri formations are chemically similar: TiO_2 can reach high contents (1.3-3.6 wt%), and Ba/Zr and Zr/Nb ratios have a similar range (about 0.9-1.5, and 11-14, respectively); the Neral formation shows the lowest Pb/Nb ratio (0.15-0.25), and low La/Nb (1.1-1.6) (Beane, 1988; Peng et al., 1994).

In the isotopic space, the lower formations depart from a similar region, named "common signature" (Peng et al., 1994), and define different trends. The Igatpuri-Jhawar formations have quite enriched compositions with $^{87}Sr/^{86}Sr_i$ and ε_{Ndi} ranging respectively between 0.7085 and 0.7128, and -3 and -8.5; Pb isotopic compositions can reach very high values (e.g. $^{206}Pb/^{204}Pb_i$ 22.6, $^{208}Pb/^{204}Pb_i$ 43.3; Peng et al., 1994). The isotopic composition of the Neral formation is much more variable in ε_{Ndi} (-2.5 to -16) and Pb isotopes (e.g. $^{206}Pb/^{204}Pb_i$ 16.5-20) rather than in $^{87}Sr/^{86}Sr_i$ (0.7062-0.7104). The overlying Thakurvadi formation shows quite highly variable isotopic composition, with $^{87}Sr/^{86}Sr_i$ ranging between 0.7066 and 0.7112, ε_{Ndi} between 0 and -13,

and $^{206}Pb/^{204}Pb_i$ between 17.2 and 20.2. The Bhimashankar has quite homogeneous composition, similar to that of the "common signature" ($^{87}Sr/^{86}Sr_i$ 0.7067-0.7076, ε_{Ndi} from -2 to -6; $^{206}Pb/^{204}Pb_i$ 20-21), whereas the Khandala formation displays high variability, reaching the lowest ε_{Ndi} (-20).

Among the upper formations, the Bushe is characterized by low TiO_2 (about 1 wt%), Zr (less than 100 ppm), and Sr (150-50 ppm) content, together with relatively high Mg# (57-60), Ba (up to 200 pmm), Rb (20-40 ppm); the Poladpur formation shows an increase in TiO_2, Zr and Sr content, and presents distinctively lower Mg# ($Mg/Mg+Fe^{2+}$, 40-53). The Ambenali formation is characterized by low Ba, Rb, and K_2O; whereas the Mahabaleshwar formation is enriched in Sr, Ba, Nb, Rb, and K_2O (Cox and Hawkesworth, 1985). The uppermost Panhala formation is characterized by high Zr/Nb (14-19), low TiO_2(1.5-2.3%), low Sr (140-200 ppm), Ba and Rb (Lightfoot et al. 1990). The Ambenali formation presents the most depleted isotopic composition with $^{87}Sr/^{86}Sr_i$ ranging from 0.7038 to 0.7044, and ε_{Ndi} from +8 to +3. From its isotopic composition two trends depart toward low and relatively high $^{87}Sr/^{86}Sr$, respectively. The first trend is defined by the Panhala and Mahabaleshwar formations, which are enriched especially in Nd isotopic composition (down to -6), whereas the second trend is described by the Poladpur and Bushe formations, having very enriched compositions with $^{87}Sr/^{86}Sr_i$ higher than 0.72 and ε_{Ndi} lower than -15 for Bushe formation.

The isotopic characteristics together with trace elements suggest that the Ambenali formation is substantially uncontaminated by the continental crust; the higher contamination of the most mafic compositions in the Ambenali-Poladpur-Bushe trend may be due to temperature-controlled assimilation of Archean granites, with more primitive magmas characterized by higher temperature and thus capable of assimilating larger amounts of the basement. ; and the Mahabaleswar trend suggests an involvement of a mantle enriched in large-ion lithophile elements (LILE), being the crustal contamination almost insignificant (Cox et al., 1984).

Conversely, the evolution of the lower formations has been explained through the involvement of at least three different continental crust end-members with variable Sr and Pb isotopic compositions (Peng et al., 1994), which would have contaminated the more depleted "common signature", which is turn considered the result of the contamination of Ambenali- or Reunion-like parental magma with high-degree melts of Archean basic amphibolites of the Indian shield (Peng et al., 1994).

The wide isotopic range of the Deccan formations has been explained through different processes that affected the different formations, but the restricted isotopic region from which these

compositions depart, strongly suggest a common mantle source. The nature of this mantle source has been inferred from the least contaminated Ambenali rocks, and taking into account the geodynamical background in which the Deccan Traps have formed, i.e. the presence of the Reunion hot spot, and the extensional setting which would have led to the formation of the Central Indian Ridge. excluding the exclusive involvement of Réunion- or CIR-type magma, the mantle source of the tholeiitic flows is thought to be a mixture of Reunion- and Central Indian Ridge (CIR)-like magmas (Mahoney, 1988), even if other models do not require the presence of a hot spot and owe the great magma production and composition of the Deccan traps to the involvement of old, eclogitized (and low solidus) oceanic crust trapped in the ancient Indian suture zone (Sheth, 2004).

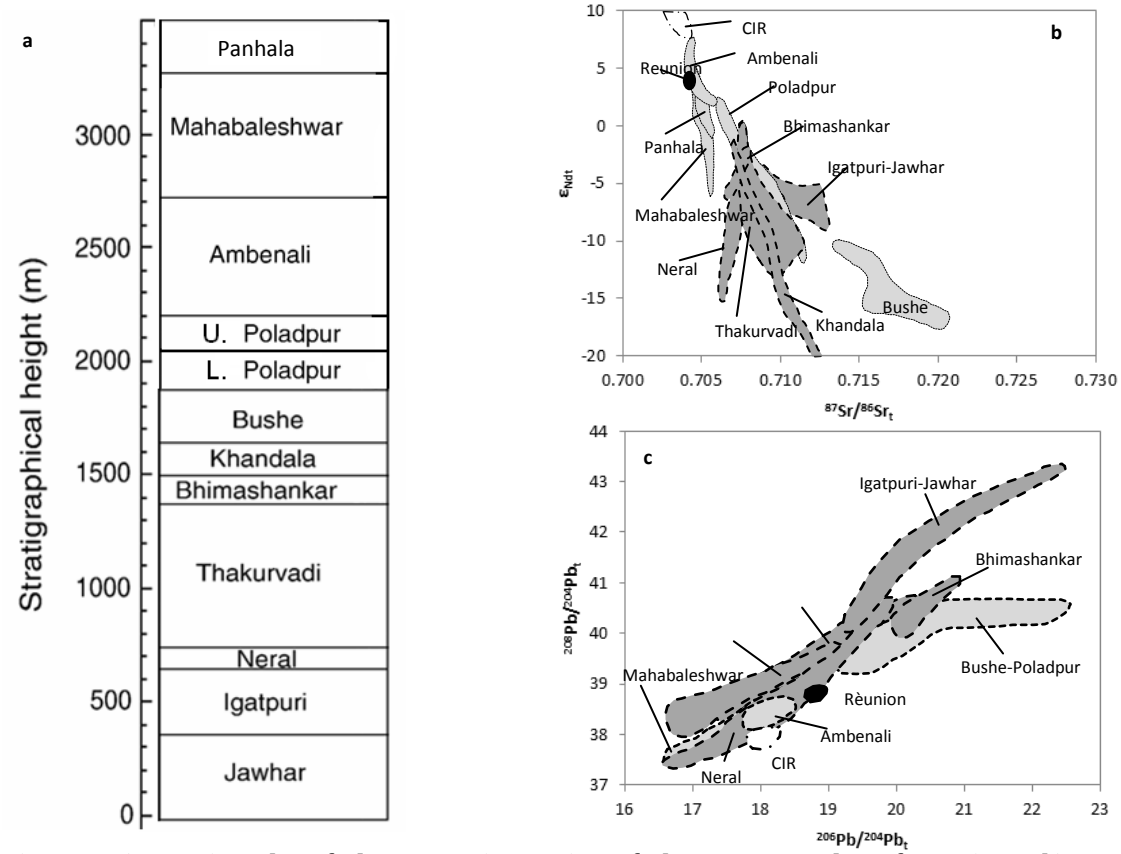

Fig. 1.2. a) Stratigraphy of the composite section of the Western Ghats formations; b) Sr-Nd isotopic compositions of the Western Ghats Formations, in dark grey are the lower formations, and in light grey are the upper formations; Réunion and CIR fields are also shown; c) $^{206}Pb/^{204}Pb_i$ vs. $^{208}Pb/^{204}Pb_i$ plot of the Western Ghats Formations (after Peng et al., 1994).

1.2. Alkaline bodies

Beside the tholeiitic lava flows, which constitute the main portion of the province, a distinctive feature of the Deccan Traps is the presence of several alkaline complexes, associated with the major fault zones. The Cambay graben is a N-S extensional structure in the northern part of the

province, and two complexes are associated with it: Sarnu-Dandali and Mundwara in Rajasthan state. In the Kutch and Saurashtran peninsulae the complexes (Bhuj and Mount Girnar) are associated with the Kutch rift departing the from the Cambay basin and extending to the W. The Narmada valley is a W-E rift that extends from the Cambay basin to the eastern part of the province and along it outcrop many alkaline-carbonatite bodies: Phenai Mata, Amba Dongar, Netrang in Gujarat state, and Barwaha in Madya Pradesh.

The northernmost complexes (Barmer and Mundwara) consist of plug-like bodies and plutons of alkali pyroxenite, nephelinite, ijolite and phonolite, with also the occurrence of carbonatite.

Basu et al. (1993) dated biotite grains from the complexes at 69.62±0.08 Ma and 69.58±0.16 Ma, respectively, suggesting that they can be considered among the first expressions of the Reunion hotspot, as would be consistent with their LREE enriched patterns, and high $^{3}He/^{4}He$ ratios (up to 13.9 times the atmospheric ratio), indicating the contribution of a primitive non-degassed mantle plume. Further investigations conducted by Simonetti et al. (1998), highlighted the depleted isotopic composition of such rocks, not far from that of the Reunion plume, and proposed an important contribution of the hotspot in the generation of this complexes, as well as in the generation of Bhuj nephelinites in Kutch, which show even more depleted compositions. Further south, the complexes represent subsequent phases during the northward migration of India, with lithospheric thinning becoming more important. Therefore, an increasing contribution of the sub-continental lithospheric mantle (SCLM) in the generation of complexes is suggested, differently to what has been proposed for other alkaline provinces, such as that in East Africa for which a two-stage model has been described: a first release by the plume of HIMU metasomatizing agents with the subsequent metasomatization of EMI-like lithosphere, and evolution through different degrees of partial melting of the metasomatized and heterogeneous lithosphere (Bell and Simonetti, 1996).

South of Mumbai other alkaline complexes outcrop, such as nepheline syenite, nephelinites, and lamprophyre in the Murud area (Melluso et al., 2002). In this case, while the lamprophyre show isotopic compositions comparable to those of the northern alkaline complexes, the nephelinites display a distinctive enriched composition, with very low ε_{Nd} (down to -16.2) and moderately radiogenic $^{87}Sr/^{86}Sr$ (0.70468); isotopic compositions and the high incompatible element content of the former suggest their derivation from low degree partial melting (2-3%) of a metasomatized lithospheric mantle; whereas the involvement of a Lewisian-like lower crust is required to reproduce the unusual isotopic composition of the nephelinites.

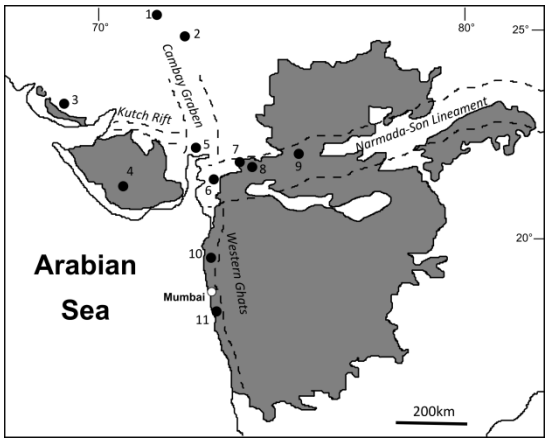

Fig. 1.3. Map showing the approximate location of the intrusive and alkaline bodies in NW India. 1) Barmer; 2) Mundwara; 3) alkaline olivine basalts in Kutch; 4) Mount Girnar; 5) Kadi; 6) Netrang; 7) Phenai Mata; 8) Amba Dongar; 9) Barwaha; 10) Jawhar; 11) Murud. Dashed lines indicate the main fault zones.

Given the presence of both alkaline and tholeiitic rocks in a relatively limited area, a comprehensive study is needed for defining the evolution of the province, in terms of geodynamic evolution, mantle source, and timing. One of the goals of the present work is also to provide constraints for determining the relationship, if any, between alkaline and tholeiitic rocks. Therefore samples from northwestern portion of the province have been collected in an area of about 5000 km^2, and characterized by the co-presence of both alkaline and tholeiitic rocks. This study will enlarge the present knowledge of the Deccan LIP by providing new data in terms of age of emplacement, major and trace elements, and isotopic compositions with the aim of defining the processes which have led to its formation.

CHAPTER 2.
GEOLOGY OF INDIA

The Deccan Traps presently cover one-sixth of the Indian surface, and they emplaced in a intracratonic environment, overlaying at least three of the cratonic blocks that form the Indian peninsula. It is important to consider and characterize such blocks in order to provide further constraints for the understanding of the contamination processes which may have taken place during the formation of the Deccan Traps.

The Indian Shield is composed by different Mid- to Late- Archean cratonic domains, bordered by fold belts which have formed as a consequence of the collisions between the cratons.
An overview of the Precambrian crustal evolution of Peninsular India is presented by Meert et al. (2010) and it can be summarized as below.
The history of the Indian shield as a unique block started when the North and South Indian Blocks collided about 1.8Ga along the Central Indian Tectonic Zone (CITZ), during the final phase of the formation of the pre-Rodinian supercontinent.
The southern protocontinent of the Indian shield is constituted by Dharwar, Bastar and Singhbhum Cratons which are located south of the Son-Narmada lineament; the Aravalli-Bundelkhand craton constitutes the northern portion of the shield.
The CITZ is a ENE-WSW trending mobile belt which joins the Aravalli-Bundelkhan Craton in the N and the Bastar Craton in the S.
The Aravalli-Bundelkhan craton is located in the north-central portion of India and can be divided into two blocks separated by the Great Boundary Fault: the Aravalli block to the west of the fault and the Bundelkhan craton to the east.
The Aravalli basement is composed by the Banded Gneissic Complex (BGC), constituted by migmatites, gneisses, meta-sedimentary rocks and to a minor extent by amphibolites for which a stabilization age of ca. 2.5Ga has been proposed (Wiedenbeck et al., 1996).
The Aravalli and Delhi fold belts represent part of the Rodinia supercontinent and they are associated to the Aravalli and Delhi Supergroups which lay over the BGC and are the oldest metasediments of the area.

The Aravalli Supergroup presents polyphase deformation and metamorphism; the lower groups represent a shelf sedimentation environment, whereas the upper group is composed by turbidite sequence, representing deep sea facies sedimentation. The intrusion of the Darwal Granite (1850Ma, Choudhary et al., 1984) marked the end of the deposition of the Aravalli Supergroup.

The Delhi Supergroup shows a diachronous deposition between the northern sector and the southern one, the former being older than the latter. It is composed by conglomerate, quartzite, phyllites, carbonaceous shales and its upper group by pillow lavas.

From about 1800Ma, several generation of granitoid intrusions have emplaced in the Aravalli Craton. In the northern sector of the Delhi Fold Belt, two granitoid plutons emplaced respectively in periods between 1780-1710Ma and 1711-1660Ma, suggesting a protracted period of extensional tectonics (Kaur et al., 2007), which have been shown to broadly coincide with the main phase of metamorphism and the outset of the Delhi Orogenic Cycle (1725-1621Ma, Roy et al., 2005).

In the southern sector of the Delhi Fold Belt younger intrusions have been recognized: the Sendra Granite (ca. 1Ga, Pandit et al., 2003) is composed by different deformed plutons ranging in composition from tonalite to granite and its formation is compatible with the processes of convergent margin in early Neoproterozoic; the Erinpura Granite (860-800Ma, Deb et al., 2001) constitutes the principal intrusion in the Delhi Supergroup and marks the closure of the Sirohi basin (upper Delhi Supergroup) and one of the phases of the Rodinia breakup through the early stage of the opening of the Mozambique Ocean.

After a metamorphic shear episode about 940-950Ma (Buick et al., 2006), another magmatic episode occurred with the emplacement of the Malani Igneous Suite (MIS, 800-750Ma) which is the largest felsic magmatic province of India and is formed by minor basaltic volcanics and predominant felsic volcanics followed by the emplacement of granitic bodies and predominantly felsic and minor mafic dykes (Torsvik et al., 2001).

One of the phase of Gondwana assembly developed through the formation of sag basins, one of which is represented by the Neoproterozoic/Cambrian Marwar Supergroup (635-515Ma, Naqvi and Rogers, 1987) which overlay the MIS in the western part of the Aravalli mountain range and it constituted by deltaic to shallow marine facies sequences made up of evaporites, carbonates, sandstones and red beds.

The Bundelkhand Craton is located to the E of the Delhi Fold Belt and is composed by three litho-tectonic unit.

The basement (enclave suite) is highly deformed and is mainly formed by 3 generation of gneisses from 3.2 to 2.5Ga old, the latter being the expression of the stabilization of the craton.
The basement is intruded by the undeformed Bundelkhand Igneous Complex which is composed by two main bodies of trondhjemitic gneisses: the Bundelkhan granite and the Berach granite (2492 and 2530Ma, respectively; Mondal et al., 2002; Wiedenbeck et al., 1996) which are in turn intruded by mafic dyke swarms (2.15 and 2Ga; Rao, 2004).

The Vindhyan Basin is an ancient sedimentary basin that outcrop between the Aravalli-Bundelkhand craton and the Deccan Traps. The sequence overlay the basement of the Bundelkhand Igneous Complex and with an age of the sedimentation in the lower units of 1750-1500Ma (Gregory et al., 2006; Patranabis-Deb et al., 2007; Azmi et al., 2008; Basu et al., 2008), and the end of sedimentation in the upper sequence by 1000Ma (Malone et al., 2008). The lower units of the basin are made up by alternating formations of shale and carbonates, whereas the upper units consist of sandstones, which define the transition into shallower marine or fluvial environment, and of carbonates in the uppermost part of the sequence. The lower units and part of the upper unit are intruded by the Majhgawan Kimberlite (1073Ma, Gregory et al. 2006). It is one of several Proterozoic-age kimberlites/lamproites intruding the peninsular Indian crust and represents a phase of widespread anorogenic activity that lead to the emplacement of intrusive bodies as a result of the dispersion of cratonic blocks from the Rodinia.

The Bastar Craton (central-eastern India) is bordered by different tectonic lineaments such as the Pranhita-Godavari rift, the Mahandi rift (to the south and northeast, respectively), the Satpura Mobile Belt and the Eastern Ghats Mobile Belt (to the north and east, respectively), and by the Deccan Traps to the west. It's made up mainly by granites and granites gneisses.

The supracrustal rocks are constituted by three sequences. The Dongargarh Supergroup can be further subdivided into three groups consisting of granites and gneisses formed during the Amagaon orgeny (2.3Ga), volcanic suites unconformably overlain by shale, sandstones and two volcanic suites of tholeiitic basalts.
The Sakoli fold belt has been reworked during the CITZ mobile belt orogeny and the correspondent Sakoli group consists of polideformed and low grade metamorphosed volcano-sedimentary sequence made up by conglomerate, mafic volcanics and BIF overlain by metapelites.
The Sausar orogenic cycle is part of the assembly process of Rodinia, which lead to the juxtaposition of Dharwar and Bastar cratons with Bundelkhand craton. The Sausar Group is constituted by different lithotectonic units including metamorphosed sediments such as

amphibolite facies metapelites and other marble and calc-silicatic rocks intruded by at least two generation of acid plutons (Bandyopadhyay et al., 2001), and the main phase of metamorphism occurred between 800 and 900Ma (Roy et al., 2006).

In the Bastar Craton different mafic dyke swarms outcrop, having formed mostly in the period of major activity dated to 1.9Ga (French et al., 2008). In the southern portion of the craton the emplacement of the swarms occurred through preexisting faults and the dykes trend mostly NW-SE parallel to the Godvari rift; in the northern region they trend NNW-SSE.

The sedimentary basins in the Bastar Craton formed in an extensional setting resulting in subsidence and the consequent evolution of the depositional environment from narrow shallow-water basin to deep continental sea.

The Chhattisgarh basin (~1Ga, Patranabis-Deb et al., 2007; Das et al., 2009) is characterized in its lower series by a shale-dominated sequence formed also by conglomerate and sandstone, storm-dominated shelf deposits and high-energy shoreface; in the upper series by limestone and shale as expression of outer shelf, slope and basin deposition (Chauduri et al., 2002; Deb, 2004).

The sequence in the Indravati basin is expression of shallow marine or lagoonal depositional environment (Maheshwari et al., 2005), being constituted by shale, dolomites, sandstones, limestone and conglomerate.

The Dharwar Craton is located in the central-southern part of the peninsula and it's divided by the Closepet Granite into Eastern and Western Dharwar Cratons: these two block differ for the abundance of greenstones, age of the basement and metamorphic grade. The early to middle Archean tonalitic-trondhjemitic-granodioritic (TTG) basement is mostly present in the Western Dharwar Craton (WDC) along with the volcano-sedimentary greenstone belts. A late Archean calc-alkaline to K-rich granitic intrusion is outcrop mostly in the Eastern Dharwar Craton (EDC) and represent the last magmatic event in the craton.

The WDC is bordered by the Deccan Traps and younger sediments in the north, by the EDC on the east, by the Sothern Granulite Terrain on the south and by the Arabian Sea on the west.

The WDC constitutes a N-S cross section of Archean continental crust in that shows an increase of the metamorphic grade from greenschist facies to amphibolite facies in the north, and granulite facies in the south, representing a pressure increase from 3-4kbar to 9-10kbar.

The Peninsular Gneisses of the WDC constitute the basement of the craton and have been dated at about 3Ga (Friend and Nutman, 1992); after about 500Ma it underwent extensive migmatization and a granulitic overprint which is contemporaneous with the emplacement of the Closepet Batholith.

The Sargur Group is one of the greenstone belts of the WDC, and it composed by a volcano-sedimentary sequence with mafic-ultramafic volcanic rocks and a transition to felsic rocks upward (Subba Rao and Naqvi, 1999; Paranthaman, 2005).

The Dharwar Supergroup outcrop in two large schist belts which are divided in two sub-units. The first one, the Bababudan Group, is composed by three schist belts: the Bababudan, the Western Ghats and the Shimoga schist belts. The first one is the expression of different environment ranging from braided fluvial systems to subaerial lava flows. It is composed at the base by a conglomerate which grades into quartzites, overlain by metabasites, gabbroic sills, BIF and phyllites.

The Western Ghats are similar to the Bababudan schist belt with major basalts, felsic rocks and pyroclastic units in the upper levels.

The Shimoga schist belt is divided from the other two by the TTG basement and is bordered by high metamorphic grade zone (kyanite and garnet bearing).

The second sub-unit, the Chitradurga succession, comprises a near-shore sedimentary sequence with basal quartz pebble conglomerate and quartzites and an off-shore volcanic sequence that shows a transition to siliceous phyllites and BIF. It is overlain by a turbidite sequence, formed as a consequence of the uplift of the surrounding gneissic land (Bhattacharyya et al., 1988).

Among the Proterozoic Indian basins, The Kalagi-Badami Basin is located along the northern border of the craton and show a E-W trend. The Kaladgi Supergroup consists of sandstones, mudstones and carbonates divided into two groups by an unconformity which testify an uplift period during the evolution of the basin (Dey et al., 2009).

The Eastern Dharwar Craton (EDC) is bordered by the Deccan Traps and Bastar Craton on the north, The Eastern Ghats Mobile Belt on the east and by the Southern Granulite Terrain on the south. It is composed by intrusive bodies, greenstone belts and sedimentary basins.

The Dharwar Batholith consists of a series of parallel plutonic belts, mainly granitic, separated by greenstone belts. They trend from NW to SE, and in the southern sector the trend became mainly N-S. These bodies are late Archean in age (2700-2500Ma; Nutman and Ehlers, 1998), younging eastward.

As mentioned before, the Closepet Granite is located at the margin of the EDC; it is N-S trending and it is bordered by shear zones, thus suggesting its formation to be linked with the suturing between Eastern and Western Dharwar Cratons. It formed 2513Ma (Friend and Nutman, 1991) during the Neo-Archean phase of the widespread plutonism that occurred throughout the Dharwar Craton and marking the stabilization of the craton. The Bangalore granites have formed

as large sheets and dykes intruding the Peninsular Gneisses; eastward of the Bangalore granites large granodioritic to granitic plutons outcrop up to the Kolar schist belt; near the western margin of this belt the intrusive bodies consist dark grey quartz monzonite; whereas near the eastern margin they consist of dark grey granodiorite and granite (Jayananda et al., 2000).

The greenstones belts are localized mostly on the western portion of the craton and show a general N-S trend; the metamorphic grade ranges from greenschist to amphibolite facies. The rocks are younger from west to east. In the EDC different greenstone schist belts have been recognized.

The Sandur Schist Belt is located in the northern margin of the Closepet Granite and, unlike all other belts, trends E-W. The rocks present mainly greenschist facies metamorphism, and minor amphibolites facies metamorphism which is confined to the borders of the belt.

Dating of the belt have been carried out on the granites, rhyolites, basalts and komatiites that are located in the center of the belt, and yielded ages ranging from 2700 to 2500Ma (Ramakrishnan and Vaidyanadhan, 2008; Nutman et al., 1996; Naqvi et al., 2002).

The Kolar-Kadiri-Jonnagiri-Hutti superbelt is composed by several discontinuous belts in the southern portion of the craton and the metamorphism facies is mainly amphibolitic.

These belts are intruded by several felsic dykes whose dating allows to define the minimum age of the hosting rocks: an age of 2700Ma for the protholith has been proposed and it is consistent with the age of granites and gneisses of the belt (Ramakrishnan and Vaidyanadhan, 2008).

The Ramagiri-Hungund superbelt consist of two discontinuous belts that outcrop eastern of the Sandur Belt. Rocks are mostly greenschist facies with minor higher grades. The dating of intruding granites and gneisses provides a minimum age of 2500-2700Ma (Zachariah et al., 1995), consistent with that of the Sandur Belt.

The Veligallu-Raichur-Gadwal superbelt outcrops on the north and the south of the Cuddapah Basin. It is composed by metabasalts (amphibolites facies) in the southern portion, whereas in the northern portion it is made up by pillow metabasalts and boninites.

Several intrusive post cratonization events occurred between 2300 and 1000Ma, and consist in the intrusion of mafic dykes, kimberlites and lamproites which haven’t undergone metamorphism nor deformation being their formation occurred after the migmatitic activity on the granites.

Many of the dykes cluster around and under the Cuddapah Basin and show three principal trends (NW-SE, E-W, NE-SW). The dykes range in composition from dolerites to gabbros, and some late alkaline dykes have been recognized (Murthy, 1995; Pradhan et al., 2008).

Kimberlites and lamproites define several fields around the Cuddapah Basin and are composed by different pipes. Their age are well constrained between 1100 and 1050Ma (Kumar et al., 2007) and formed during the same event which lead to the formation of other kimberlites fields in other Indian cratons.

Three Proterozoic basins formed in the EDC.

The Cuddapah Basin occupies the eastern portion of the craton and it is filled by about 12km thick pack of sediments which can be divided into two different stratigraphic groups, the lower being present throughout the basin and the upper covering mostly the western part of it.

The onset of the sedimentation can be constrained through the dating of the dykes formed around the basin probably after the thermal impulse which brought to the formation of the basin; it had been proposed an age of about 1.9Ga (Chatterjee and Bhattacharji, 2001).

The Pranhita-Godavari Basin consists of two NW-SE trending basins located between the EDC and the Bastar Craton. The sedimentation took place in different deposition environment ranging from continental to deep marine and reflecting episodic changes in the base level due to the dominant extensional regime. The Godavari Supergroup is constituted by three groups: the lower made up by limestone and quartzarenites, and by conglomerate and carbonatite shelf sequence; the second group consists of sandstones and shale, whereas the upper group starts with a basal conglomerate followed by aeolian sandstones. This proterozoic sequence has been dated at 1330-790Ma (Chauduri, 2003).

The Bhima Basin is located between the EDC and the Deccan Traps. The basement consists of granites and gneisses and it's overlain by a basal sequence composed by sandstones and conglomerate, in turn overlain by limestones.

The smallest cratonic block in the Indian shield is the Singhbhum Craton in the eastern part of the peninsula. The nucleus of the craton is mainly formed by Archean granitoid batholiths. The Older Metamorphic Group (OMG) is composed by what remains of the oldest basement that is micaceous schists, quartzites, calc-silicates, and para- and ortho-amphibolites. Dating of these rocks have yielded different ages but they range between 3.6 and 3.2Ga (Mondal et al., 2007; Misra et al., 1999), probably indicating different stages of metamorphism.

The Singhbhum Granite intrudes the OMG and it is composed by twelve magmatic bodies emplaced in several magmatic phases between 3.4 and 0.9Ga (Naqvi and Rogers, 1987; Mondal et al., 2007; Misra, 2006).

The Iron Ore Group (IOG) is a greenstone gneiss terrain composed by three fold belts and divided into Older and Younger Sections. The Older IOG formed in a shallow marine

environment during a large scale rifting. It is composed by sedimentary clastic rocks and volcanic rocks. It predates the formation of the SGC and its age has been placed between 3.5 and 3.1Ga (Mondal et al., 2007). The Younger IOG (3.0-2.5Ga) formed after the emplacement of the SGC, and it is composed by shelf or shallow marine greenstone deposits, and BIF (Eriksson et al., 2006).

Among the Proterozoic basins in the Singhbhum Craton, the Dhanjori Basin is the oldest one, though its age is still debated (about 2.5Ga from Acharyya et al., 2008; 2.8Ga from Mishra and Johnson, 2005). It presents a fluvial sequence formed by sedimentary clastic rocks overlain by mafic and ultramafic volcanics and volcanoclastic rocks.

The Singhbhum Group is formed by different formations which are expression of several depositional environment. At the base, the Chaibasa formation represent a transgression on the craton and consists of tidal sandstones and offshore shale facies. The Dhalbhum formation formed in a aeolian/fluvial depositional environment and is constituted by phyllites, shales, and quartzite overlain by tuff. The Dhalma formation consists of mafic and ultramafic volcanic rocks; whereas the Chandil formation is a belt of metasedimentary rocks and volcanics and represents a aeolian/fluvial or shallow marine depositional environment (Mazumder, 2005; Eriksson et al., 2006).

The Kolhan Group is a minor supracrustal suite (1.1Ga, Mukhopadhyay et al., 2006) composed by a transgressive sequence formed by sandstones, limestones and shale that probably developed in a rift setting during the Rodinia fragmentation (Bandopadhyay and Sengupta, 2004).

The southernmost portion of the Indian Shield is constituted by the Southern Granulite Province. It is formed by three late Archean to Neoproterozoic blocks which show high grade metamorphism assemblages and are joined through different shear zones.

The Northern Block is located south of the Dharwar Craton and is bordered by the Palghat-Cauvery Shear Zone (PCSZ) to the south. It consists of granulite massif with pyroxene granite, migmatites and gneisses. Seismic studies indicate that the Northern Block was accreted onto the Dharwar Craton in a mid-Archean collision (Rao et al., 2006).

The PCSZ is thought to be linked to shear zones in Madagascar and Antartica, and related to the final stages of assembly of East Gondwana (Windley et al., 1994; Harris et al., 1994; de Wit et al., 1998; Clark et al., 2009).

The Central Block is divided by the PCSZ into the Nilgiri and Madras Blocks.

The Nilgiri Block represents one of the deepest exhumed crust of Indian Peninsula, with the paleopressure ranging from 6-7kbar to 9-10kbar (Raith et al., 1999). It consists of garnet-bearing

granulites, gabbroic to anorthositic pyroxenites, kyanite gneisses and quartzites. The granulitic metamorphism occurred 2.4Ga (Raith et al., 1999), as in the Northern Block (Clark et al., 2009).

The Madras Block is east of the PCSZ and consists of medium- high- pressure charnockites and gneisses. The granulite formation has been dated at 2.5-2.6Ga (Bernard-Griffiths, 1987) with a second thermal pulse at 2-1.7Ga (Santosh et al., 2002).

The Madurai Block is the largest one in the Soutehrn Granulite Terrain and it is bordered by the PCSZ on the north, and the NW-SE trending Achankovil Shear Zone (ACSZ) to the south. The western portion of the block consists of charnockites showing ultra-high pressure (8-11kbar) and ultra-high temperature (1000-1100°C) metamorphism (Braun et al., 2007). Basement gneisses and metasedimentary complexes constitute the eastern part of the block. Several metamorphic intervals have been recognized and ranging from 2100-1600 to 600-450Ma (Santosh et al., 2002; Braun et al., 2007; Collins et al., 2007), the latter probably indicating the final stage of Gondwana assembly.

The ACSZ is made up by different lithologies such as garnet-biotite and orthopyroxene-cordierite gneisses, aluminous metapelites, mafic granulites, and is thought to be the prosecution of the shear zone in Madagascar (Naganjaneyulu and Santosh, 2010).

The Trivandrum Block constitutes the southernmost portion of the Indian Shield; it is composed by supracrustal rock showing UHT conditions, such as sillimanite-, garnet- and orthopyroxenes-granulites, garnet and biotite gneisses. Dating of zircon cores yielded an age of 3460Ma and it has been attributed to old relicts of continental crust (Zeger et al., 1996); other dating (Santosh et al., 2006) provided ages probably related with the different phases of the geodynamic evolution of the Earth, in particular the assembly of Columbia (1600Ma), Rodinia (1000Ma), and Gondwana/Pangea (600-400Ma).

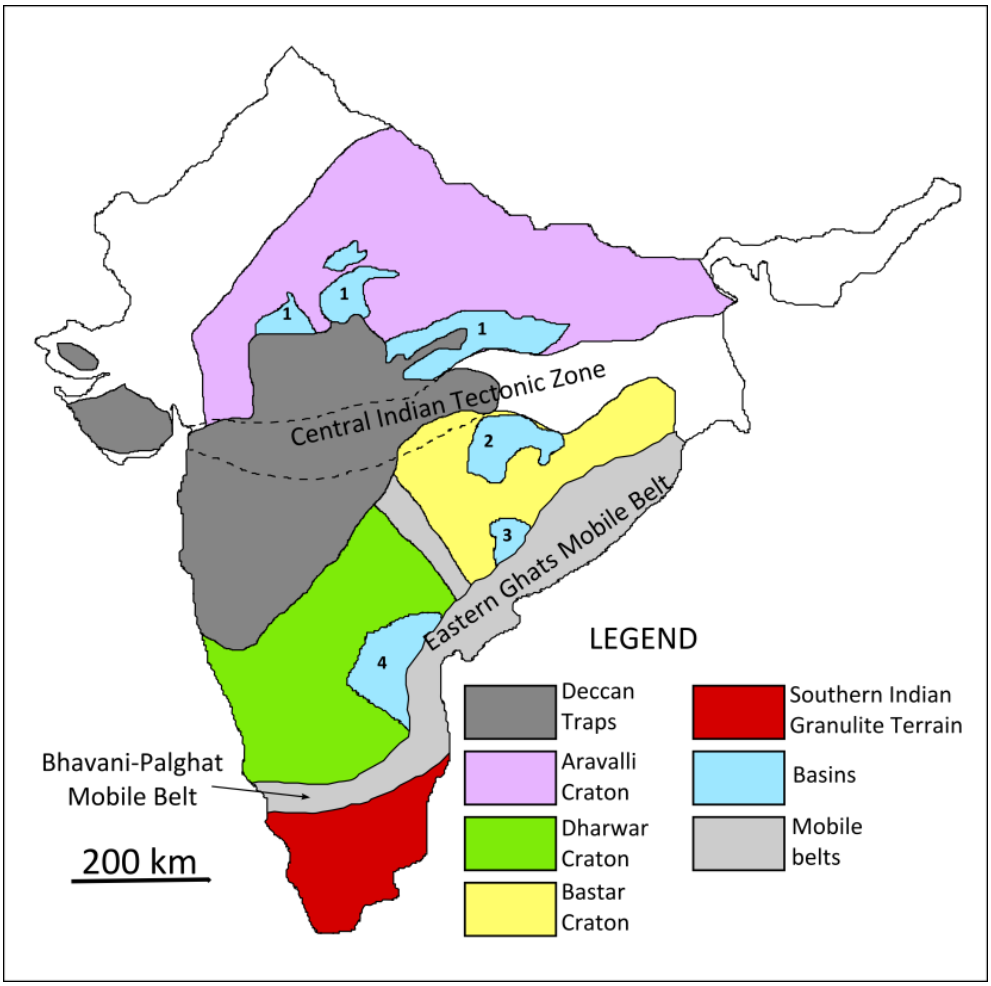

Fig. 2.1. Sketch map of Indian subcontinent. 1) Vindhyan Basin; 2) Chhattisgarh Basin; 3) Indravati Basin; 4) Cuddapah Basin.

CHAPTER 3.
SAMPLING

The sampling activity has been carried out in 2011 in north-western India; the investigated region is situated 400km North of Mumbai in Gujarat and Madhya Pradesh states and consists of three areas; the largest sampled area (≈ 1200 km^2) is the Chhota Udaipur sub-province which, following the description of Gwalani et al. (1993), has been divided into five sectors based on their predominant lithology.

1) The Phenai-Mata sector is located in the northen portion of the area, and shows an association between alkaline rocks and a layered tholeiitic intrusion. The Phenai Mata monadock consists of gabbro associated with anorthosite, granophyre, nepheline syenite and a series of dykes crosscutting the complex (Sukheswala et al., 1973). Nepheline-syenite presents medium-coarse texture mainly constituted by k-felspars and amphiboles, with minor nepheline; the gabbro is present with different modal compositions ranging from olivine-rich samples to bimodal samples constituted mainly by plagioclase and pyroxene. The granophyre is present at the base and at the top of the hill, where it's intercalated with basalt.

Further north, tinguaite and trachyte samples have been collected.

2) East of Phenai Mata, the Panwad-Kanwant sector is mainly characterized by syenite, phonolite, lamprophyre and tinguaite which form plugs and dykes, phonolite in the northeastern part of the sector show ENE trend, whereas lamprophyre dykes are mainly WNW striking. In the southern part of the sector late basic-ultrabasic dolerite dyke outcrop. Phonolitic dykes are porphyritic with felspars phenocryst and present strong alteration; lamprophyre present fine-grained groundmass and phenocryst of euhedral pyroxene and biotite.

3) Further east, the Bakhatgarh-Phulmahal sector contains basic and ultrabasic dykes mostly with ENE to E-W trend, they consist of dolerites and picrite basalts. Lamprophyre dykes may occur as extension of those in the Panwad-Kawant sector. In this area picrite samples have been collected with porphyric texture and abundant phenocrysts of olivine and pyroxenes.

4) The southernmost sector is Amba Dongar and it is characterised by a carbonatite-ring complex which intruded Cretaceous sediments (Bagh sandstone); this complex consists of an innermost ring of carbonatite breccia rimmed by calciocarbonatite which is intruded by ferrocarbonatite

plugs and dykes and cored by basalt (Simonetti et al., 1995). In this sector samples of carbonatite and dolerite have been collected. The carbonatite shows intrusive medium-grained texture composed by carbonatic grains. The dolerites are medium-grained with plagioclase phenocrysts, pyroxenes and olivine. Little south of the complex nephelinite samples have been collected, they present fine-medium groundmass with green pyroxene and brownish garnet as phenocrysts.

5) Little east from Amba Dongar the Siriwasan-Dugdha sector contains tinguaites and trachytic rocks within the flow basalts. In this area almot aphyric trachytes have been collected with greenish fine grained ground mass.

50km eastern of the Amba Dongar area, the Rajpipla area shows a succession with early tholeiites (lava flows) overlain by K-rich alkaline flows which constitute the main exposed sequence, in turn cut by late tholeiitic dykes (Krishnamurty et al., 1980). The Rajpipla alkalic suite has a maximum thickness of 200m in the north-eastern part and is composed by highly porphyritic basaltic and trachybsaltic flows, with minor ankaramite and mugearite and is cut by plug-like masses of K-rhyolites. The latest activity in this area is represented by E-W and WSW-ENE trending tholeiitic dykes. Basalts are aphyric with plagioclase and femic phases in the groundmass, the collected tinguaite present porphyritic texture and big phenocrysts (up to 1mm in size) of amphiboles and pyroxenes.

Mount Pavagadh is the northernmost sampled area (50km NE of Phenai Mata) and consists of a 550m thick sequence of igneous rocks ranging from alkali olivine basalt to rhyolite lavas with a thin layer of pitchstone (Sheth et al., 2008; Greenough et al., 1998). Olivine basalts are characterized by plagioclase phenocrysts which occur also in aggregate and big olivine phenocrysts which can reach 5mm in size. Pitchstone are black aphyric rocks with typical conchoidal fracture.

CHAPTER 4.
METHODS

4.1. Major and trace elements.

After removing alteration crusts, sample have been reduced into chips of less than 4mm in size through a jaw crusher (Retsch BB200), and then reduced into powder by means of agate disc mill (Retsch RS100).

Major elements contents have been determined on 61 samples at the University of Naples Federico II by means of a Philips PW1400 X-Ray fluorescence (XRF) spectrometer. Samples have been prepared as pressed powder pellets. Errors are estimated to be within 1% for SiO_2, TiO_2, Al_2O_3, Fe_2O_{3t} and CaO, less than 6% for K_2O, about 0.03 wt% for MnO and P_2O_5, generally between 5 and 10% for Sc, V, Cr, Ni, Ba, Sr, Y and Zr, and ±1 ppm for Rb and less than 10 ppm Nb.

Loss on ignition (LOI) have been determined at University of Padua by weighting about 1g of sample powder in a ceramic crucible and heating it into a furnace at 100°C overnight, and into a muffle at 1100°C for 4.30 hours, and weighting after each heating.

Trace and REE element contents were measured at University of Ferrara by means of inductively coupled plasma mass spectrometer (ICP-MS) VG Plasma Quad2 Plus, using JP-1 (peridotite at 0·1 chondritic REE) and UB-N (serpentine at 1 chondritic REE) as international standards.

Mineralogical compositions were measured at the IGG-CNR of Padua, by means of the electron microprobe CAMECA SX50, through core-rime traverses. For all analyzed phases an acceleration voltage of 15kV was used, and a take-off angle of 40°, the beam current was set at 10nA for olivine and pyroxenes, and at 15nA for plagioclases.

4.2. Isotopic analyses.

Samples size has been reduced by means of a hand screw-press, covering the crushing surfaces with two plexiglass tablets (1x10x10 cm) to prevent steel contamination. Chips of 1.6-2mm in size were carefully hand-picked under binocular microscope and washed with distilled water in ultra-sonic bath, then powder was obtained through crushing with agate mortar and pestle.

Sr, Nd and Pb isotopic analyses were performed on 30 selected samples at the University of Geneva.

About 150mg of sample were weighted into Teflon beaker, and dissolved in a sub-boiling solution of 4ml HF and 1ml HNO_3. After evaporation 3ml HNO_3 15M were added to the samples and put on the hot plate for 3 days. After evaporation, Sr was separated twice from the matrix by chromatography using a Sr-spec resin, Nd with a REE-spec resin, and Pb with a TRU-spc one.

Analyses were carried in solution mode (through an ARIDUS desolvation nebulizer) by means of a Neptune Thermo Scientific multicollector ICP-MS.

Os isotopic compositions have been determined at Curtin University (Perth, Australia) on 10 samples through isotopic diluition.

About 2g of powder were put into Carius Tube together with 2ml HCl, 4 (or 6)ml HNO_3, 200µl Os spike and 900µl Re spike. After sealing with a torch, the tubes were put in steel jacket and heated at 220°C for 48h for the dissolution. Once cooled, in order to separate Os from Re, carbon tetrachloride was added to the solution, centrifuged, extracted with a pipette, poured into vessels containing HBr, and then heated on a hot plate at 85°C for 3 hours; after partial evaporation, the remaining ca. 40µl of HBr (containing the Os fraction) were transferred onto the center of a flat cap of 5ml conical bottom Teflon vessel, and dried completely for microdistillation. 15µl of conc HBr were added to the tip of these vessels, whereas 20-30 µl of dichromate were added to the flat cap, covering the dried sample. Once capped and wrapped into Al foil, the vessel were put on the hot plate at 85°C for 2-3 hours. In this time, Os is transferred (through a redox reaction) from the dichromate to the HBr, and in order to verify the complete oxidation of Os, the cap have been unscrewed and a little Milli-Q water have been added to the residue, which has to be red-yellow in color, otherwise the microdistillation has to be repeated. the samples were then loaded on Pt filament together with $Ba(OH)_2$ as activator.

For the extraction of Re, the residue from the centrifuge tubes was put into 15ml beakers to evaporate until highly viscous. 10ml 0.8N HNO_3 were added to the sample sludge and put on the hot plate at 70°C overnight. Re was then extracted through chromatography using AG1x8 anion resin, and HNO_3 and HCl for the elution.

Concentrations and isotopic compositions were measured by means of Thermal Ionization Mass Spectrometry (TIMS) in negative mode (NTIMS).

4.3. Datings.

$^{40}Ar/^{39}Ar$ dating were performed on plagioclase, biotite and amphibole separates. In order to separate the freshest grains, they were carefully hand-picked under binocular microscope. The

optimal size for each phase was: 150-200µm for plagioclase, 150-315µm for amphibole and 500-800µm for biotite. The separates were washed with distilled water and acetone.

The $^{40}Ar/^{39}Ar$ analyses were performed at the Western Australian Argon Isotope Facility at Curtin University through step-heating technique. Amphibole and biotite were step-heated using a 110 W Spectron Laser Systems, with a continuous Nd-YAG (IR; 1064 nm) laser rastered over the sample during 1 minute to ensure an homogenously distributed temperature.

Plagioclase were loaded in 0-blank Cu-foil packages and step-heated using a Pond Engineering® double vacuum resistance Furnace.

The gas was purified in a stainless steel extraction line using a GP50 and two AP10 SAES getters and a liquid nitrogen condensation trap. Ar isotopes were measured in static mode using a MAP 215-50 mass spectrometer (resolution of ~ 500; sensitivity of 2x10-14 mol/V) with a Balzers SEV 217 electron multiplier. The data acquisition was performed with the Argus program written by M.O. McWilliams and ran under a LabView environment. The raw data were processed using the ArArCALC software (Koppers 2002) and the step ages have been calculated using the decay constants recommended by Steiger & Jäger (1977).

Blanks were monitored every 3 samples.

CHAPTER 5.
$^{40}Ar/^{39}Ar$ DATING

5.1. Previous geochronology

Dating Deccan Traps magmatic rocks has been the aim of many works (e.g. Courtollot et al., 1988; Ducan and Pyle, 1988; Baksi et al., 1994; Hofmann et al., 2000) , providing an important tool in defining the evolution of the province (e.g. eruptive centers and rate of extrusion), and in establishing their link with the KPg mass extinction, which occurred ~66Ma (Renne et al., 2013), and whose causes are still debated. In order to compare the ages obtained so far, they have been recalculated relative to the age of Fish Canyon sanidine (28.294±0.037 Ma) using the decay constants of Renne et al. (2010, 2011), and all uncertainties are given at 2σ level. Reliable ages must satisfy the criteria for the definition of a plateau age (i.e. at least 70% ^{39}Ar released, at least 3 consecutive steps yielding the same apparent age with 95% confidence level); if excess Ar is present, robust (MSWD<1) isochron ages will be considered. Moreover, it has to be taken into account that some of the ages are relative to standards (MMhb-1, SB-3, LP-6) that are poorly intercalibrated with the FCs standard or not reliable (cf. Jourdan and Renne, 2007) and therefore they will not be considered any further. The available and recalculated Ar/Ar ages are listed in Table 1 and fig. 5.1.

Western Ghats represent the most voluminous sequence in the Deccan Traps, erupted in the main pulse during the formation of the province. Many geochronological analyses of the lava flows have revealed that at least 1800m of the entire sequence were extruded in a short interval of the order of 1 Ma (Baksi, 1994; Hofmann et al. 2000), being the ages of the bottom (mean age 66.07±0.7 Ma; Hofmann et al. 2000) almost indistinguishable from those at the top (65.87±0.4 Ma; Hofmann et al. 2000). To further characterize the evolution of the province, rocks thought to belong to the early and late phases of Deccan volcanism have been dated. Mahoney et al. (2002) proposed the Bibai Volcanics and related suture zone magmatic rocks in the South Tethyan Suture zone (Pakistan) as the first expression of the volcanism, having isotopic and elemental compositions typical of the product of the Reunion hotspot, which produced OIB-type marine volcanism at least 6-8 Ma before the main phase of Deccan tholeiitic magmatism, having age of 74.54-73.14 Ma. In the Cambay graben the OIB characteristics of two intrusive complexes

(Sarnu Dandali and Mundwara) led Basu et al. (1993) to recognize the occurrence of an early alkaline phase of the magmatism which has been dated at ~69Ma (Sarnu Dandali 69.62±0.08Ma; Mundwara 69.58±0.16Ma), representing the incubation of a primitive high-^{3}He plume, followed by a later alkaline phase in the Narmada lineament and dated at 66.01±0.11 Ma, and represented by the Phenai Mata complex.

Further west, in Kutch, the only reliable ages are those provided by Courtillot et al. (2000), who dated lava flows from the Anjar Traps at 67.2-67.7 Ma, thus representing evidence for the eruption of small volume of lava in an early phase of the main volcanism. The late stage of the main volcanism of the Deccan traps could be represented by the lava flows outcropping along the eastern coast of India in the Rajahmundry traps (Knight et al., 2003), which can be correlated to the Western Ghats lava flows on the base of their geochemical characteristics and remnant magnetization, and have a mean age of 65.33±0.5 Ma , thus implying an original extension of the province much larger than that presently observed.

According to Renne et al. (2013), the absolute age of the K-Pg boundary is 66.043±0.043Ma, and can be considered synchronous with the Chicxulub bolide impact in the Yucatan Peninsula, which is often invoked as the main cause of the mass extinction at KPg boundary (Hildebrand et al., 1991; Schulte et al., 2010). Nevertheless, they also argued that a global climate instability (abrupt cooling and sea level drop) preceded of ~1 Ma the KPgB and hence the impact, which therefore cannot be considered the primary cause of the mass extinction, but it stroke an already stressed ecosystem. Thus the outpour of the huge quantity of lavas of the Deccan Traps, which has been estimated in more than $8x10^{6}$ km^{3} (Eldholm and Coffin, 2000), along with the age of the main phase of the volcanism provided by different works (67-66 Ma), strongly suggest that the emplacement of the magmatic province could be the cause of the global change and to a first biotic crisis eventually developed in the mass extinction. Therefore, the precise timing of Deccan rocks is essential to further constrain these events.

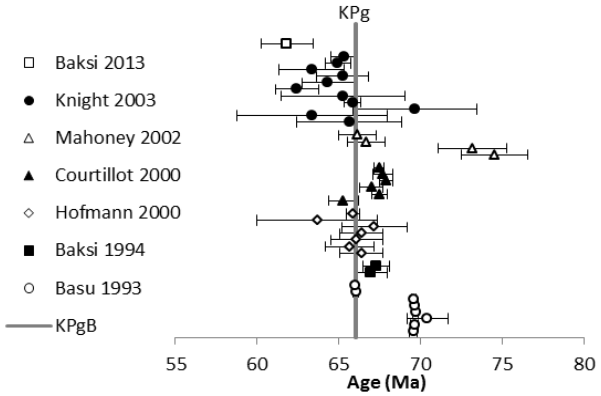

Fig. 5.1. Compilation of reliable plateau ages and respective error bars for Deccan Traps; Cretaceous/Palogene boundary is indicated (grey line).

Table 1. Compilation of $^{40}Ar/^{39}Ar$ ages from the Deccan Traps and rocks linked to the Deccan volcanism.

reference standard	sample	plateau age			isochron			inverse isochron					recalculated age	
		age	2σ	$\%^{39}Ar$	age	2σ	MSWD	age	2σ	MSWD	$^{40}Ar/^{36}Ar$	2σ	age	2σ
Courtillot et al., 1988* LP6bt= 128.5Ma	DK01-03A	66.4	1.9	93										
	86NA03	63.6	0.2	68.5										
	86NA18	63.6	0.5	79.8										
	86NA16	67.6	1.8	71										
	86NA17	65.1	0.6	98.3										
Duncan and Pyle, 1988* MMhb-1= 519.5Ma	MAP 057	68.5	2.4	89	66.9	2					305	22		
	MAP 056	64.7	2.8	65	66.7	2					289	38		
	CAT 034	64.4	1.8	94	67.7	6					286	24		
	CAT021	66.6	2	76	67.7	3					289	30		
	JEB 023	67.8	3.6	67	66.7	2					299	6		
	JEB 311	60.8	4.2	63	62.1	2.1					295	4		
	TEM 004	66.8	1.4	70	66.9	1.2					295	4		
	JEB 334B	62.7	4.2	60	66.6	4					288	8		
	IGA 004	37.5	1.2	91	68.5	1.2					279	40		
Basu et al., 1993 FCs= 27.84Ma	#79bt1	**68.5**	**0.22**					68.58	0.62	1.33	293.4	10.3	**69.55**	**0.22**
	#79bt2	**68.57**	**0.24**										**69.62**	**0.24**
	#51hbl1				**69.36**	**1.26**	**1.91**						**70.41**	**1.26**
	#C11bt-1	**68.63**	**0.16**					68.61	0.52	2.83	295.5	1.4	**69.68**	**0.16**
	#C11bt-2	**68.59**	**0.22**										**69.64**	**0.22**
	#C11bt-3	**68.53**	**0.12**										**69.58**	**0.12**
	PMbt1	**64.99**	**0.16**					64.94	0.58	0.96	298.2	4.3	**66.04**	**0.16**
	PMbt2	**64.94**	**0.14**										**65.99**	**0.14**
Venkatesan et al., 1993* MMhb-1= 520.4	MB81-24	62.4	0.8	75.2	63.1	2					290	14		
	AM83-7	62.1	1	77.6	60	1.4					331	24		
	MB81-10	64.1	1	54.3	65.2	2					262	36		
	MB-81-4	66.1	0.8	73	64.4	2					495	298		
	MB81-3b	67.5	0.8	66	69.2	17.6					126	1028		
	MB81-3a	67	0.8	65.1	68.9	3					165	170		
	IG82-39	66.8	0.6	98.7	64.1	1.4					363	24		
	IG82-34	67.5	0.6	70	68.1	1.8					272	36		
	IG82-27	66.5	0.8	54.2	67.3	1.8					269	30		
	IG82-4	66.8	0.6	81.4	68.2	1.4					218	82		
Baksi, 1994 FCbt= 27.95Ma; SB3bt= 162.8Ma*	IGA009	65.6	1.2	61	66	2	2.8				294	8	66.95	1.2
	JEB339	**65.6**	**1**	**70**	65.3	1	0.97				296.3	3.2	**66.95**	**1**
	JEB339*	66.3	1.4	52	63.7	1.8	0.59				487	140		
	JEB013	65.9	0.8	67	66.5	1.4	1.9				270	56	67.25	0.8
	JEB013			45	67.5	1	11				176	64		
	JEB013*	65.1	1.2	43	67.3	2.8	2.2				236	84		
	KOP-021*			46	66.4	1	2				264	22		
	BSH-008*			33	66	1.2	0.71				246	26		
	MAP052*	64.9	1	57	66.9	2	0.91				271	24		
	D-907*			27	62.5	1.4	0.68				306	14		
	D-921*			32	65.1	6.2	1.6				349	60		
	D-949*	64.5	1	44	65.5	2.4	0.46				278	50		
	D-961*			31	68.9	5.8	4				275	150		
	D970	64.7	2.2	52	63.4	2.4	0.9				325	76	66.05	4.4
	RP81-19	60.8	1.2	63	60.6	0.6	1.9				297	4	62.15	2.4

Table 1. Continued.

Venkatesan et al., 1996* MMhb-1= 520.4Ma	F upper Z199	65.7	0.7	63										
	F lower Z200	65.2 64.9	0.6 0.8	76 79				65.3 66.2	6.8 4.5	0.15 0.83	289 278	8 12		
Hofmann et al., 2000 Hb3gr= 1072Ma	JW2	65.4	1.3	91.2	**65.7**	**1**	**0.2**				291.8	3.6	**66.37**	**1.3**
	JW4	**65**	**1.5**	**69.5**	65.7	1.6	0.6				292.9	7	**65.67**	**1.5**
	JW5	65.4	1.6	65.74	66.2	1.2	0.1				279.8	14.4	66.07	1.6
	JW6	**65.7**	**1.3**	**73.1**	65	1.2	0.1				305.5	14.6	**66.37**	**1.3**
	JW7	65.8	2	84.6	**66.5**	**1.4**	**0.4**				289.5	3.8	**67.17**	**2**
	MA2	63.8	3.7	93.3	**63**	**2**	**0.1**				311.6	16	**63.67**	**3.7**
	D90	**65.2**	**0.4**	**96.2**	64.8	1.2	1				431	660	**65.87**	**0.4**
Courtillot et al., 2000 Hb3gr= 1072Ma	AJ4	64.8	0.9	91	**64.6**	**0.8**	**0.2**				303.4	3.2	**65.27**	**0.9**
	AJ3	66.8	0.5	69									**67.47**	**0.5**
	AJ1	66.3	0.7	86	**66.3**	**0.7**	**0.3**				299.4	1.2	66.97	0.7
		66.9	0.7	100	**67.2**	**0.4**	**1.3**				292.6	1.9	**67.87**	**0.4**
	AJ11	**67**	**0.6**	**88**	66.3	1	0.6				304.4	10.2	**67.67**	**0.6**
	AJ11	**66.8**	**0.3**	**74**									**67.47**	**0.3**
Seth et al., 2001* MMhb-1= 520.4Ma	MnTr	60.4	0.6	99.6	60.2	0.9	1.1	60.5	3.1	1.16	292	10		
	SnTr	61.8	0.6	99.6	62	0.9	1.38	61.8	5.2	1.36	312	18		
Mahoney et al., 2002 FCT-3= 28.04Ma	P60	**73.37**	**2.03**	**92.2**	73.94	2.08	0.78				290.2	12.5	**74.477**	**2.03**
	P69	**72.04**	**2.1**	**96.5**	71.93	2.39	2.93				289.4	55.2	**73.18**	**2.1**
	D1	**65.54**	**1.14**	**99.3**	65.31	1.59	2.95				300.9	27.3	**66.68**	**1.14**
	B4	**64.98**	**1.17**	**78**	65.05	1.3	3.02				292.1	18.8	**66.12**	**1.17**
Knight et al., 2003 FCs= 28.02Ma	RA99.1A	66	2.9	59.1	67	4					295	6	66.63	5.8
	RA99.1B	**65**	**1.6**	**98.9**	67	2					287	12	**65.63**	**3.2**
	RA00.1B	**62.7**	**2.3**	**73.9**	40	30					380	130	**63.33**	**4.6**
	RA991BB	65.3	1.9	89.9	**69**	**4**					280	15	**69.63**	**3.8**
	RA099.02	65.8	0.5	81.9	**65.2**	**0.5**					297	1	**65.83**	**0.5**
	RA99.06	**64.6**	**1.9**	**87.7**	64	3					300	30	**65.23**	**3.8**
	RA99.06	63.5	1.1	88.5	**61.8**	**1.3**					299	3	**62.43**	**1.3**
	RA99.11	**63.7**	**0.8**	**76.4**	63.7	1.2					296	17	**64.33**	**1.6**
	RA99.12A	**64.6**	**0.8**	**86.7**	65	0.9					286	20	**65.23**	**1.6**
	RA99.12B	64.8	0.8	87.9	**62.7**	**2**					350	50	63.33	2
	RA99.14	**64.3**	**0.4**	**75.2**	64.5	0.4					280	20	**64.93**	**0.8**
	RA99.23	**64.7**	**0.4**	**87**	64.8	0.3					289	19	**65.33**	**0.8**
Pande et al., 2004* MMhb-1= 523.2Ma	JEB127.1	66.5	0.9	80.8	66	1.4	2.7	66.1	1.4	1	291	56		
	JEB127.4	66.7	0.7	73.2	66.4	1	0.8	66.7	1.2	0.4	314	12		
Baksi, 2013 FCs=28.03 Ma	D-921			75				**61.2**	**1.6**	**0.84**	495	16	**61.81**	**1.6**
	MAP-052	64.8	0.8	59							295	22	65.41	1.6
	MAP-037	64.6	0.6	67							294.8	4.4	65.21	1.2
	BSH-008	66.6	1	47							299	8	67.21	2
	JEB-339			45				65.3	1	0.35	425	200		
	IGA-009	65.5	0.4	64							320	200	66.11	0.8

*: standard not suitable for recalculating the age of FCs

reliable ages satisfying age plateau and isochron criteria are bolded.

5.2. New $^{40}Ar/^{39}Ar$ dating

Step-heating $^{40}Ar/^{39}Ar$ dating was carried on 11 mineral separates: 4 biotites, 2 are amphiboles, and 5 plagioclases (Table 1). Samples have been heated by means of laser (biotite and amphibole) and furnace (plagioclase and ground mass).

Table 1. Samples analyzed through $^{40}Ar/^{39}Ar$ technique.

sample name	norm	mineral separate	lithology	location
PL3	ne-norm	biotite	gabbro	Phenai Mata complex
PL9	ol/hy-norm	biotite	gabbro	Phenai Mata complex
PL20	ol/hy-norm	biotite	gabbro	Phenai Mata complex
PL36	ne-norm	biotite	lamprophyre	Panwad-Kawant sector
PL2	ol/hy-norm	amphibole	syenite	Phenai Mata complex
PL48	ne-norm	amphibole	phonolite	Northern Phenai Mata sector
PL24a	qtz-norm	plagioclase	dolerite	Amba Dongar
PL54	qtz-norm	plagioclase	basalt	Raipipla area
PL60	qtz-norm	plagioclase	basaltic dyke	Phulmahal-Bakatghar sector
PL61	ol/hy-norm	plagioclase	picrite	Mount Pavagadh
PL63	qtz-norm	plagioclase	rhyolite	Mount Pavagadh

No plateau age have been obtained for samples PL48 and PL60, whereas PL24a yielded very high error (75.32 ± 22.35 Ma), making the plateau age useless.

The 4 samples from Phenai Mata provided robust plateau ages which are indistinguishable at 2 sigma level (from 66.60±0.35 to 66.24±0.37 Ma). The lamprophyric dyke PL36 yielded also a concordant age, which is however significantly younger than those of Phenai Mata rocks (65.25±0.29 Ma). Due to small quantity of fresh plagioclase available, the ages yielded by PL54 and PL61 have relatively large errors (65.9 ± 1.7, and 66.4 ± 2.8 Ma, respectively), preventing to establish if they are as old as Phenai Mata or slightly younger. Finally, a feldspar separate from the rhyolite PL63 (Pavagadh) yielded a robust plateau age (dati del plateau) with the low error (64.9 ± 0.8 Ma) and is significantly younger than the Phenai Mata complex and comparable to the dyke PL36.

All the inverse isochrones (fig. 5.2, right column) yielded identical ages (within the error bars) to those provided by the age spectra, and $^{40}Ar/^{36}Ar$ values comparable to the atmospheric one, thus indicating that negligible, if any, excess Ar was present, with the exception of amphibole PL2, which showed little excess Ar, having $^{40}Ar/^{36}Ar$ intercept=324±13.1, and for which the age provided by the isochron is more reliable.

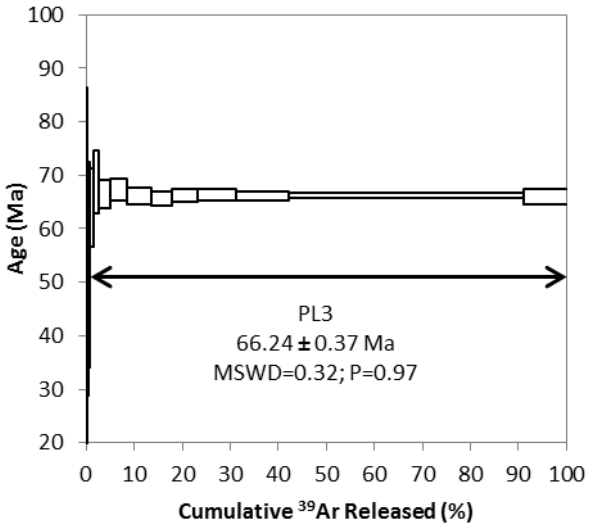
Age (Ma)
Cumulative ^{39}Ar Released (%)
PL3
66.24 ± 0.37 Ma
MSWD=0.32; P=0.97

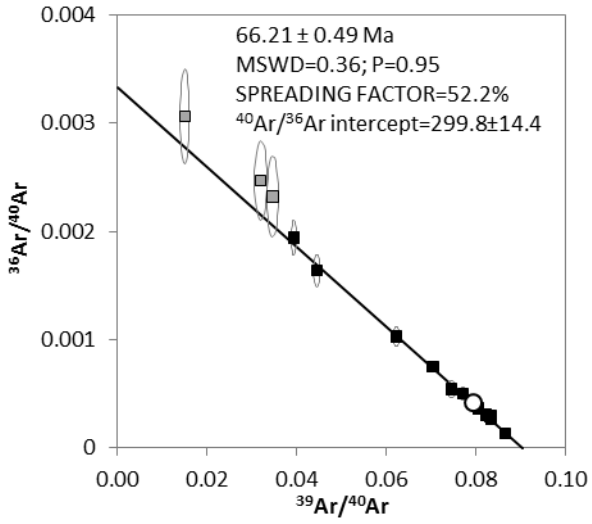
66.21 ± 0.49 Ma
MSWD=0.36; P=0.95
SPREADING FACTOR=52.2%
^{40}Ar/^{36}Ar intercept=299.8±14.4
^{36}Ar/^{40}Ar
^{39}Ar/^{40}Ar

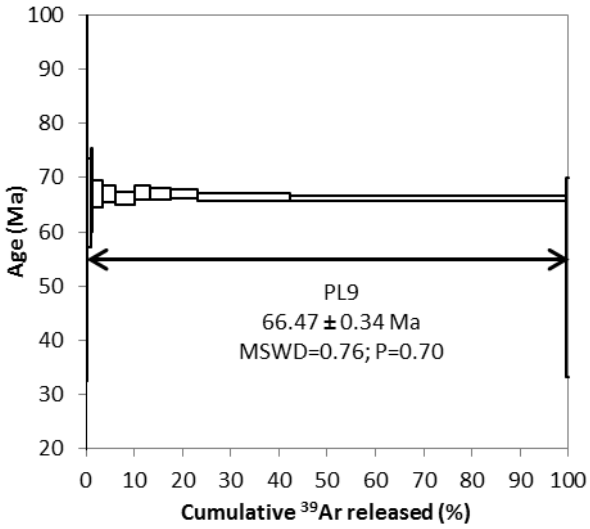
Age (Ma)
Cumulative ^{39}Ar released (%)
PL9
66.47 ± 0.34 Ma
MSWD=0.76; P=0.70

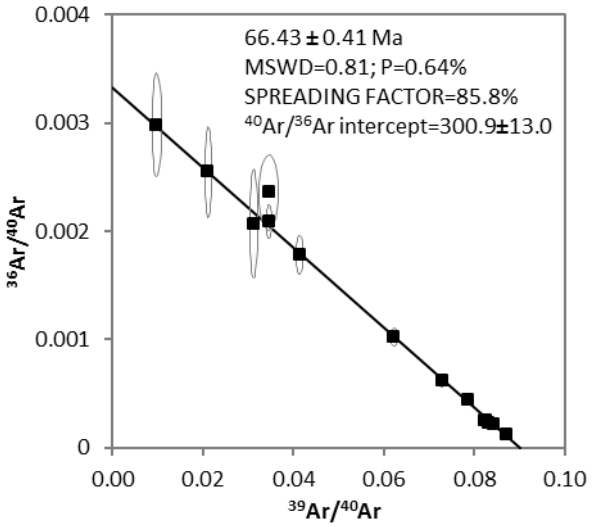
66.43 ± 0.41 Ma
MSWD=0.81; P=0.64%
SPREADING FACTOR=85.8%
^{40}Ar/^{36}Ar intercept=300.9±13.0
^{36}Ar/^{40}Ar
^{39}Ar/^{40}Ar

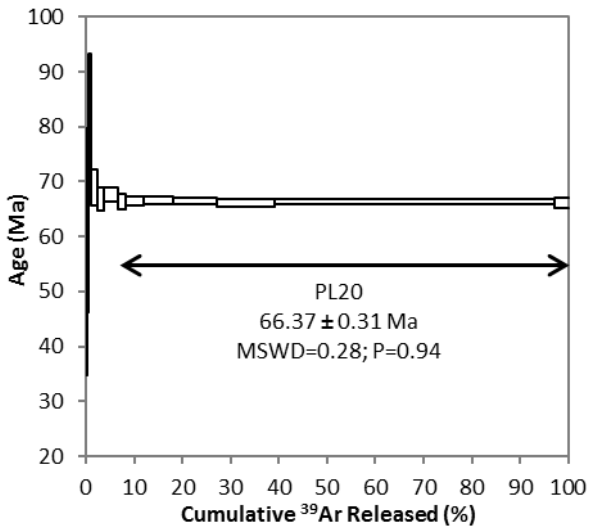
Age (Ma)
Cumulative ^{39}Ar Released (%)
PL20
66.37 ± 0.31 Ma
MSWD=0.28; P=0.94

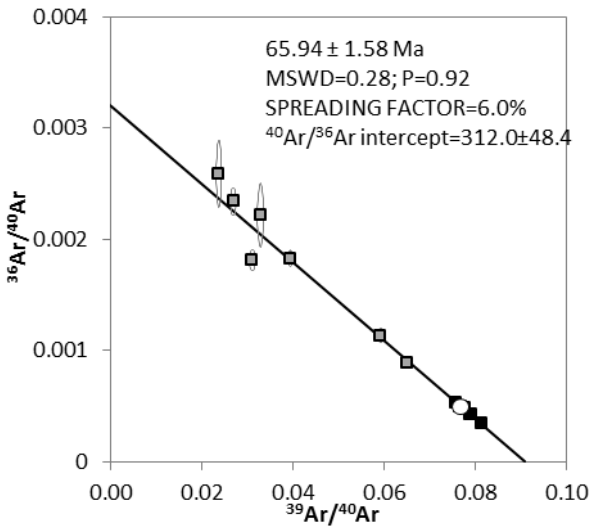
65.94 ± 1.58 Ma
MSWD=0.28; P=0.92
SPREADING FACTOR=6.0%
^{40}Ar/^{36}Ar intercept=312.0±48.4
^{36}Ar/^{40}Ar
^{39}Ar/^{40}Ar

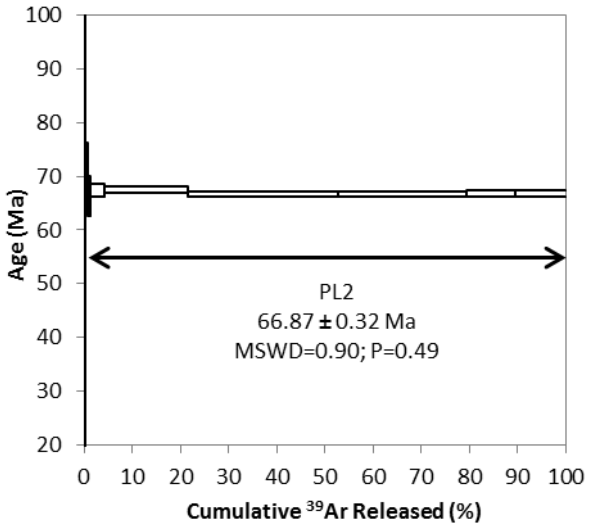
Age (Ma)
Cumulative ^{39}Ar Released (%)
PL2
66.87 ± 0.32 Ma
MSWD=0.90; P=0.49

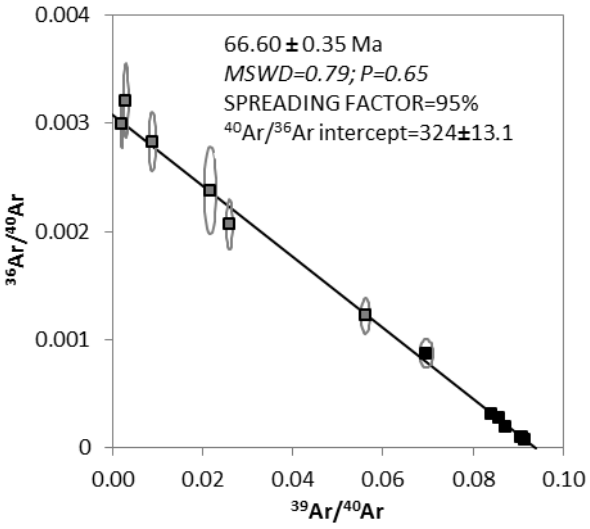
66.60 ± 0.35 Ma
MSWD=0.79; P=0.65
SPREADING FACTOR=95%
^{40}Ar/^{36}Ar intercept=324±13.1
^{36}Ar/^{40}Ar
^{39}Ar/^{40}Ar

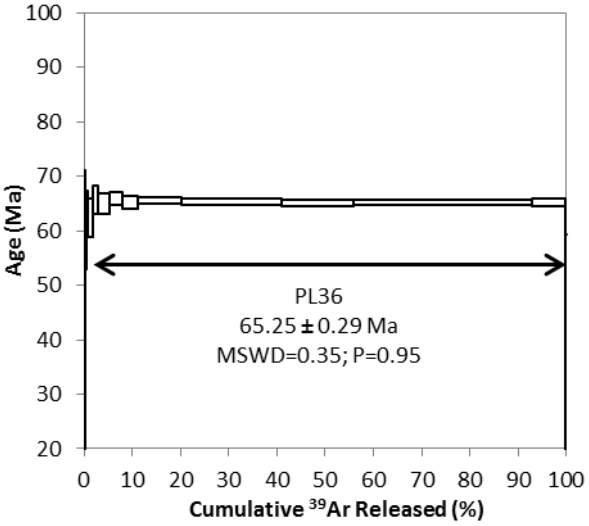
Age (Ma)
Cumulative ^{39}Ar Released (%)
PL36
65.25 ± 0.29 Ma
MSWD=0.35; P=0.95

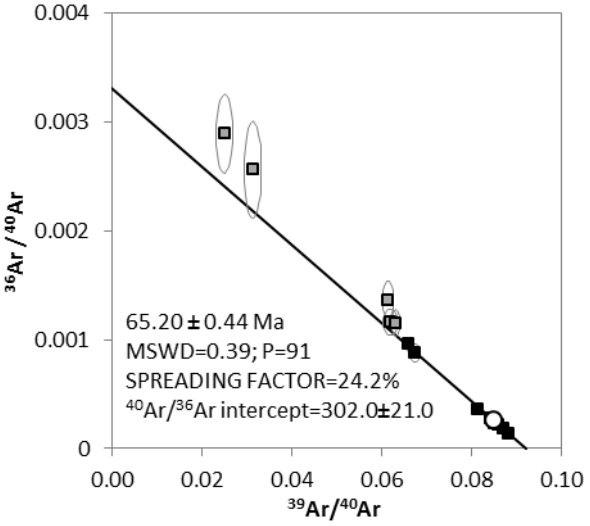
65.20 ± 0.44 Ma
MSWD=0.39; P=91
SPREADING FACTOR=24.2%
^{40}Ar/^{36}Ar intercept=302.0±21.0
^{36}Ar / ^{40}Ar
^{39}Ar/^{40}Ar

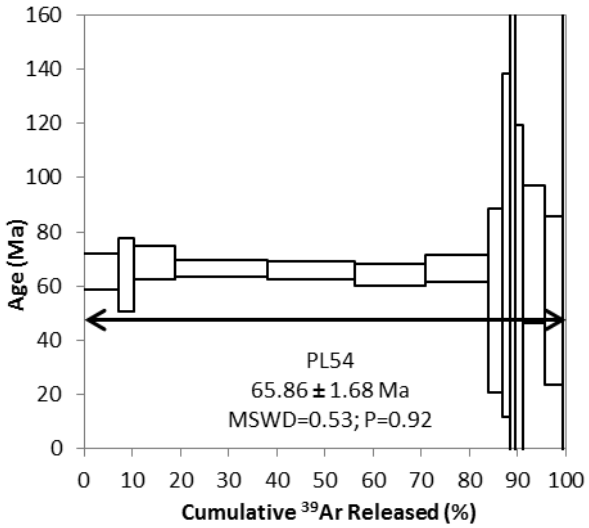
Age (Ma)
Cumulative ^{39}Ar Released (%)
PL54
65.86 ± 1.68 Ma
MSWD=0.53; P=0.92

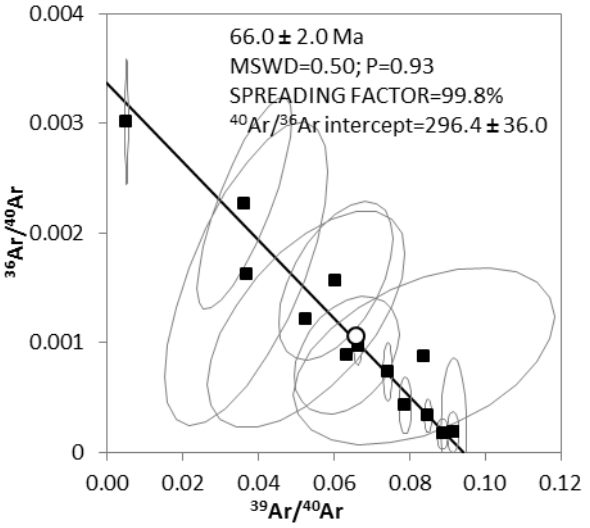
66.0 ± 2.0 Ma
MSWD=0.50; P=0.93
SPREADING FACTOR=99.8%
^{40}Ar/^{36}Ar intercept=296.4 ± 36.0
^{36}Ar/^{40}Ar
^{39}Ar/^{40}Ar

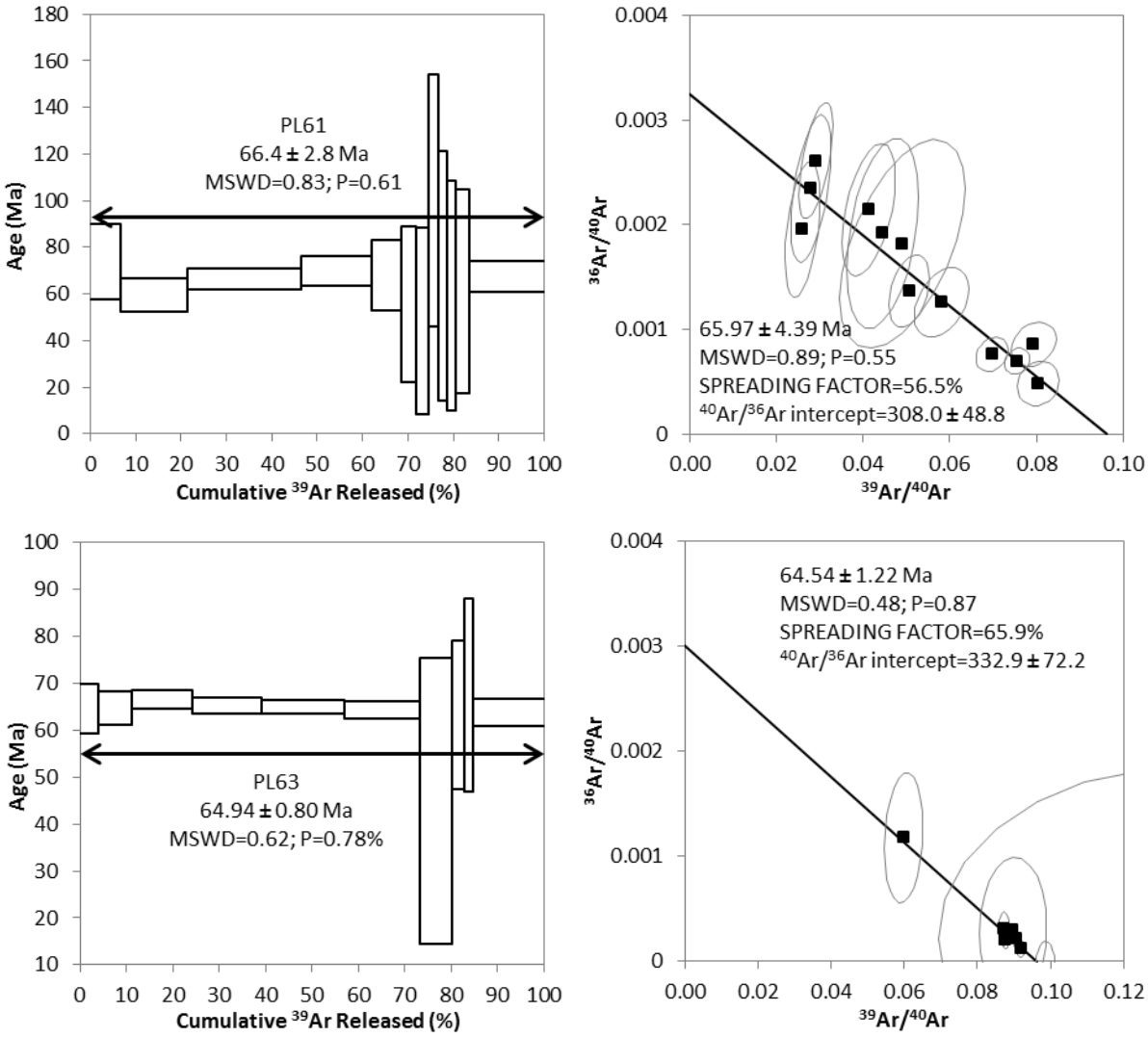

Fig. 5.2. On the left column: age spectra for sample measured using step-heating. Plateau age are indicated by the arrow; MSWD: mean square of the weighted deviates; P: probability of fit. On the right column: inverse isochron plot; black squares: plateau data points; grey squares: non plateau data points; white circle: total fusion data point.

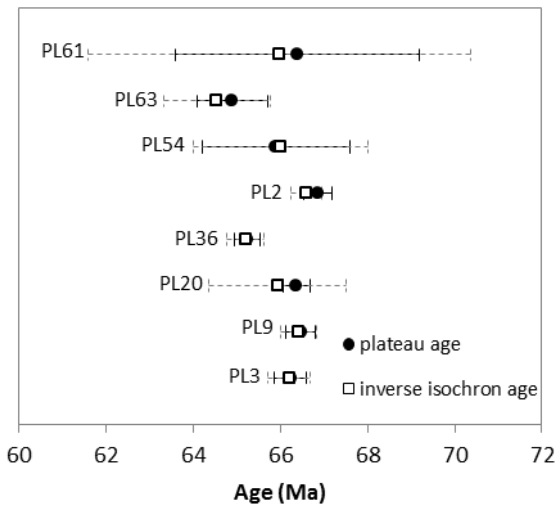

Fig. 5.3. Comparison between plateau ages (black circle), and inverse isochrones ages (white squares). Error bars are indicated: solid line for plateau age, and grey dashed lines for inverse isochron ages.

Except for PL54 and PL61 which have high uncertanties, the other samples clearly define two distinct peaks that straddle the KPgB, being on average at about 66.5 Ma and 65.2Ma, respectively, with alkaline samples belonging to both groups.

The new Ar data are in general in agreement with those described earlier. However it is noteworthy that all the samples from Phenai Mata yielded a remarkably older age than that reported by Basu et al. (1993), implying the formation of the complex within the main Deccan volcanism and not after it. On the contrary, the rocks from Pavagadh e the dyke PL36 belong to the late phase of volcanism.

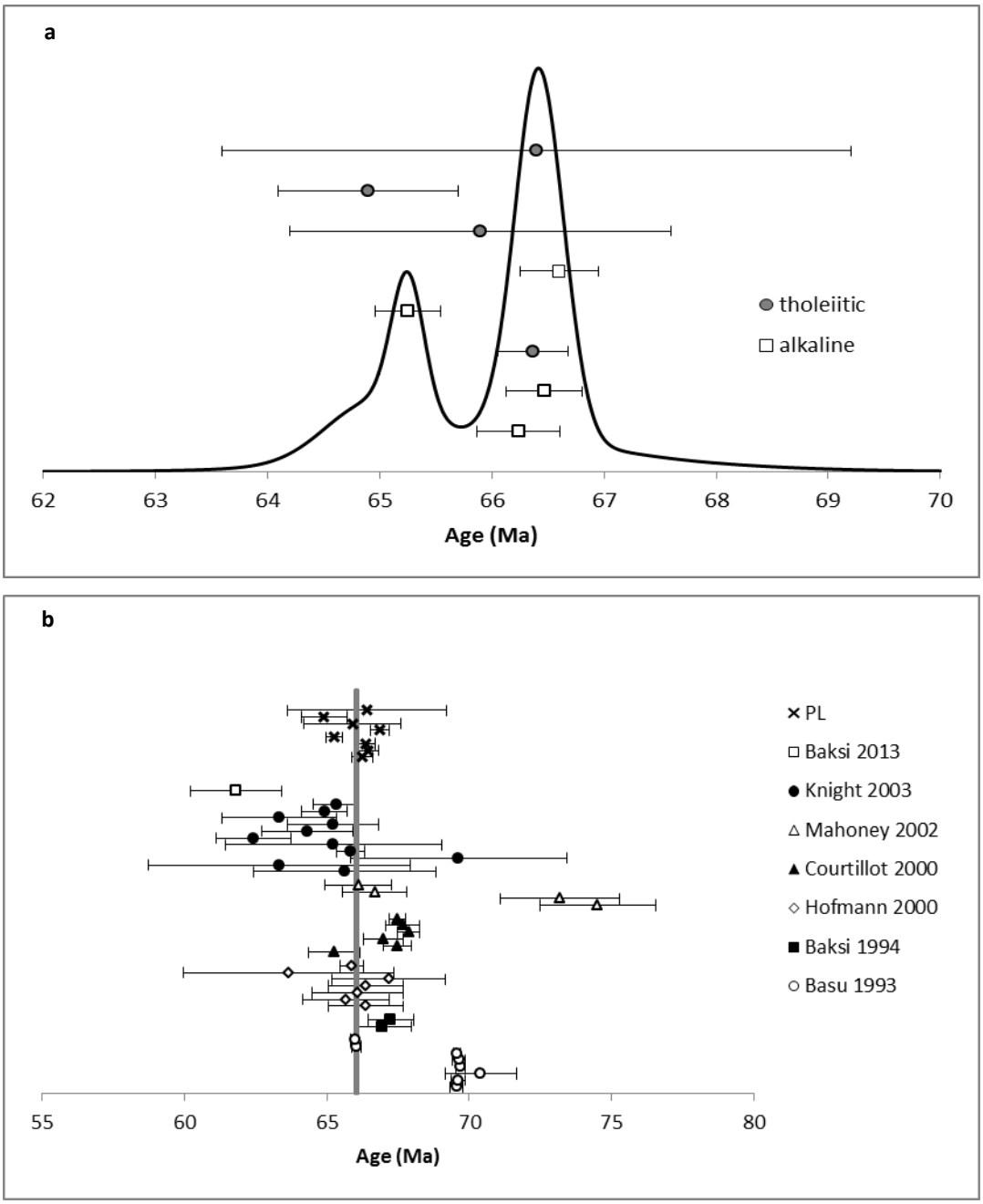

Fig. 5.4. a) Frequency distribution of the obtained ages; b) comparison between new Ar/Ar ages and the reliable ages from the literature, and their relationship with the K/Pg boundary (grey line).

Tables with results obtained per each sample are reported below, and the steps satisfying the criteria for the definition of the plateau are bolded.

PL3.

	Step	Heating	40(r)/39(k)	± 2σ	Age±2σ (Ma)		40Ar(r) %	39Ar(k) %	K/Ca	± 2σ
1	3M28318D	64 W	5.68404	± 8.67237	34.39	± 51.97	8.54	0.13	1	± 3
2	3M28319D	66 W	8.18855	± 3.46642	49.34	± 20.60	26.19	0.29	3	± 23
3	3M28320D	67 W	8.83885	± 3.23445	53.20	± 19.18	30.64	0.34	3	± 21
4	**3M28322D**	**68 W**	**10.66008**	**± 1.24969**	**63.97**	**± 7.37**	**41.99**	**0.70**	**3**	**± 13**
5	**3M28323D**	**69 W**	**11.47514**	**± 1.01442**	**68.77**	**± 5.96**	**51.10**	**1.08**	**63**	**± 3190**
6	**3M28324D**	**69 W**	**11.10079**	**± 0.44577**	**66.56**	**± 2.62**	**69.20**	**2.49**	**18**	**± 117**
7	**3M28325D**	**70 W**	**11.22023**	**± 0.34951**	**67.27**	**± 2.06**	**83.80**	**3.57**	**387**	**± 37968**
8	**3M28327D**	**70 W**	**11.02605**	**± 0.26162**	**66.12**	**± 1.54**	**85.08**	**4.97**	**12**	**± 28**
9	**3M28328D**	**71 W**	**10.93914**	**± 0.23719**	**65.61**	**± 1.40**	**91.12**	**4.39**	**230**	**± 11442**
10	**3M28329D**	**71 W**	**11.03887**	**± 0.21688**	**66.20**	**± 1.28**	**90.80**	**5.15**	**33**	**± 190**
11	**3M28330D**	**72 W**	**11.06131**	**± 0.16736**	**66.33**	**± 0.99**	**89.10**	**8.13**	**331**	**± 11609**
12	**3M28332D**	**72 W**	**11.02883**	**± 0.14486**	**66.14**	**± 0.85**	**92.11**	**11.03**	**547**	**± 23525**
13	**3M28333D**	**80 W**	**11.05680**	**± 0.08693**	**66.30**	**± 0.51**	**95.85**	**48.91**	**265**	**± 1240**

Results	40(a)/36(a)± 2σ		40(r)/39(k)±2σ		Age±2σ (Ma)		MSWD	39Ar(k)(%,n)	K/Ca± 2σ
Age Plateau			11.04614	± 0.05772	66.24	± 0.37	0.32	99.24	5 ± 12
				± 0.52%		± 0.56%	97%	11	
				Full External Error		± 0.61	1.89	2σ Confidence Limit	
				Analytical Error		± 0.34	1.0000	Error Magnification	
Total Fusion Age			11.02784	± 0.06287	66.13	± 0.40		14	70 ± 162
				± 0.57%		± 0.61%			
				Full External Error		± 0.63			
				Analytical Error		± 0.37			
Normal Isochron	299.49	± 14.42	11.03859	± 0.07955	66.20	± 0.49	0.36	99.24	
		± 4.82%		± 0.72%		± 0.75%	95%	11	
				Full External Error		± 0.69	1.94	2σ Confidence Limit	
				Analytical Error		± 0.47	1.0000	Error Magnification	
							1	Number of Iterations	
							0.0000427489	Convergence	
Inverse Isochron	299.84	± 14.43	11.04144	± 0.07965	66.21	± 0.49	0.36	99.24	
		± 4.81%		± 0.72%		± 0.75%	95%	11	
				Full External Error		± 0.69	1.94	2σ Confidence Limit	
				Analytical Error		± 0.47	1.0000	Error Magnification	
							3	Number of Iterations	
							0.0000106673	Convergence	
							52%	Spreading Factor	
J = 0.00337800 ± 0.00000405									

PL9.

	Step	Heating	40(r)/39(k)	± 2σ	Age±2σ (Ma)		40Ar(r) %	39Ar(k) %	K/Ca	± 2σ
1	**3M28336D**	**64 W**	**11.17692**	**± 14.62225**	**67.01**	**± 86.06**	**10.95**	**0.05**	**10**	**± 727**
2	**3M28337D**	**66 W**	**11.31498**	**± 5.98902**	**67.82**	**± 35.23**	**23.96**	**0.11**	**2**	**± 20**
3	**3M28338D**	**67 W**	**12.25776**	**± 4.84114**	**73.36**	**± 28.39**	**38.28**	**0.15**	**2**	**± 13**
4	**3M28340D**	**68 W**	**10.88567**	**± 1.38310**	**65.30**	**± 8.15**	**37.66**	**0.59**	**6**	**± 21**
5	**3M28341D**	**69 W**	**11.29236**	**± 1.32491**	**67.69**	**± 7.80**	**46.75**	**0.51**	**4**	**± 18**
6	**3M28342D**	**69 W**	**11.15986**	**± 0.42300**	**66.91**	**± 2.49**	**69.52**	**1.92**	**11**	**± 21**
7	**3M28343D**	**70 W**	**11.17584**	**± 0.26155**	**67.00**	**± 1.54**	**81.49**	**2.62**	**8**	**± 10**
8	**3M28345D**	**70 W**	**11.03586**	**± 0.19188**	**66.18**	**± 1.13**	**86.93**	**4.04**	**1960**	**± 342790**
9	**3M28346D**	**71 W**	**11.21928**	**± 0.22195**	**67.26**	**± 1.31**	**92.41**	**3.25**	**26**	**± 81**
10	**3M28347D**	**71 W**	**11.16819**	**± 0.18193**	**66.96**	**± 1.07**	**92.45**	**4.23**	**29**	**± 80**
11	**3M28348D**	**72 W**	**11.17793**	**± 0.14909**	**67.02**	**± 0.88**	**93.03**	**5.59**	**27**	**± 48**
12	**3M28350D**	**72 W**	**11.07224**	**± 0.11128**	**66.39**	**± 0.66**	**93.44**	**19.11**	**145**	**± 459**
13	**3M28351D**	**80 W**	**11.02738**	**± 0.08121**	**66.13**	**± 0.48**	**96.21**	**57.47**	**329**	**± 893**
14	**3M28352D**	**82 W**	**8.55612**	**± 3.09234**	**51.52**	**± 18.36**	**29.56**	**0.36**	**3**	**± 9**

Results	40(a)/36(a)± 2σ		40(r)/39(k)±2σ		Age±2σ (Ma)		MSWD	39Ar(k)(%,n)	K/Ca± 2σ
Age Plateau			11.08465	± 0.05154	66.47	± 0.34	0.76	100.00	3 ± 5
				± 0.46%		± 0.51%	70%	14	
				Full External Error		± 0.59	1.78	2σ Confidence Limit	
				Analytical Error		± 0.30	1.0000	Error Magnification	
Total Fusion Age			11.05723	± 0.05811	66.31	± 0.38		14	133 ± 266
				± 0.53%		± 0.57%			
				Full External Error		± 0.61			
				Analytical Error		± 0.34			
Normal Isochron	299.07	± 12.79	11.07845	± 0.06512	66.43	± 0.41	0.83	100.00	
		± 4.28%		± 0.59%		± 0.62%	62%	14	
				Full External Error		± 0.64	1.82	2σ Confidence Limit	
				Analytical Error		± 0.38	1.0000	Error Magnification	
							1	Number of Iterations	
							0.0000543218	Convergence	
Inverse Isochron	300.92	± 12.96	11.07782	± 0.06505	66.43	± 0.41	0.81	100.00	
		± 4.31%		± 0.59%		± 0.62%	64%	14	
				Full External Error		± 0.64	1.82	2σ Confidence Limit	
				Analytical Error		± 0.38	1.0000	Error Magnification	
							4	Number of Iterations	
							0.000017080	Convergence	
							86%	Spreading Factor	
J = 0.00337800 ± 0.00000405									

PL2.

	Step	Heating	40(r)/39(k)	± 2σ	Age±2σ (Ma)		40Ar(r) %	39Ar(k) %	K/Ca	± 2σ
1	3M28797D	62 W	52.63970	± 32.70602	307.37	± 175.62	10.75	0.02	0.071	± 0.117
2	3M28798D	64 W	17.69853	± 9.29998	109.28	± 55.72	15.53	0.05	1.109	± 9.137
3	3M28801D	67 W	14.20862	± 34.51846	88.24	± 209.24	4.21	0.02	0.245	± 1.537
4	3M28802D	68 W	13.38005	± 5.62191	83.22	± 34.17	28.97	0.05	0.400	± 1.125
5	3M28804D	69 W	14.82908	± 2.71809	92.00	± 16.44	38.45	0.15	0.339	± 0.294
6	3M28806D	69 W	11.33756	± 0.89985	70.76	± 5.51	63.63	0.43	0.236	± 0.052
7	**3M28807D**	**69 W**	**10.62101**	**± 0.61105**	**66.37**	**± 3.75**	**73.97**	**0.66**	**0.177**	**± 0.023**
8	**3M28808D**	**70 W**	**10.77882**	**± 0.19423**	**67.33**	**± 1.19**	**90.69**	**2.73**	**0.169**	**± 0.014**
9	**3M28809D**	**71 W**	**10.79004**	**± 0.09579**	**67.40**	**± 0.59**	**94.14**	**17.40**	**0.162**	**± 0.012**
10	**3M28811D**	**71 W**	**10.68443**	**± 0.08302**	**66.76**	**± 0.51**	**97.14**	**31.11**	**0.162**	**± 0.012**
11	**3M28812D**	**72 W**	**10.66147**	**± 0.08047**	**66.61**	**± 0.49**	**97.62**	**26.81**	**0.160**	**± 0.012**
12	**3M28813D**	**79 W**	**10.69076**	**± 0.10622**	**66.79**	**± 0.65**	**97.01**	**10.03**	**0.162**	**± 0.012**
13	**3M28814D**	**82 W**	**10.68682**	**± 0.10978**	**66.77**	**± 0.67**	**91.66**	**10.55**	**0.150**	**± 0.011**

Results	40(a)/36(a)± 2σ		40(r)/39(k)±2σ		Age±2σ (Ma)		MSWD	39Ar(k)(%,n)	K/Ca± 2σ	
Age Plateau			10.70257	± 0.04051	66.87	± 0.32	0.90	99.29	0.161	± 0.005
				± 0.38%		± 0.48%	49%	7		
				Full External Error		± 0.58	2.15	2σ Confidence Limit		
				Analytical Error		± 0.25	1.0000	Error Magnification		
Total Fusion Age			10.72073	± 0.04272	66.98	± 0.33		13	0.161	± 0.006
				± 0.40%		± 0.50%				
				Full External Error		± 0.59				
				Analytical Error		± 0.26				
Normal Isochron	319.55	± 34.68	10.65926	± 0.07133	66.60	± 0.48	0.92	99.29		
		± 10.85%		± 0.67%		± 0.72%	47%	7		
				Full External Error		± 0.68	2.26	2σ Confidence Limit		
				Analytical Error		± 0.44	1.0000	Error Magnification		
							1	Number of Iterations		
							0.0000853641	Convergence		
Inverse Isochron	315.77	± 35.32	10.67370	± 0.07215	66.69	± 0.49	0.90	99.29		
		± 11.19%		± 0.68%		± 0.73%	48%	7		
				Full External Error		± 0.68	2.26	2σ Confidence Limit		
				Analytical Error		± 0.44	1.0000	Error Magnification		
							5	Number of Iterations		
							0.0000220833	Convergence		
							23%	Spreading Factor		
J = 0.00352000 ± 0.00000546										

PL20.

	Step	Heating	40(r)/39(k)	± 2σ	Age±2σ (Ma)		40Ar(r) %	39Ar(k) %	K/Ca	± 2σ
1	3M28354D	64 W	9.52044	± 3.78192	57.23	± 22.38	22.66	0.12	1	± 4
2	3M28355D	66 W	11.17818	± 1.41920	67.02	± 8.35	30.19	0.21	8	± 72
3	3M28356D	67 W	10.26059	± 2.60727	61.61	± 15.39	33.82	0.20	2	± 7
4	3M28358D	68 W	14.71324	± 0.97111	87.71	± 5.65	45.87	0.52	9	± 47
5	3M28359D	69 W	11.49954	± 0.55196	68.91	± 3.25	45.45	1.23	7	± 10
6	3M28360D	69 W	11.14867	± 0.34209	66.84	± 2.01	66.16	1.30	9	± 19
7	3M28361D	70 W	11.29078	± 0.21489	67.68	± 1.26	73.62	3.16	31	± 78
8	**3M28363D**	**70 W**	**11.07245**	**± 0.23639**	**66.40**	**± 1.39**	**85.32**	**1.56**	**30**	**± 160**
9	**3M28364D**	**71 W**	**11.09019**	**± 0.14699**	**66.50**	**± 0.87**	**84.16**	**3.61**	**66**	**± 339**
10	**3M28365D**	**71 W**	**11.10557**	**± 0.12201**	**66.59**	**± 0.72**	**85.21**	**6.11**	**42**	**± 78**
11	**3M28366D**	**72 W**	**11.10038**	**± 0.10384**	**66.56**	**± 0.61**	**87.49**	**9.13**	**37**	**± 43**
12	**3M28368D**	**72 W**	**11.03069**	**± 0.10563**	**66.15**	**± 0.62**	**87.40**	**11.85**	**470**	**± 4760**
13	**3M28369D**	**80 W**	**11.05406**	**± 0.08707**	**66.29**	**± 0.51**	**89.92**	**58.17**	**190**	**± 180**
14	**3M28370D**	**82 W**	**11.02807**	**± 0.16074**	**66.13**	**± 0.95**	**85.69**	**2.84**	**54**	**± 294**

Results	40(a)/36(a)± 2σ		40(r)/39(k)±2σ		Age±2σ (Ma)		MSWD	39Ar(k)(%,n)	K/Ca± 2σ
Age Plateau			11.06780	± 0.04544	66.37	± 0.31	0.28	93.27	44 ± 35
Overstimated error				± 0.41%		± 0.47%	94%	7	
				Full External Error		± 0.58	2.15	2σ Confidence Limit	
				Analytical Error		± 0.27	1.0000	Error Magnification	
Total Fusion Age			11.08942	± 0.05600	66.50	± 0.37		14	71 ± 54
Overstimated error				± 0.50%		± 0.55%			
				Full External Error		± 0.61			
				Analytical Error		± 0.33			
Normal Isochron	311.34	± 48.51	10.99811	± 0.26651	65.96	± 1.58	0.28	93.27	
		± 15.58%		± 2.42%		± 2.39%	92%	7	
Overstimated error									
				Full External Error		± 1.65	2.26	2σ Confidence Limit	
				Analytical Error		± 1.57	1.0000	Error Magnification	
							40	Number of Iterations	
							0.0001092658	Convergence	
Inverse Isochron	311.95	± 48.45	10.99537	± 0.26633	65.94	± 1.58	0.28	93.27	
		± 15.53%		± 2.42%		± 2.39%	92%	7	
Overstimated error									
				Full External Error		± 1.65	2.26	2σ Confidence Limit	
				Analytical Error		± 1.57	1.0000	Error Magnification	
							3	Number of Iterations	
							0.0000014570	Convergence	
							6%	Spreading Factor	
J = 0.00337800 ± 0.00000405									

PL36.

	Step	Heating	40(r)/39(k)	± 2σ	Age±2σ (Ma)		40Ar(r) %	39Ar(k) %	K/Ca	± 2σ
1	3M28372D	64 W	7.56053	± 4.28853	45.60	± 25.54	23.70	0.08	1.8	± 13.2
2	3M28373D	66 W	9.66123	± 0.87572	58.07	± 5.18	59.28	0.35	22.3	± 431.5
3	3M28374D	67 W	10.56089	± 0.65494	63.38	± 3.86	65.34	0.41	5.3	± 18.3
4	3M28376D	68 W	10.39711	± 0.58770	62.42	± 3.47	65.59	0.95	5.7	± 12.7
5	**3M28377D**	**69 W**	**10.95170**	**± 0.42625**	**65.68**	**± 2.51**	**73.78**	**1.06**	**21.6**	**± 122.8**
6	**3M28378D**	**69 W**	**10.82853**	**± 0.31478**	**64.96**	**± 1.85**	**71.43**	**2.30**	**28.7**	**± 111.7**
7	**3M28379D**	**70 W**	**10.98403**	**± 0.20487**	**65.88**	**± 1.21**	**89.32**	**2.73**	**3080.2**	**± 1218200.1**
8	**3M28381D**	**70 W**	**10.87985**	**± 0.20536**	**65.26**	**± 1.21**	**91.76**	**3.21**	**146.1**	**± 2014.9**
9	**3M28382D**	**71 W**	**10.92863**	**± 0.11325**	**65.55**	**± 0.67**	**93.11**	**8.98**	**129.4**	**± 611.5**
10	**3M28383D**	**71 W**	**10.88487**	**± 0.08731**	**65.29**	**± 0.51**	**93.61**	**20.83**	**40.9**	**± 23.4**
11	**3M28384D**	**72 W**	**10.85116**	**± 0.09267**	**65.09**	**± 0.55**	**94.60**	**14.88**	**92.1**	**± 161.1**
12	**3M28386D**	**72 W**	**10.86192**	**± 0.08486**	**65.16**	**± 0.50**	**95.83**	**37.17**	**31.4**	**± 8.4**
13	**3M28387D**	**80 W**	**10.85153**	**± 0.11963**	**65.09**	**± 0.70**	**92.77**	**6.86**	**20.5**	**± 18.9**
14	3M28388D	82 W	5.49056	± 4.35313	33.23	± 26.10	13.73	0.19	4.9	± 38.7

Results	40(a)/36(a)± 2σ		40(r)/39(k)±2σ		Age±2σ (Ma)		MSWD	39Ar(k)(%,n)	K/Ca± 2σ
Age Plateau			10.87820	± 0.04091	65.25	± 0.29	0.35	98.02	30.8 ± 7.3
				± 0.38%		± 0.44%	95%	9	
				Full External Error		± 0.56	2.00	2σ Confidence Limit	
				Analytical Error		± 0.24	1.0000	Error Magnification	
Total Fusion Age			10.85190	± 0.04425	65.10	± 0.30		14	39.1 ± 17.8
				± 0.41%		± 0.46%			
				Full External Error		± 0.56			
				Analytical Error		± 0.26			
Normal Isochron	302.40	± 20.89	10.86540	± 0.06919	65.18	± 0.44	0.37	98.02	
		± 6.91%		± 0.64%		± 0.67%	92%	9	
				Full External Error		± 0.65	2.07	2σ Confidence Limit	
				Analytical Error		± 0.41	1.0000	Error Magnification	
							57	Number of Iterations	
							0.0001057286	Convergence	
Inverse Isochron	301.98	± 21.03	10.86916	± 0.06947	65.20	± 0.44	0.39	98.02	
		± 6.97%		± 0.64%		± 0.67%	91%	9	
				Full External Error		± 0.65	2.07	2σ Confidence Limit	
				Analytical Error		± 0.41	1.0000	Error Magnification	
							3	Number of Iterations	
							0.0000687151	Convergence	
							24%	Spreading Factor	
J = 0.00337800 ± 0.00000405									

PL54.

	Step	Heating	40(r)/39(k)	± 2σ	Age±2σ (Ma)		40Ar(r) %	39Ar(k) %	K/Ca	± 2σ
1	**3B28993D**	**600 °C**	**10.51178**	**± 1.07879**	**65.24**	**± 6.58**	**78.14**	**7.18**	**0.0184**	**± 0.0015**
2	**3B28994D**	**700 °C**	**10.32262**	**± 2.23976**	**64.08**	**± 13.66**	**94.64**	**3.26**	**0.0198**	**± 0.0021**
3	**3B28995D**	**700 °C**	**11.06433**	**± 1.00610**	**68.60**	**± 6.12**	**87.34**	**8.51**	**0.0179**	**± 0.0015**
4	**3B28996D**	**800 °C**	**10.70584**	**± 0.50515**	**66.42**	**± 3.08**	**95.06**	**19.06**	**0.0161**	**± 0.0013**
5	**3B28997D**	**870 °C**	**10.60582**	**± 0.55389**	**65.81**	**± 3.38**	**90.10**	**18.12**	**0.0156**	**± 0.0012**
6	**3B28998D**	**950 °C**	**10.33670**	**± 0.63029**	**64.17**	**± 3.84**	**94.59**	**14.76**	**0.0157**	**± 0.0013**
7	**3B28999D**	**1020 °C**	**10.69446**	**± 0.81525**	**66.35**	**± 4.97**	**71.05**	**12.88**	**0.0155**	**± 0.0012**
8	**3B29000D**	**1080 °C**	**8.80208**	**± 5.52755**	**54.79**	**± 33.89**	**73.84**	**3.14**	**0.0159**	**± 0.0015**
9	**3B29001D**	**1130 °C**	**12.11066**	**± 10.42057**	**74.96**	**± 63.18**	**63.87**	**1.63**	**0.0163**	**± 0.0017**
10	**3B29002D**	**1180 °C**	**13.91953**	**± 17.70637**	**85.89**	**± 106.70**	**51.46**	**0.98**	**0.0223**	**± 0.0046**
11	**3B29003D**	**1230 °C**	**8.82089**	**± 10.51991**	**54.90**	**± 64.49**	**32.17**	**1.63**	**0.0192**	**± 0.0025**
12	**3B29004D**	**1280 °C**	**11.59165**	**± 4.16853**	**71.81**	**± 25.32**	**73.60**	**4.49**	**0.0155**	**± 0.0014**
13	**3B29005D**	**1350 °C**	**8.79123**	**± 5.08256**	**54.72**	**± 31.16**	**53.29**	**3.77**	**0.0156**	**± 0.0014**
14	**3B29006D**	**1425 °C**	**133.97100**	**± 126.98531**	**694.43**	**± 546.57**	**29.48**	**0.18**	**0.2109**	**± 1.4067**
15	**3B29007D**	**1500 °C**	**19.00048**	**± 32.40853**	**116.25**	**± 192.05**	**10.08**	**0.76**	**0.0135**	**± 0.0021**

Results	40(a)/36(a)± 2σ		40(r)/39(k)±2σ		Age±2σ (Ma)		MSWD	39Ar(k)(%,n)	K/Ca± 2σ	
Age Plateau			10.61441	± 0.27320	65.86	± 1.68	0.53	100.00	0.0163	± 0.0008
				± 2.57%		± 2.56%	92%	15		
				Full External Error		± 1.75	1.76	2σ Confidence Limit		
				Analytical Error		± 1.66	1.0000	Error Magnification		
Total Fusion Age			10.40543	± 0.59939	64.59	± 3.66		15	0.0162	± 0.0005
				± 5.76%		± 5.67%				
				Full External Error		± 0.56				
				Analytical Error		± 0.26				
Normal Isochron	287.48	± 33.61	10.50661	± 0.31799	65.21	± 1.96	0.64	100.00		
		± 11.69%		± 3.03%		± 3.00%	82%	15		
				Full External Error		± 2.01	1.78	2σ Confidence Limit		
				Analytical Error		± 1.94	1.0000	Error Magnification		
							100	Number of Iterations		
							0.0001837101	Convergence		
Inverse Isochron	296.38	± 36.00	10.62905	± 0.32027	65.95	± 1.97	0.50	100.00		
		± 12.15%		± 3.01%		± 2.98%	93%	15		
				Full External Error		± 2.03	1.78	2σ Confidence Limit		
				Analytical Error		± 1.95	1.0000	Error Magnification		
							4	Number of Iterations		
							0.0000053942	Convergence		
							100%	Spreading Factor		
J = 0.00349500 ± 0.00000699										

PL61.

	Step	Heating	40(r)/39(k)	± 2σ	Age±2σ (Ma)		40Ar(r) %	39Ar(k) %	K/Ca	± 2σ
1	**3B29612D**	**600 °C**	**11.29728**	**± 4.40805**	**71.59**	**± 27.39**	**72.00**	**6.50**	**0.0185**	**± 0.0019**
2	**3B29613D**	**700 °C**	**9.06636**	**± 1.92002**	**57.68**	**± 12.02**	**96.42**	**14.72**	**0.0226**	**± 0.0021**
3	**3B29614D**	**800 °C**	**10.33961**	**± 1.14449**	**65.63**	**± 7.13**	**94.14**	**25.07**	**0.0229**	**± 0.0022**
4	**3B29615D**	**870 °C**	**10.95546**	**± 1.78618**	**69.47**	**± 11.11**	**102.34**	**15.62**	**0.0224**	**± 0.0021**
5	**3B29616D**	**950 °C**	**10.77411**	**± 4.34989**	**68.34**	**± 27.08**	**119.30**	**6.39**	**0.0235**	**± 0.0024**
6	**3B29617D**	**1020 °C**	**9.17316**	**± 8.96379**	**58.35**	**± 56.10**	**91.44**	**3.24**	**0.0268**	**± 0.0035**
7	**3B29618D**	**1080 °C**	**8.59172**	**± 11.15940**	**54.70**	**± 69.99**	**47.30**	**2.54**	**0.0402**	**± 0.0078**
8	**3B29619D**	**1130 °C**	**17.98947**	**± 14.68810**	**112.70**	**± 89.21**	**98.16**	**1.99**	**0.0259**	**± 0.0051**
9	**3B29620D**	**1180 °C**	**12.82199**	**± 14.12904**	**81.04**	**± 87.33**	**84.94**	**2.05**	**0.0217**	**± 0.0036**
10	**3B29621D**	**1230 °C**	**11.69680**	**± 13.64000**	**74.07**	**± 84.63**	**330.38**	**2.04**	**0.0223**	**± 0.0035**
11	**3B29622D**	**1280 °C**	**11.36994**	**± 10.22520**	**72.04**	**± 63.52**	**596.41**	**2.98**	**0.0233**	**± 0.0029**
12	**3B29623D**	**1400 °C**	**10.99957**	**± 1.72598**	**69.74**	**± 10.73**	**219.48**	**16.86**	**0.0216**	**± 0.0020**

Results	40(a)/36(a)± 2σ		40(r)/39(k)±2σ		Age±2σ (Ma)		MSWD	39Ar(k)(%,n)	K/Ca± 2σ	
Age Plateau			10.43667	± 0.73858	66.24	± 4.61	0.40	100.00		
				± 7.08%		± 6.95%	96%	12	0.0223	± 0.0016
				Full External Error		± 4.63	1.85	2σ Confidence Limit		
				Analytical Error		± 4.60	1.0000	Error Magnification		
Total Fusion Age			10.62866	± 0.99406	67.43	± 6.19				
				± 9.35%		± 9.18%		12	0.0226	± 0.0008
				Full External Error		± 6.21				
				Analytical Error		± 6.19				
Normal Isochron	296.86	± 76.40	11.45213	± 0.85379	72.55	± 5.31	0.59	100.00		
no convergence		± 25.74%		± 7.46%		± 7.31%	82%	12		
				Full External Error		± 5.33	1.89	2σ Confidence Limit		
				Analytical Error		± 5.30	1.0000	Error Magnification		
							100	Number of Iterations		
							0.0042857480	Convergence		
Inverse Isochron	321.43	± 156.51	10.38264	± 0.85960	65.90	± 5.36	0.42	100.00		
		± 48.69%		± 8.28%		± 8.13%	94%	12		
				Full External Error		± 5.38	1.89	2σ Confidence Limit		
				Analytical Error		± 5.36	1.0000	Error Magnification		
							7	Number of Iterations		
							0.0002952050	Convergence		
							838%	Spreading Factor		
J = 0.00357500 ± 0.00000501										

PL63.

	Step	Heating	40(r)/39(k)	± 2σ	Age±2σ (Ma)		40Ar(r) %	39Ar(k) %	K/Ca	± 2σ
1	**3B29077D**	**600 °C**	**10.39349**	**± 0.86402**	**64.55**	**± 5.27**	**102.48**	**4.01**	**0.084**	**± 0.009**
2	**3B29078D**	**700 °C**	**10.40459**	**± 0.58159**	**64.62**	**± 3.55**	**90.81**	**7.13**	**0.084**	**± 0.007**
3	**3B29079D**	**800 °C**	**10.69331**	**± 0.32304**	**66.38**	**± 1.97**	**93.81**	**13.07**	**0.082**	**± 0.007**
4	**3B29080D**	**870 °C**	**10.50334**	**± 0.28972**	**65.22**	**± 1.77**	**96.50**	**15.02**	**0.080**	**± 0.007**
5	**3B29081D**	**950 °C**	**10.44597**	**± 0.23282**	**64.87**	**± 1.42**	**91.74**	**17.68**	**0.082**	**± 0.007**
6	**3B29082D**	**1020 °C**	**10.34158**	**± 0.29447**	**64.24**	**± 1.80**	**93.61**	**16.43**	**0.082**	**± 0.007**
7	**3B29083D**	**1080 °C**	**7.19778**	**± 4.93848**	**44.95**	**± 30.46**	**88.67**	**6.97**	**0.131**	**± 0.019**
8	**3B29084D**	**1130 °C**	**10.16647**	**± 2.59112**	**63.17**	**± 15.82**	**91.24**	**2.42**	**0.090**	**± 0.014**
9	**3B29085D**	**1180 °C**	**10.85078**	**± 3.36952**	**67.34**	**± 20.53**	**64.91**	**1.92**	**0.091**	**± 0.018**
10	**3B29087D**	**1400 °C**	**10.24378**	**± 0.47971**	**63.64**	**± 2.93**	**114.15**	**15.35**	**0.080**	**± 0.007**

Results	40(a)/36(a)± 2σ		40(r)/39(k)±2σ		Age±2σ (Ma)		MSWD	39Ar(k)(%,n)	K/Ca± 2σ	
Age Plateau			10.45656	± 0.12867	64.94	± 0.80	0.62	100.00	0.083	± 0.005
				± 1.23%		± 1.24%	78%	10		
				Full External Error		± 0.93	1.94	2σ Confidence Limit		
				Analytical Error		± 0.78	1.0000	Error Magnification		
Total Fusion Age			10.20838	± 0.37750	63.42	± 2.31		10	0.084	± 0.003
				± 3.70%		± 3.64%				
				Full External Error		± 2.36				
				Analytical Error		± 2.30				
Normal Isochron	330.61	± 67.24	10.34647	± 0.19367	64.27	± 1.19	0.34	100.00		
		± 20.34%		± 1.87%		± 1.86%	95%	10		
				Full External Error		± 1.28	2.00	2σ Confidence Limit		
				Analytical Error		± 1.18	1.0000	Error Magnification		
							1	Number of Iterations		
							0.0000746435	Convergence		
Inverse Isochron	332.90	± 72.25	10.39178	± 0.19864	64.54	± 1.22	0.48	100.00		
		± 21.70%		± 1.91%		± 1.90%	87%	10		
				Full External Error		± 1.31	2.00	2σ Confidence Limit		
				Analytical Error		± 1.21	1.0000	Error Magnification		
							4	Number of Iterations		
							0.0000054498	Convergence		
							66%	Spreading Factor		
J = 0.00349700 ± 0.00000490										

CHAPTER 6.
WHOLE-ROCK COMPOSITIONS

6.1. Major elements

XRF analyses were carried out on 61 samples and the compositions are reported in table 1. Though the samples are both intrusive and effusive, their compositions have been plotted in a TAS diagram (total alkali vs. silica, Le Bas et al., 1986; fig. 6.1), which shows the high compositional variability of the samples. The normative compositions have permitted distinguishing nepheline (Ne-) normative samples (alkaline samples), and olivine/hypersthene (Ol/Hy-), and quartz (Qtz-) normative rocks (subalkaline, tholeiitic samples).

The samples span a wide compositional range varying from little-evolved compositions such as picro-basalts (43.09 wt.% SiO_2), to fairly evolved ones such as those plotting in the rhyolite field (78.58 wt.% SiO_2). The large variation is observed in the total alkali content (Na_2O+K_2O) as well, ranging from the basalt field (<5 wt.% $Na_2O + K_2O$), up to strongly alkaline samples like phonolites (>12 wt.%).

MgO ranges from 17 to <1 wt.%, and both alkaline and tholeiitic samples show similar ranges in MgO contents with maximum values being 10.39 and 8.93 wt.%, respectively, and two tholeiitic samples reaching the values of 13.43 and 16.97 wt.%. MgO and SiO_2 describe a negative correlation (fig. 6.2a), with steeper slope for the samples with lower MgO content (<2.7 %). A similar behavior can be observed for Na_2O and, to a lesser extent, K_2O (fig. 6.2b, c).

Fe_2O_3 and CaO contents vary from almost 16 (and one sample yields nearly 22 wt.%) to 1 wt.%, and from 16 to near 0 wt.%, respectively, and define positive correlations with MgO (fig. 6.2 d, e); alkaline samples are slightly enriched in CaO and NaO with respect to the tholeiites.

Al_2O_3 contents are largely scattered, yet a broadly positive correlation with MgO is shown by tholeiitic samples and a negative one by alkaline rocks (fig. 6.2f).

Also TiO_2 shows a very rough positive correlation with MgO (in particular at MgO <5 wt.%), even if a very large scatter can be observed for samples at a given MgO. Notably, low-Ti samples are from Phenai Mata, Amba Dongar and Mount Pavagadh; whereas high-Ti samples are from Phulmahal-Bakhatgarh, Jaspur, and Panwad-Kawant.

On a P_2O_5 vs. MgO plot, all the samples are scattered, and no correlation can be observed; the maximum value of 1.13 wt.% is reached.

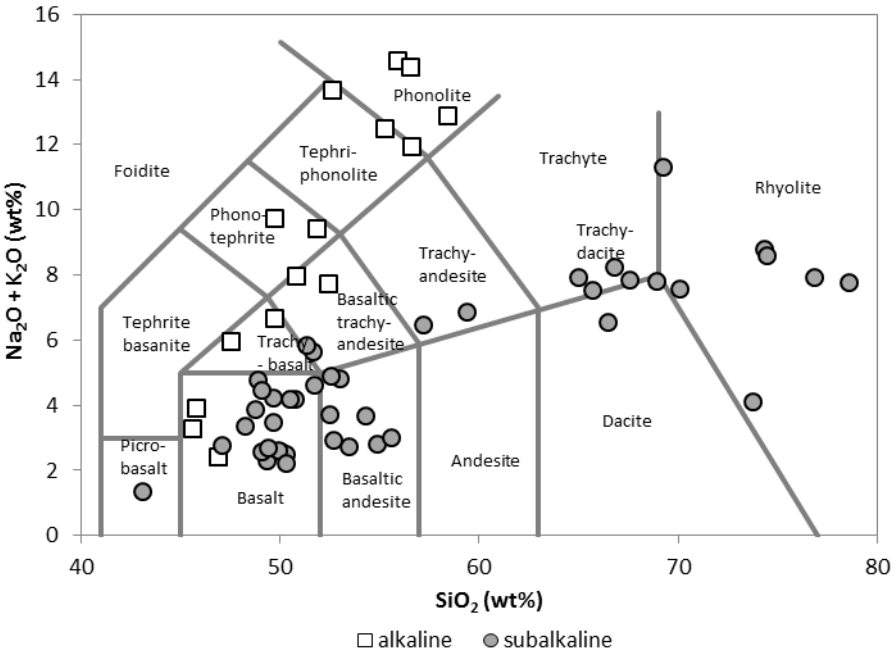

Fig. 6.1. TAS diagram of the samples analyzed by XRF. Grey lines mark the boundaries of the different compositional fields.

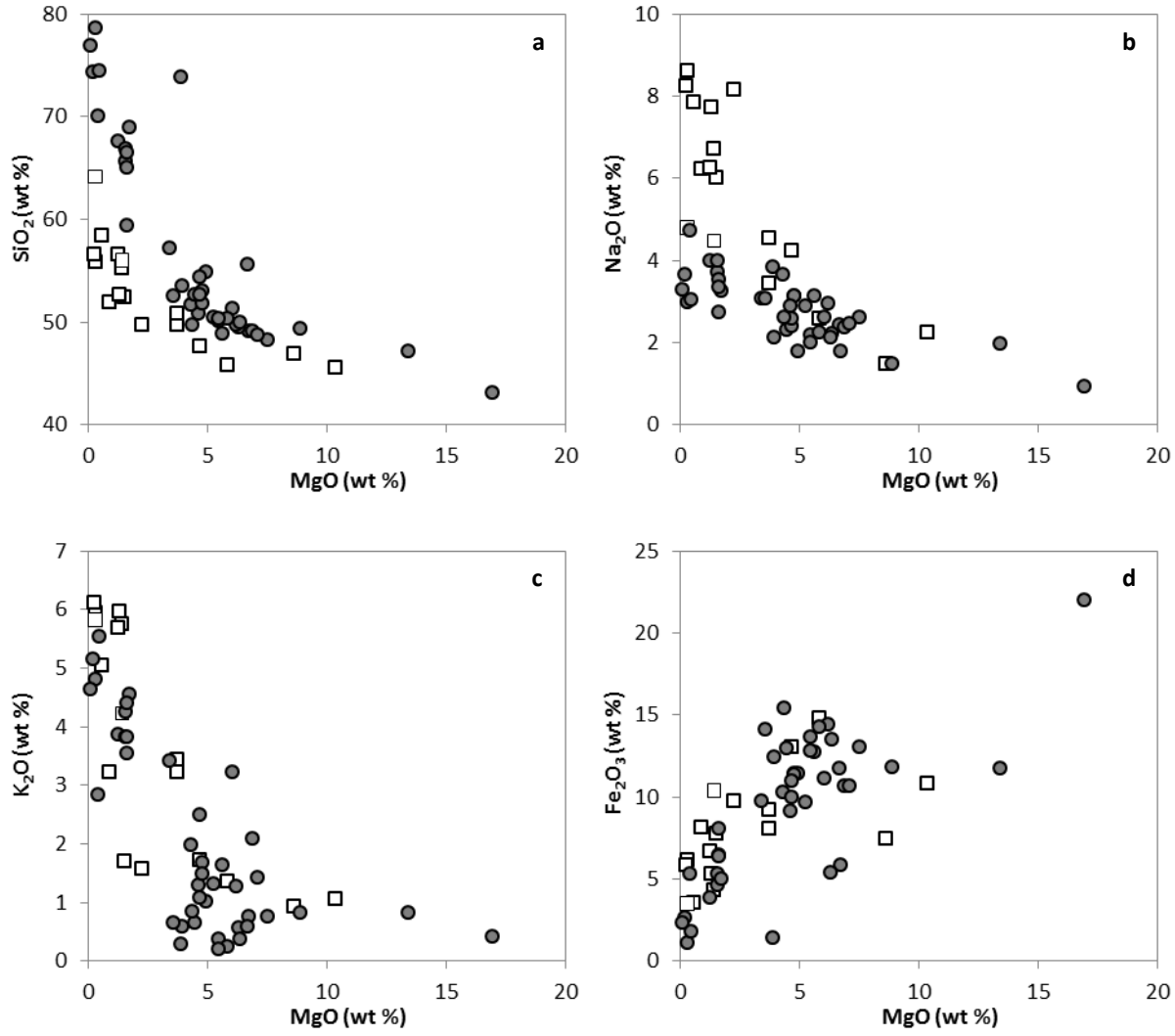

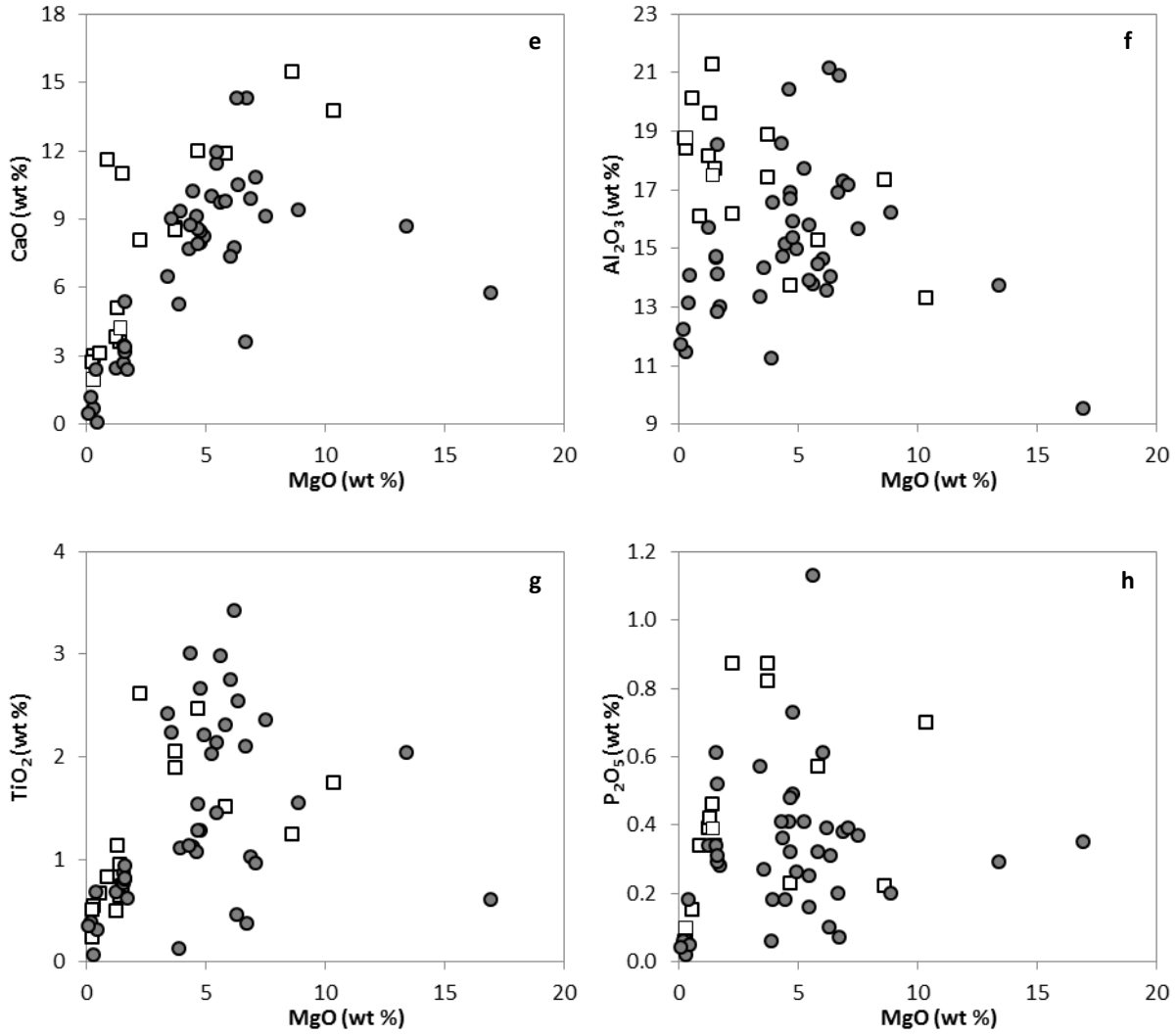

Fig. 2 a-h. Major elements vs. MgO variations. Symbols as in fig. 6.1.

6.2. Trace elements

Ni, Sc and Cr are positively correlated with MgO, whereas V variations are roughly similar to those of TiO_2 (fig. 6.3 a, b).

Due to the different degree of evolution, the samples show large variations in incompatible trace element concentrations, and the patterns are not very homogeneous in each series. All samples show PM-normalized patterns (primitive mantle-normalized values, Sun and McDonough, 1989) enriched in the most incompatible elements, and alkaline samples are the most enriched ones, with element contents up to 800 times PM values. Alkaline samples in particular are characterized by a strong negative K anomaly, which is shown only by some tholeiitic samples, and by a slight negative Ta anomaly. Some of them also show Pb spikes. Most of the tholeiitic samples present negative Sr anomaly, and some of the them show marked

negative Zr-Hf anomaly. Ti shows absent to negative anomalies in alkaline samples, and negative to slightly positive anomalies in tholeiitic samples.

Rare Earth element (REE) contents normalized to chondritic values (C1, Sun and McDonough, 1989) display patterns enriched in light (LREE) vs heavy (HREE) elements. This enrichment is strongest and most variable in the alkaline rocks (La/Yb_N = 19.52-68.79, and PL30 with La/Yb_N = 312.60), whereas tholeiitic samples have significantly lower range of $(La/Yb)_N$ (2.18-22.35), still slightly more enriched than E-MORBs. The patterns are in general concave, with strong enrichment of LREE over intermediate (M) REE and low MREE/HREE.

All the analyzed trace elements define a negative correlation with MgO, and display low and almost constant values for MgO > 3.5 wt.%, whereas they increase describing steeper slope with lower MgO contents (fig. 6 a-f). Alkaline samples are enriched in most of the IE, while tholeiitic rocks are enriched in HREE and Y (e.g. fig. 6f). All samples are rich in Ba and Sr, in particular alkaline ones (670-3480 ppm, and 207-3849 ppm, respectively).

Rb (9-208 ppm) and Zr are similar for both groups, but most of the tholeiitic rocks display slightly lower values.

While Zr/Y is similar in the alkaline and subalkaline rocks, they show some difference in the Zr/Nb ratio, the alkaline samples having the lowest values, and the tholeiitic ones higher values, with a group which have particularly high values (10-13).

Alkaline samples show a marked positive correlation between Nb/Y and Nb/Zr ratios, whereas tholeiitic samples display almost constant Nb/Y values, and highly variable Nb/Zr (8-210).

The groups have similar range in Ba/Nb (1-24), whereas they can be distinguished based on the Sm/Nd ratio, which is highest in the tholeiitic rocks (0.13-0.3) and lowest in alkaline samples (up to 0.17).

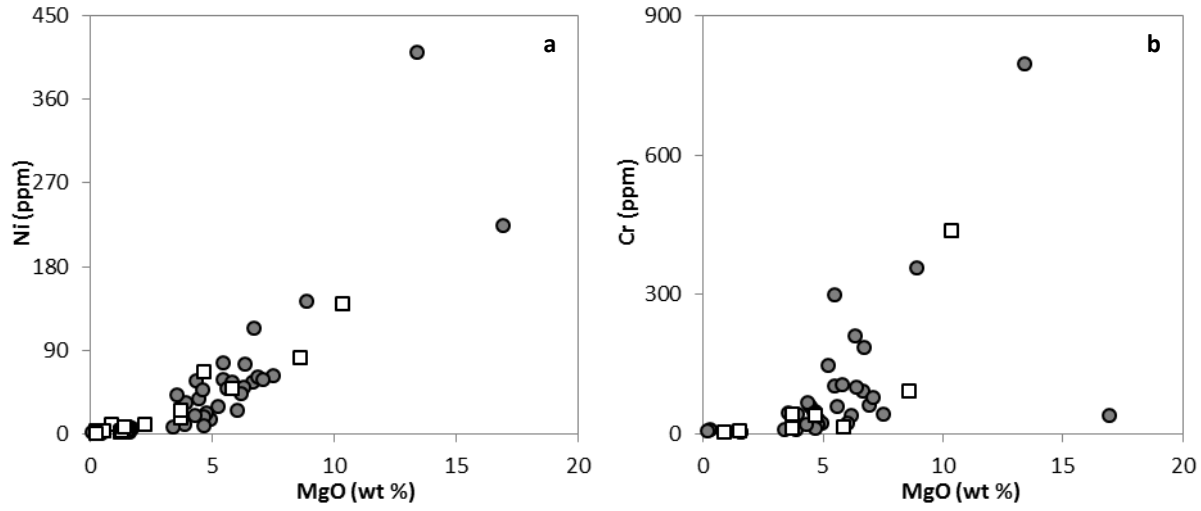

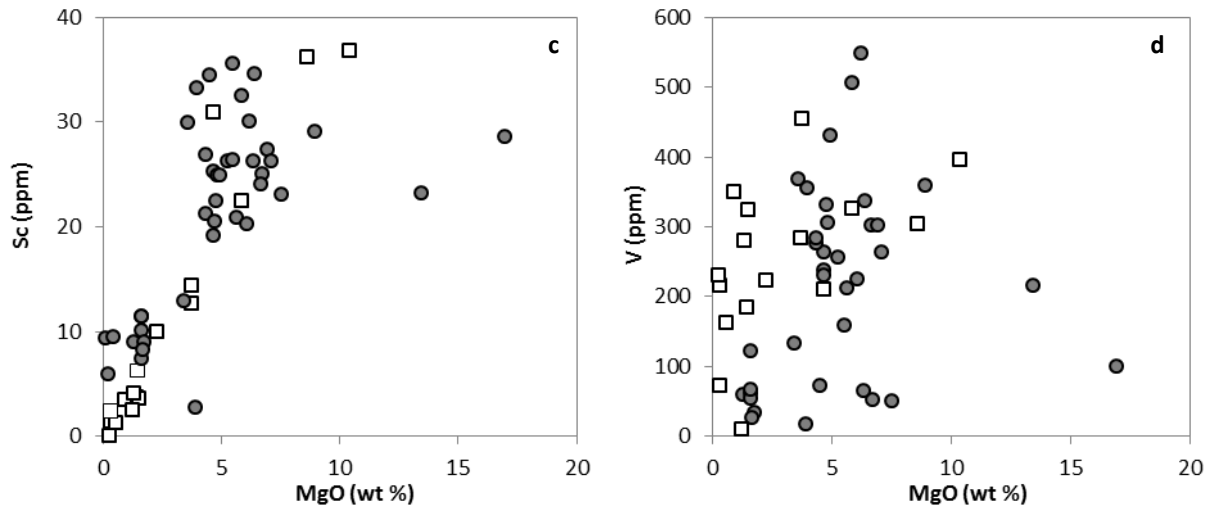

Fig. 6.3 a-d. Bivariate plots of compatible trace elements vs. MgO content.

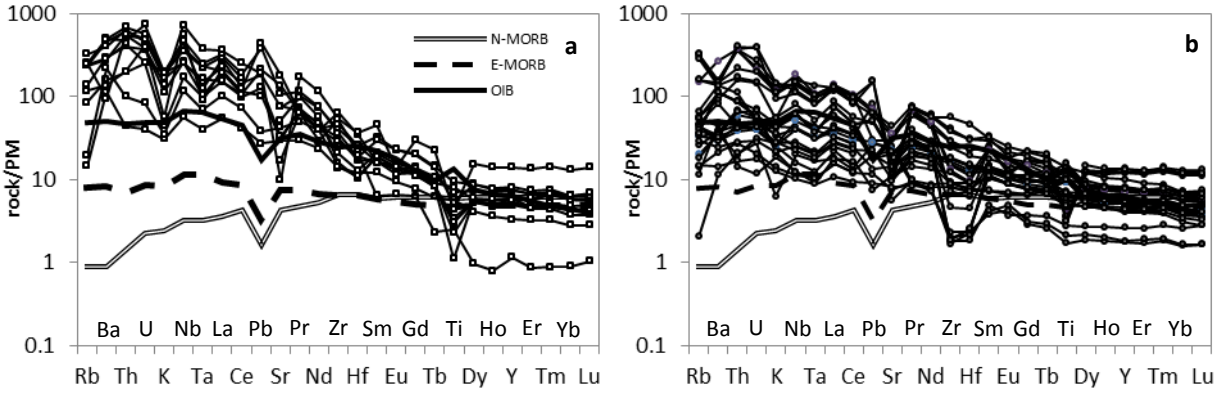

Fig. 6.4. Spider diagrams of trace elements content normalized to primitive mantle values. a) Alkaline samples; b) Tholeiitic samples; N-MORB, E-MORB and OIB patterns (Sun and McDonough, 1989) are shown.

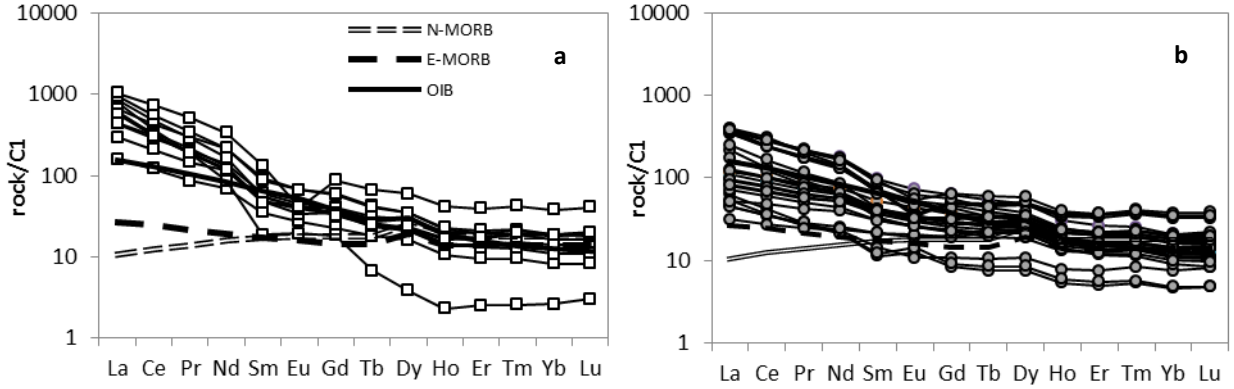

Fig. 6.5. REE element contents normalized to chondritic value. a) alkaline samples; b) tholeiitic samples.

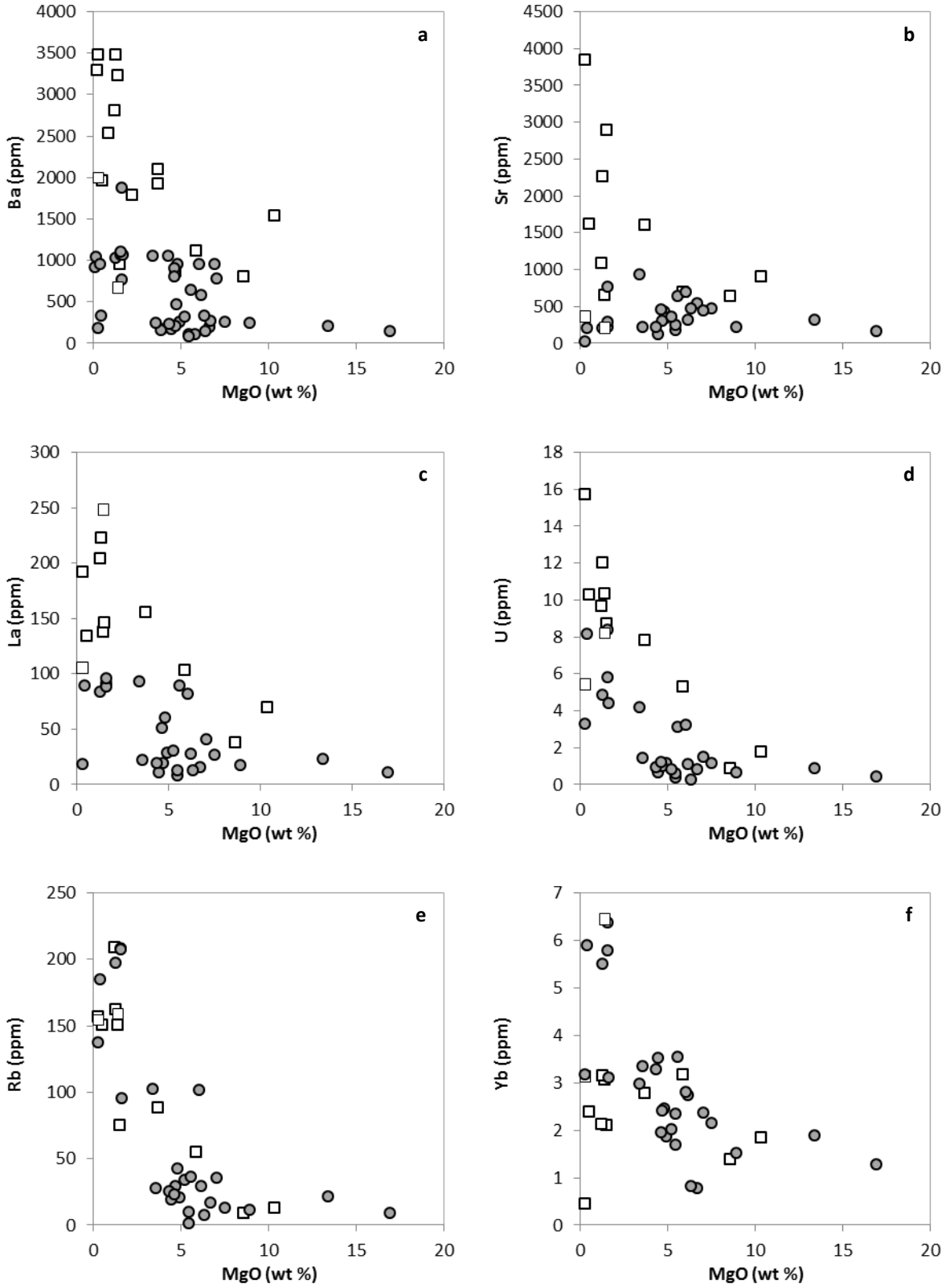

Fig. 6.6 a-f. Bivariate plots of incompatible trace elements vs. MgO contents.

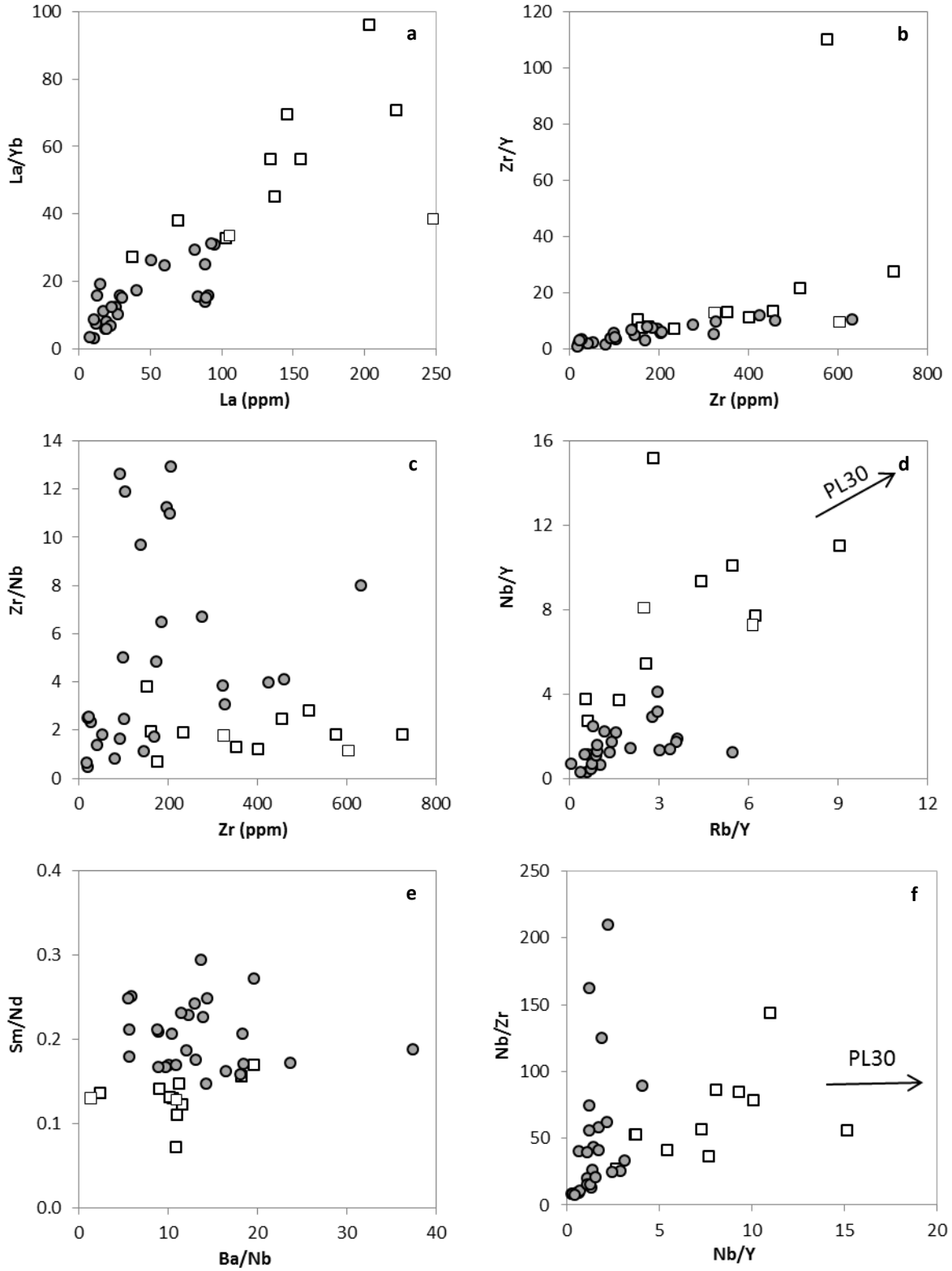

Fig.6.7a-f. Bivariate diagrams between incompatible elements ratios and incompatible elements (a-c); and between incompatible elements ratios (d-f).

Table 1. Major and trace element compositions.

	PL1	PL2	PL3	PL4	PL5	PL6	PL7	PL8	PL9	PL10
	alk	alk	alk	alk	alk	thol	thol	thol	thol	thol
SiO_2 (wt.%)	64.09	55.91	46.89	55.24	49.69	50.73	67.54	65.64	49.07	43.06
TiO_2	0.24	0.94	1.24	0.64	1.89	1.07	0.68	0.86	0.37	0.6
Al_2O_3	18.78	17.47	17.33	21.24	18.87	20.4	15.69	14.64	20.89	9.5
Fe_2O_3	3.49	10.39	7.48	4.31	9.17	9.15	3.88	5.32	5.82	21.98
MnO	0.11	0.3	0.12	0.11	0.17	0.14	0.1	0.13	0.1	0.34
MgO	0.28	1.42	8.62	1.41	3.72	4.64	1.28	1.6	6.72	16.96
CaO	1.96	4.22	15.46	3.62	8.63	9.08	2.44	3.45	14.28	5.75
Na_2O	4.8	4.48	1.49	6.72	3.45	2.89	3.98	3.72	1.79	0.94
K_2O	5.82	4.22	0.93	5.75	3.21	1.29	3.86	3.81	0.76	0.42
P_2O_5	0.1	0.39	0.22	0.46	0.82	0.41	0.34	0.61	0.07	0.35
Tot	99.67	99.74	99.78	99.5	99.62	99.8	99.79	99.78	99.87	99.9
LOI	2.41	1.87	1.20	1.21	0.94	0.07	0.61	0.56	0.76	-0.75
Rb (ppm)	154.19	159.13	9.22	150.70		23.04	196.94		16.41	9.16
Ba	1998.20	669.30	798.50	3226.80		798.00	1026.80		268.00	147.80
Th	36.70	47.09	3.76	51.74		7.37	30.73		3.87	2.33
U	5.43	8.19	0.85	10.35		1.20	4.82		0.83	0.43
Nb	182.79	517.47	40.75	277.80		43.97	102.07		11.31	8.04
Ta	6.76	15.47	1.66	9.65		1.51	4.03		0.50	0.43
La	105.41	248.03	37.67	137.70		50.96	83.79		15.04	10.84
Ce	187.85	447.77	73.63	203.64		82.28	150.28		25.80	21.19
Pb		35.06	5.08	18.97		9.49	19.00		4.86	2.13
Sr	364.34	206.96	632.75	656.29		457.42	208.90		533.06	157.85
Pr	17.78	48.49	8.20	20.12		8.85	17.02		2.71	2.55
Nd	55.06	156.38	32.11	60.90		31.49	61.19		9.97	10.59
Zr	324.24	603.49	153.74	354.02		20.94	81.64		26.11	20.04
Hf	6.03	11.42	3.79	5.27		0.79	1.92		0.72	0.57
Sm	7.06	20.34	5.42	7.43		4.95	10.34		1.71	2.19
Eu	2.54	2.35	1.59	2.32		1.49	2.12		0.72	0.62
Gd	6.61	17.91	4.65	7.24		4.74	9.91		1.70	2.18
Tb	0.91	2.47	0.67	0.91		0.72	1.70		0.28	0.39
Dy	4.38	11.23	3.03	4.21		3.49	8.83		1.39	2.01
Ho	0.94	2.32	0.60	0.90		0.74	1.91		0.30	0.44
Y	25.09	64.01	15.12	27.55		19.81	54.46		8.02	11.99
Er	2.86	6.54	1.57	2.75		2.07	5.50		0.82	1.23
Tm	0.50	1.07	0.24	0.48		0.34	0.93		0.14	0.21
Yb	3.14	6.44	1.38	3.05		1.96	5.50		0.78	1.28
Lu	0.51	1.04	0.21	0.48		0.30	0.83		0.12	0.21
Re (ppt)										
Os										22.86

Table 1. Continued.

	PL11	PL12	PL13	PL14	PL15	PL16	PL17	PL18	PL19	PL20
	thol	thol	thol	thol	thol	alk	thol	thol	thol	thol
SiO_2 (wt.%)	66.78	52.96	54.86	55.52	78.55	45.74	68.87	50.46	74.3	49.41
TiO_2	0.76	1.28	2.21	2.09	0.07	1.51	0.61	2.02	0.38	0.46
Al_2O_3	14.69	15.89	14.98	16.9	11.43	15.24	12.97	17.71	12.23	21.12
Fe_2O_3	4.61	11.44	11.44	11.71	1.11	14.75	5.01	9.68	2.59	5.38
MnO	0.11	0.17	0.14	0.13	0.01	0.27	0.11	0.14	0.05	0.08
MgO	1.6	4.81	4.94	6.66	0.29	5.86	1.73	5.25	0.2	6.34
CaO	2.66	7.93	8.22	3.62	0.67	11.85	2.41	9.98	1.19	14.3
Na_2O	3.99	3.13	1.79	2.42	2.97	2.57	3.26	2.87	3.66	2.11
K_2O	4.24	1.67	1.01	0.58	4.81	1.35	4.54	1.32	5.14	0.56
P_2O_5	0.34	0.49	0.26	0.2	0.02	0.57	0.28	0.41	0.06	0.1
Tot	99.78	99.77	99.85	99.83	99.93	99.71	99.79	99.84	99.8	99.86
LOI	1.16	2.30	1.58	0.44	0.90	3.45	1.22	0.26	0.81	0.83
Rb (ppm)	207.73	42.05	20.93		137.60	54.79		33.62		7.30
Ba	1067.30	955.30	256.50		178.90	1107.70		319.70		332.70
Th	32.29	9.59	5.85		14.84	16.83		4.36		1.22
U	5.77	1.07	1.16		3.29	5.30		0.83		0.25
Nb	98.34	57.74	28.72		30.40	122.84		30.54		8.87
Ta	3.91	2.13	1.28		1.62	4.12		1.31		0.38
La	90.71	59.85	28.81		18.29	103.48		30.27		12.70
Ce	151.38	100.74	60.35		37.44	176.64		62.59		22.67
Pb	24.00	9.05	15.39			23.96				3.74
Sr	215.62	425.29	335.42		25.82	698.76		349.44		461.37
Pr	17.61	10.92	7.34		4.96	18.79		7.58		2.54
Nd	63.59	39.63	30.61		19.39	65.34		31.54		9.89
Zr	169.13	92.89	51.96		41.06	233.85		18.85		22.61
Hf	3.53	2.21	1.38		1.59	3.96		0.70		0.67
Sm	10.72	6.42	6.39		4.86	9.21		6.49		1.86
Eu	2.12	1.94	1.91		0.13	2.57		2.02		0.82
Gd	10.25	6.13	6.01		4.65	8.35		6.08		1.85
Tb	1.76	0.95	1.02		0.96	1.17		1.02		0.31
Dy	9.14	4.61	4.76		5.09	5.42		4.81		1.59
Ho	1.98	0.98	0.92		1.10	1.15		0.95		0.33
Y	57.65	26.90	24.21		25.09	33.09		24.80		8.25
Er	5.74	2.66	2.29		3.13	3.25		2.42		0.91
Tm	0.96	0.42	0.34		0.53	0.53		0.37		0.14
Yb	5.78	2.44	1.85		3.17	3.17		2.01		0.81
Lu	0.87	0.37	0.26		0.45	0.49		0.29		0.12
Re (ppt)										
Os										

Table 1. Continued.

	PL23	PL24A	PL24B	PL26	PL27A	PL27B	PL28	PL30	PL31	PL32
	thol	thol	thol	thol	alk	alk	thol	alk	alk	thol
SiO_2 (wt.%)	69.17	53.44	52.68	50.02	51.8	52.39	48.86	55.86	56.54	51.72
TiO_2	0.29	1.1	1.12	1.45	0.82	0.74	2.98	0.54	0.5	2.66
Al_2O_3	13.63	16.56	15.12	15.79	16.06	17.71	13.76	18.38	18.74	15.33
Fe_2O_3	1.78	12.42	12.99	12.83	8.13	7.74	12.73	6.11	5.8	11.38
MnO	0.15	0.16	0.18	0.19	0.26	0.31	0.2	0.27	0.25	0.16
MgO	0.68	3.97	4.5	5.5	0.9	1.51	5.61	0.32	0.24	4.79
CaO	2.83	9.35	10.22	11.44	11.56	10.98	9.73	3	2.69	8.43
Na_2O	0.16	2.13	2.29	2.17	6.21	6.02	3.12	8.62	8.24	3.14
K_2O	11.12	0.58	0.64	0.38	3.21	1.7	1.64	5.94	6.11	1.49
P_2O_5	0.01	0.18	0.18	0.16	0.34	0.34	1.13	0.07	0.06	0.73
Tot	99.82	99.89	99.92	99.93	99.29	99.44	99.76	99.11	99.17	99.83
LOI	4.15	2.97	2.08	1.55	10.53	11.35	3.66	5.03	4.39	5.40
Rb (ppm)			18.63	9.44		75.39	36.33	156.63		
Ba			171.20	99.80		951.50	646.30	3479.50		
Th			2.41	1.43		17.25	13.66	40.35		
U			0.62	0.37		8.68	3.10	15.69		
Nb			8.71	7.29		404.36	113.15	320.55		
Ta			0.42	0.36		3.70	5.57	5.14		
La			10.70	7.44		146.00	88.73	191.51		
Ce			21.62	16.58		198.31	176.57	224.20		
Pb				1.67		39.60	5.49	82.46		
Sr			118.83	170.94		2890.11	632.53	3848.64		
Pr			2.72	2.31		17.54	20.68	17.38		
Nd			11.85	11.15		53.67	82.47	39.77		
Zr			103.40	91.93		725.92	461.10	577.82		
Hf			2.44	2.25		10.89	9.54	6.71		
Sm			3.22	3.27		7.28	14.73	2.84		
Eu			1.10	1.18		1.94	4.19	1.11		
Gd			4.00	3.89		7.19	12.98	3.78		
Tb			0.88	0.80		0.93	2.01	0.25		
Dy			5.16	4.35		4.06	8.97	0.71		
Ho			1.19	0.93		0.81	1.71	0.13		
Y			32.98	24.66		26.64	45.98	5.25		
Er			3.40	2.50		2.22	4.32	0.42		
Tm			0.59	0.41		0.35	0.64	0.06		
Yb			3.51	2.34		2.10	3.54	0.44		
Lu			0.55	0.35		0.32	0.51	0.08		
Re (ppt)										
Os				23.48						

Table 1. Continued.

	PL33	PL34	PL35	PL36	PL37	PL38	PL39	PL41	PL42	PL43
	alk	thol	alk	alk	thol	thol	thol	thol	thol	thol
SiO_2 (wt.%)	49.65	73.79	47.55	50.78	48.26	49.64	50.29	64.96	66.43	52.56
TiO_2	2.61	0.12	2.47	2.05	2.36	3.42	2.30	0.80	0.81	1.28
Al_2O_3	16.13	11.26	13.74	17.40	15.65	13.55	14.46	12.81	14.10	16.87
Fe_2O_3	9.76	1.4	13.02	8.08	13.03	14.44	14.23	8.04	6.45	10.98
MnO	0.28	0.08	0.18	0.17	0.17	0.22	0.21	0.17	0.14	0.15
MgO	2.26	3.89	4.68	3.73	7.54	6.20	5.83	1.61	1.65	4.67
CaO	8.06	5.23	11.95	8.47	9.13	7.73	9.74	3.16	3.38	7.89
Na_2O	8.14	3.84	4.24	4.53	2.61	2.96	2.25	3.52	2.74	2.40
K_2O	1.57	0.28	1.73	3.43	0.76	1.26	0.25	4.40	3.82	2.50
P_2O_5	0.87	0.06	0.23	0.87	0.37	0.39	0.32	0.29	0.31	0.48
Tot	99.33	99.95	99.79	99.51	99.88	99.81	99.88	99.76	99.83	99.78
LOI	6.37	4.83	10.08	4.28	2.72	2.08	2.06	2.45	3.72	2.23
Rb (ppm)				88.00	12.86	29.38		207.10		
Ba				2100.40	251.30	577.50		1106.40		
Th				34.35	5.12	3.88		32.11		
U				7.80	1.12	1.06		8.35		
Nb				187.06	28.66	41.31		84.42		
Ta				6.08	1.32	1.78		3.46		
La				155.76	26.13	27.74		88.36		
Ce				266.38	55.20	63.03		148.95		
Pb				34.06	5.24	3.66		28.67		
Sr				1604.77	470.72	310.26		283.00		
Pr				28.00	6.80	7.96		16.46		
Nd				98.56	28.65	34.89		60.00		
Zr				456.42	185.86	275.72		323.83		
Hf				8.03	4.05	5.99		7.14		
Sm				14.40	6.05	7.86		10.48		
Eu				3.85	1.93	2.50		1.97		
Gd				12.15	5.79	7.57		10.19		
Tb				1.57	0.99	1.33		1.81		
Dy				6.49	4.80	6.39		9.54		
Ho				1.22	0.96	1.26		2.08		
Y				34.39	26.01	32.15		61.64		
Er				3.20	2.48	3.24		6.12		
Tm				0.49	0.38	0.49		1.04		
Yb				2.77	2.15	2.74		6.37		
Lu				0.41	0.32	0.40		0.97		
Re (ppt)										
Os										

Table 1. Continued.

	PL44	PL45	PL46	PL47	PL48	PL49	PL50	PL51	PL52	PL53
	thol	thol	thol	thol	alk	thol	thol	thol	thol	thol
SiO_2 (wt.%)	49.33	49.05	48.73	51.65	56.57	59.35	54.31	74.41	57.15	51.29
TiO_2	1.55	1.02	0.96	1.13	0.49	0.93	1.53	0.31	2.41	2.75
Al_2O_3	16.19	17.29	17.14	18.54	18.12	18.52	16.66	14.04	13.35	14.60
Fe_2O_3	11.80	10.66	10.66	10.28	6.65	6.36	10.00	1.77	9.71	11.13
MnO	0.17	0.15	0.17	0.15	0.21	0.11	0.14	0.09	0.17	0.13
MgO	8.92	6.92	7.08	4.32	1.24	1.62	4.69	0.49	3.40	6.05
CaO	9.38	9.87	10.79	7.66	3.83	5.36	8.58	0.09	6.46	7.36
Na_2O	1.49	2.36	2.45	3.65	6.26	3.33	2.58	3.05	3.06	2.60
K_2O	0.82	2.08	1.41	1.97	5.68	3.54	1.08	5.54	3.42	3.22
P_2O_5	0.20	0.38	0.39	0.41	0.39	0.52	0.32	0.05	0.57	0.61
Tot	99.85	99.78	99.78	99.76	99.44	99.64	99.89	99.84	99.70	99.74
LOI	4.28	3.52	2.93	2.61	2.35	1.36	3.15	1.83	2.33	2.40
Rb (ppm)	11.49		35.46		208.92	95.43	28.93		101.90	101.42
Ba	247.60		779.40		2807.30	1869.80	202.00		1045.00	957.30
Th	1.68		7.51		54.97	32.20	3.86		18.90	14.68
U	0.66		1.48		9.68	4.38	0.98		4.19	3.20
Nb	20.11		42.17		253.94	130.66	17.61		106.95	107.17
Ta	0.89		1.65		9.16	4.41	0.83		4.38	4.16
La	16.93		40.79		203.85	95.35	19.51		92.85	81.58
Ce	36.68		74.60		292.15	188.42	43.00		177.85	146.37
Pb			3.32			13.03	2.48		11.93	11.25
Sr	216.76		440.52		1090.48	755.80	300.09		930.41	696.68
Pr	4.70		7.90		27.16	19.20	5.59		21.04	16.73
Nd	20.54		29.12		77.05	67.04	24.57		79.85	66.03
Zr	100.20		102.68		177.01	146.94	197.96		425.09	326.51
Hf	2.79		2.33		3.22	2.92	4.39		9.30	7.06
Sm	4.68		4.96		8.49	9.87	5.66		13.28	11.00
Eu	1.50		1.48		2.36	2.71	1.76		3.63	3.01
Gd	4.59		4.87		8.15	8.92	5.56		11.32	9.67
Tb	0.82		0.81		0.93	1.27	1.01		1.65	1.45
Dy	3.98		4.14		3.87	5.92	5.03		7.16	6.41
Ho	0.78		0.90		0.78	1.21	1.02		1.37	1.24
Y	18.31		24.78		23.02	32.16	27.86		36.70	34.24
Er	1.94		2.47		2.22	3.35	2.69		3.56	3.25
Tm	0.29		0.40		0.35	0.53	0.42		0.54	0.50
Yb	1.52		2.36		2.13	3.09	2.42		2.98	2.79
Lu	0.21		0.36		0.31	0.45	0.36		0.44	0.41
Re (ppt)										
Os										

6.3. Isotopic compositions

6.3.1. Sr-Nd-Pb isotopic compositions

Sr, Nd and Pb isotopic analyses were performed on 30 selected samples and the results are shown in Table 2.

On ε_{Ndt} vs. $^{87}Sr/^{86}Sr_t$ plot, the most straightforward feature is that the samples define two different arrays with negative slope both departing from a similar composition (ε_{Ndt} ca. +3 and $^{87}Sr/^{86}Sr_t$ ca. 0.705): one trend points towards low ε_{Ndt} and relatively low $^{87}Sr/^{86}Sr_t$ (-12.96 and 0.71061, respectively), the other one towards high $^{87}Sr/^{86}Sr_t$ (0.72788) and low ε_{Ndt} (-12.50). Tholeiitic samples belong to both trends and show the widest range of compositions, $^{87}Sr/^{86}Sr_t$ varying from 0.70524 to 0.72788, and ε_{Ndt} from +2.81 to -12.96. Alkaline samples (including evolved ones, e.g. phonolites) present quite homogeneous isotopic compositions ($^{87}Sr/^{86}Sr_t$ 0.70626- 0.70762, ε_{Ndt} -3.1 to -7.3).

On $^{206}Pb/^{204}Pb_t$ vs. $^{207}Pb/^{204}Pb_t$ and vs. $^{208}Pb/^{204}Pb_t$ diagrams, all the samples plot well above the North Hemisphere Reference Line, and span a wide range of compositions (e.g., $^{206}Pb/^{204}Pb_t$ 17.77-21.04), tholeiitic samples result enriched in Pb isotopic compositions ($^{206}Pb/^{204}Pb_t$ 17.6-21.04, $^{207}Pb/^{204}Pb_t$ 15.64-15.96, $^{208}Pb/^{204}Pb_t$ 39.3-42.7); alkaline samples have the lowest isotopic compositions .

The same trends as in the Sr-Nd isotopic diagram can be recognized in Sr vs Pb and Nd vs Pb isotopic space, although less well defined. The common origin of the two trends is at $^{206}Pb/^{204}Pb_t$ of about 19.0, and $^{87}Sr/^{86}Sr_t$ ca. 0.705, and ε_{Ndt} of 3.5, from which the trends one and two show slightly decreasing and increasing Pb isotopic compositions, respectively.

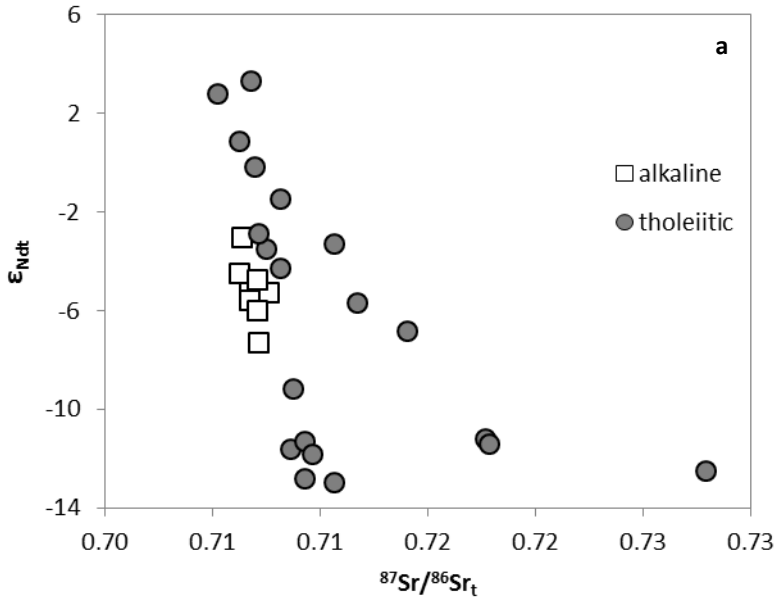

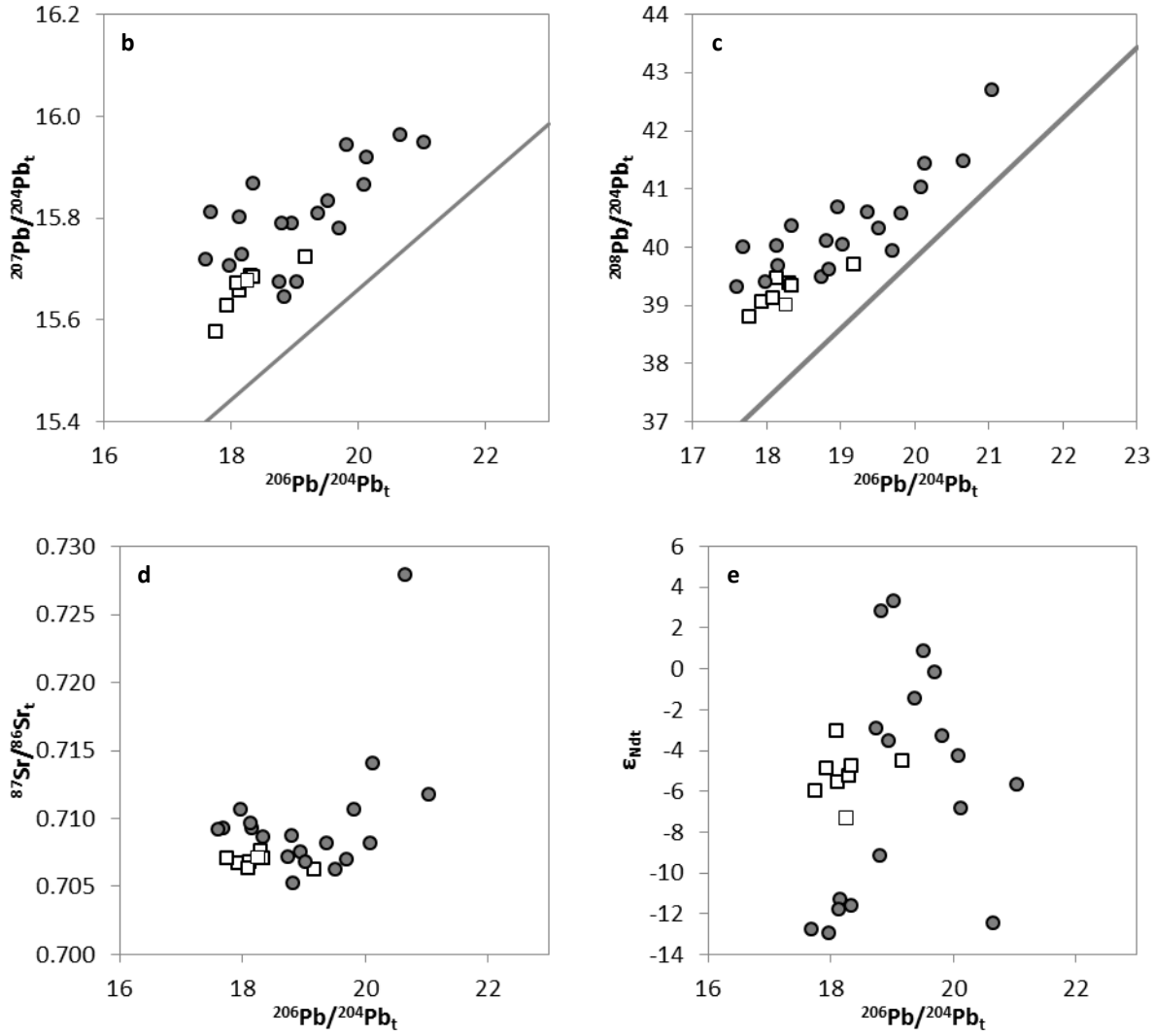

Fig. 6.8 a-e. Initial isotopic compositions. The grey line in $^{206}Pb/^{204}Pb_t$ vs. $^{207}Pb/^{204}Pb_t$ and vs. $^{208}Pb/^{204}Pb_t$ diagrams is North Hemisphere Reference Line (NHRL, from Zindler and Hart, 1986).

6.3.2. Os isotopic compositions

Os isotopic compositions have been determined at Curtin University (Perth) on 10 samples, which have been selected among the 30 samples previously analyzed for other isotopes, taking those with higher MgO content and lower $^{87}Sr/^{86}Sr_t$, thus belonging to the trend1.

The most depleted samples show values of 0.1584 and 0.1648, whereas the most enriched one (a gabbro from Phenai Mata) has a value of 0.2457; all of them have very similar Os content (from 22.9 to 27.7 ppt)

Table 2. Isotopic compositions.

	PL2	PL3	PL4	PL6	PL7	PL9	PL10	PL11	PL12	PL13
$^{87}Sr/^{86}Sr_m$	0.70919	0.70672	0.70734	0.70938	0.72020	0.70971	0.71075	0.72042	0.70884	0.71080
$^{87}Sr/^{86}Sr_t$	0.70713	0.70670	0.70674	0.70927	0.71766	0.70965	0.71061	0.71783	0.70860	0.71066
$^{143}Nd/^{144}Nd_m$	0.51221	0.51235	0.51230	0.51194	0.51202	0.51199	0.51194	0.51201	0.51200	0.51249
$^{143}Nd/^{144}Nd_t$	0.51218	0.51230	0.51227	0.51190	0.51198	0.51195	0.51189	0.51197	0.51196	0.51239
ε_{Ndt}	-7.31	-4.89	-5.59	-12.81	-11.18	-11.82	-12.96	-11.39	-11.61	-3.28
$^{206}Pb/^{204}Pb_m$	18.08	17.93	18.13	17.69	20.08	18.14	17.98	20.07	18.35	19.82
$^{206}Pb/^{204}Pb_t$	17.92	17.82	17.77	17.61	19.91	18.02	17.85	19.90	18.27	19.77
$^{207}Pb/^{204}Pb_m$	15.67	15.63	15.66	15.81	15.87	15.80	15.71	15.88	15.87	15.94
$^{207}Pb/^{204}Pb_t$	15.66	15.62	15.64	15.81	15.87	15.80	15.70	15.87	15.86	15.94
$^{208}Pb/^{204}Pb_m$	39.34	39.06	39.46	40.00	40.91	40.02	39.40	40.93	40.35	40.59
$^{208}Pb/^{204}Pb_t$	39.05	38.90	38.88	39.84	40.55	39.85	39.17	40.62	40.12	40.50
$^{187}Os/^{188}Os_m$							0.2865			
$^{187}Os/^{188}Os_t$							0.2457			

Table 2. Continued.

	PL16	PL20	PL26	PL27B	PL28	PL30	PL36	PL37	PL38	PL41
$^{87}Sr/^{86}Sr_m$	0.70977	0.70919	0.70638	0.70631	0.70537	0.70643	0.70775	0.70817	0.70701	0.72984
$^{87}Sr/^{86}Sr_t$	0.70958	0.70917	0.70625	0.70626	0.70524	0.70634	0.70762	0.70812	0.70677	0.72788
$^{143}Nd/^{144}Nd_m$	0.512378		0.51267	0.51236	0.51274	0.51242	0.51232	0.51253	0.51278	0.51196
$^{143}Nd/^{144}Nd_t$	0.51233		0.51260	0.51232	0.51270	0.51240	0.51228	0.51248	0.51272	0.51191
ε_{Ndt}	-4.32		0.85	-4.50	2.81	-3.06	-5.25	-1.47	3.30	-12.50
$^{206}Pb/^{204}Pb_m$		17.60	19.51	19.17	18.84	18.09	18.30	19.37	19.02	20.66
$^{206}Pb/^{204}Pb_t$		17.56	19.36	19.03	18.47	17.97	18.15	19.23	18.83	20.46
$^{207}Pb/^{204}Pb_m$		15.72	15.83	15.72	15.64	15.67	15.69	15.81	15.67	15.96
$^{207}Pb/^{204}Pb_t$		15.72	15.83	15.71	15.63	15.67	15.68	15.80	15.66	15.95
$^{208}Pb/^{204}Pb_m$		39.30	40.31	39.70	39.62	39.12	39.37	40.59	40.03	41.48
$^{208}Pb/^{204}Pb_t$		39.23	40.12	39.61	39.08	39.02	39.15	40.37	39.80	41.22
$^{187}Os/^{188}Os_m$			0.2215							
$^{187}Os/^{188}Os_t$			0.1648							

Table 2. Continued.

	PL46	PL49	PL50	PL52	PL53	PL56	PL58	PL59	PL60	PL63
$^{87}Sr/^{86}Sr_m$	0.70894	0.70957	0.71195	0.70776	0.70852	0.70725	0.70701	0.70711	0.70741	0.71649
$^{87}Sr/^{86}Sr_t$	0.70874	0.70925	0.71171	0.70749	0.70815	0.70708	0.70694	0.70709	0.70711	0.71403
$^{143}Nd/^{144}Nd_m$	0.51213	0.51201	0.51232	0.51242	0.51238	0.51234	0.51261	0.51229	0.51247	0.51225
$^{143}Nd/^{144}Nd_t$	0.51208	0.51197	0.51226	0.51237	0.51233	0.51231	0.51254	0.51225	0.51240	0.51220
ε_{Ndt}	-9.18	-11.31	-5.70	-3.52	-4.30	-4.74	-0.19	-6.00	-2.90	-6.86
$^{206}Pb/^{204}Pb_m$	18.81	18.16	21.04	18.96	20.09	18.34	19.70	17.77	18.75	20.13
$^{206}Pb/^{204}Pb_t$	18.51	17.94	20.76	18.72	19.90	18.23	19.41	17.60	18.60	19.94
$^{207}Pb/^{204}Pb_m$	15.79	15.73	15.95	15.79	15.87	15.68	15.78	15.58	15.67	15.92
$^{207}Pb/^{204}Pb_t$	15.77	15.72	15.93	15.78	15.86	15.68	15.76	15.57	15.67	15.91
$^{208}Pb/^{204}Pb_m$	40.09	39.67	42.70	40.69	41.03	39.33	39.93	38.79	39.49	41.43
$^{208}Pb/^{204}Pb_t$	39.60	39.13	42.33	40.34	40.74	39.15	39.65	38.54	39.31	41.16
$^{187}Os/^{188}Os_m$									0.40	
$^{187}Os/^{188}Os_t$									0.16	

6.4. Comparison with other Deccan rocks

The trace elements and isotopic compositions of the tholeiitic samples have been compared with those of the most studied Deccan lava sequence of the Western Ghats (lower and upper formations) in order to evaluate similarities and differences between them, and to establish whether they may have a similar mantle source or have undergone similar differentiation processes. Moreover, alkaline rocks from different parts of the province have been considered in order to compare them with the Narmada alkaline samples, and following the criteria of Simonetti et al. (1998), only alkaline samples with Mg#>50 have been used (as our samples PL3, PL36, PL59). The considered alkaline rocks are from the alkaline complexes of Barmer and Mundwara, in the northernmost part of the province, Bhuj (Kutch) and Amba Dongar (Chotta Udaipur region; Simonetti et al., 1998); basanites from Kutch (Karmalkar et al., 2005), and alkaline rocks from the Mumbai area (Melluso et al., 2002).

6.4.1. Trace elements – tholeiitic samples

The least evolved Narmada samples have trace element contents and patterns comparable to those of Deccan formations, for example, negative Sr anomalies. Some difference relative to the Western Ghat formations can be observed in terms of Zr/Nb ratios (generally lower in the Narmada). Narmada tholeiities are also less enriched in La/Nb than the strongly contaminated Bushe formation.

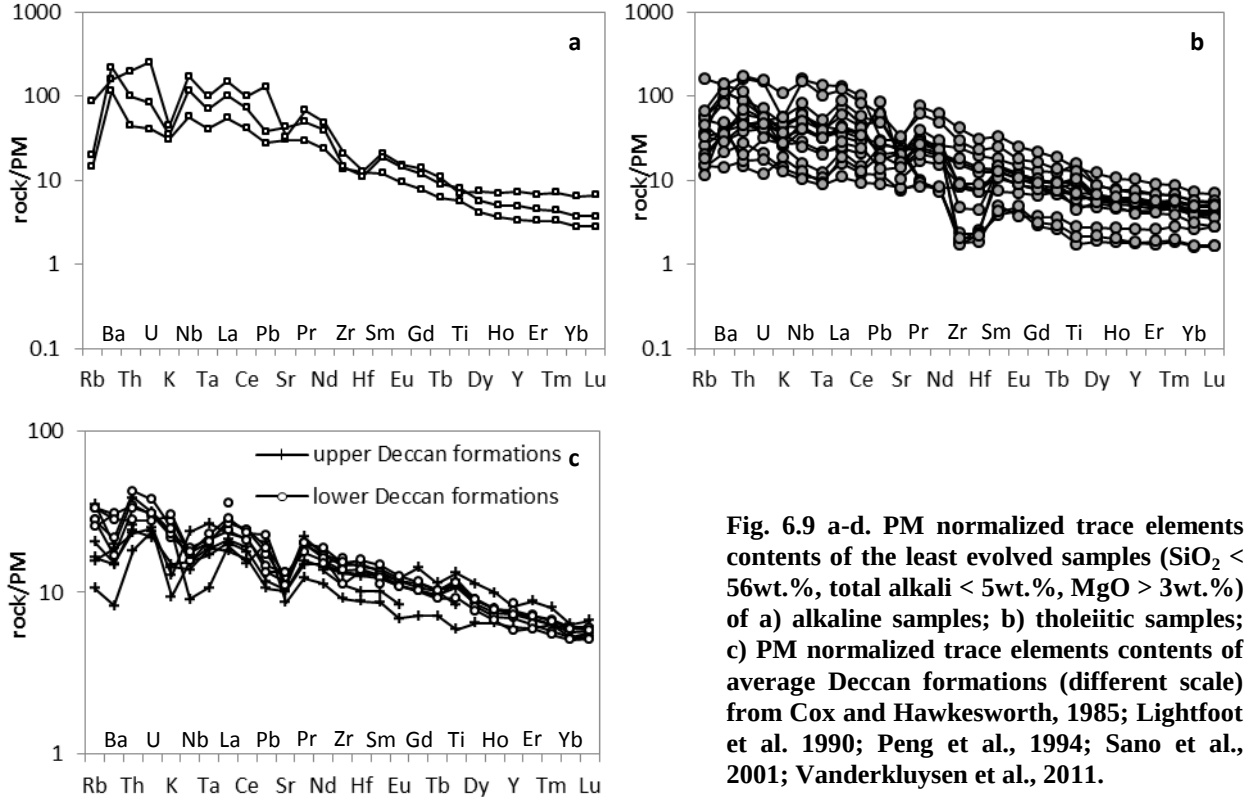

Fig. 6.9 a-d. PM normalized trace elements contents of the least evolved samples (SiO_2 < 56wt.%, total alkali < 5wt.%, MgO > 3wt.%) of a) alkaline samples; b) tholeiitic samples; c) PM normalized trace elements contents of average Deccan formations (different scale) from Cox and Hawkesworth, 1985; Lightfoot et al. 1990; Peng et al., 1994; Sano et al., 2001; Vanderkluysen et al., 2011.

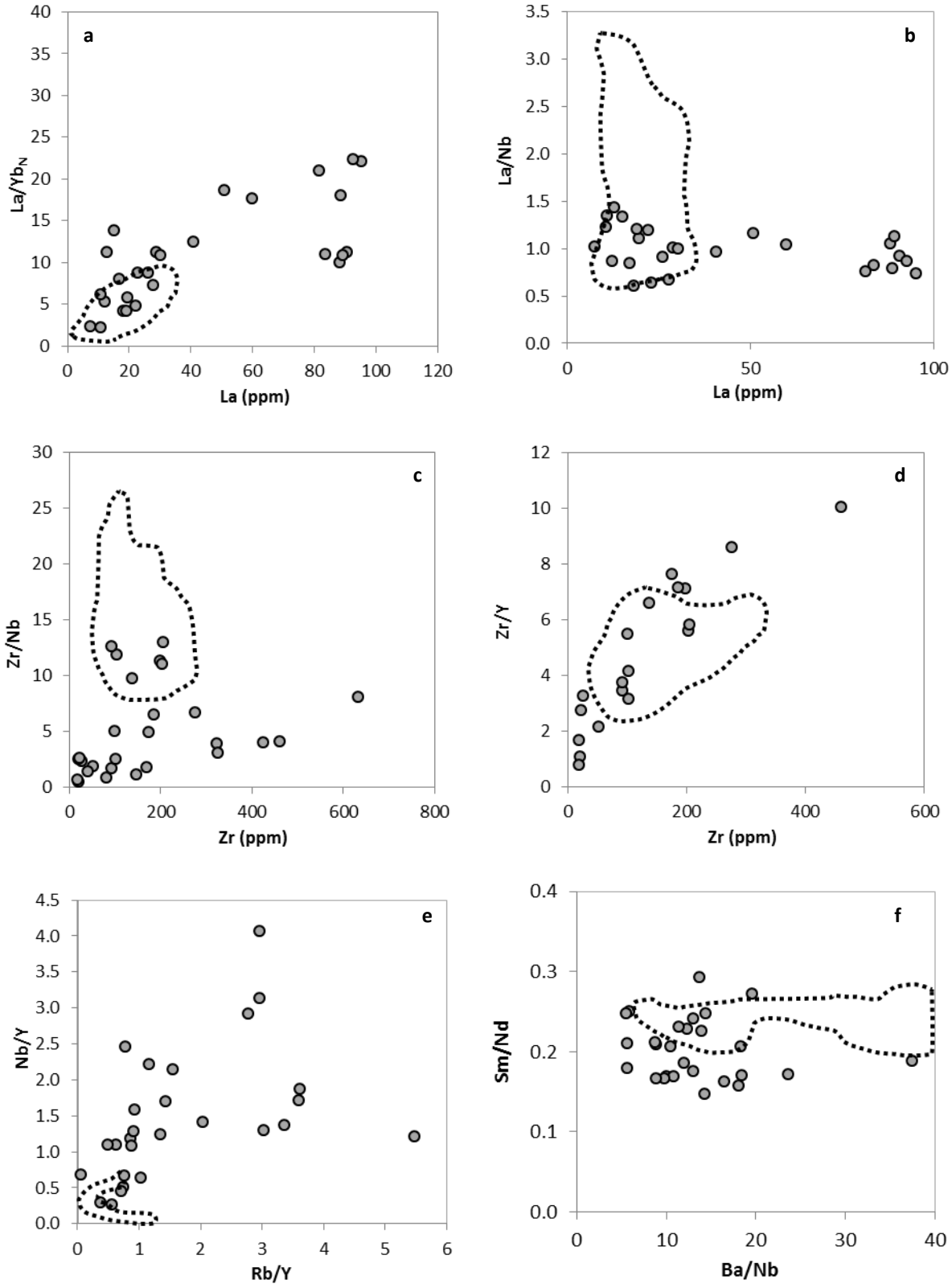

Fig. 6.10 a-f. Bivariate diagrams for incompatible element ratios vs. incompatible elements and between incompatible element ratios of the tholeiitic samples compared to those of the Western Ghats lava formations. Due to the general overlap, no distinctions have been made for the Deccan formations, and they are indicated by the dashed-line region. See text for explanation.

6.4.2. Isotopes – tholeiitic samples

The isotopic compositions of the analyzed samples are in general similar to those of the Western Ghats lava formations. In particular, considering Sr and Nd isotopic compositions, the most depleted tholeiitic samples (e.g., PL28) fall between the fields of the more depleted formations of the upper Deccan lava sequence (Ambenali and Panhala fm), and slightly more enriched formations such as Poladpur and Bimashankar. Samples pointing to low ε_{Ndt} at low $^{87}Sr/^{86}Sr_t$ (TREND 1) have compositions similar to those of Thakurvadi and Kandhala formations; whereas samples trending to high $^{87}Sr/^{86}Sr_t$ (TREND 2) are similar to those of Igatpuri-Jawhar and Bushe formations, yet at higher ε_{Ndt} (fig. 6.11 a).

Despite having $^{206}Pb/^{204}Pb_t$ comparable to those of Western Ghats formations, $^{207}Pb/^{204}Pb_t$ and $^{208}Pb/^{204}Pb_t$ of Narmada samples are distinctly higher (at equal $^{206}Pb/^{204}Pb_t$). In particular, for values of $^{206}Pb/^{204}Pb_t$ between 17.5 and 18.9, the samples result to be enriched both in $^{207}Pb/^{204}Pb_t$ and in $^{208}Pb/^{204}Pb_t$, whereas for $^{206}Pb/^{204}Pb_t > 18.9$, they follow the trend defined by Deccan lava flows (fig. X d and e).

The most depleted samples in Os isotopic compostion, have $^{187}Os/^{188}O_t$ ratio comparable to the most enriched lava flows analyzed in Deccan province, which reach maximum values of 0.158 (Allègre et el., 1999).

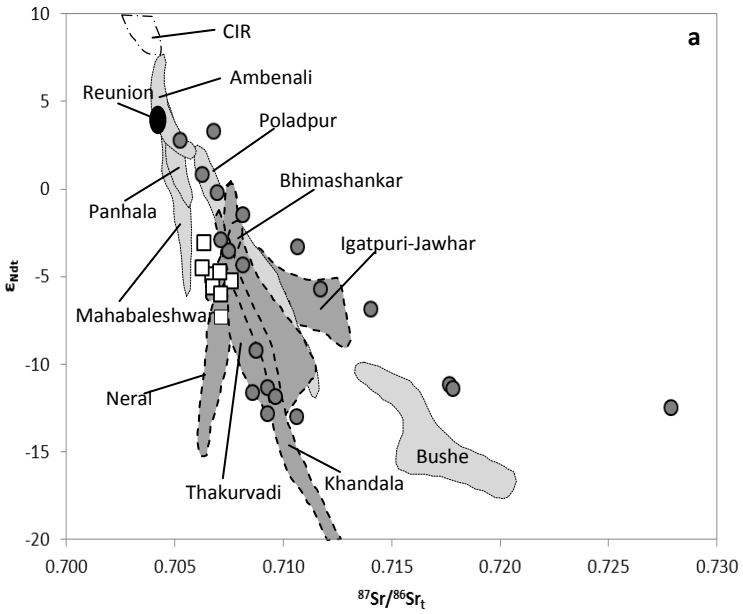

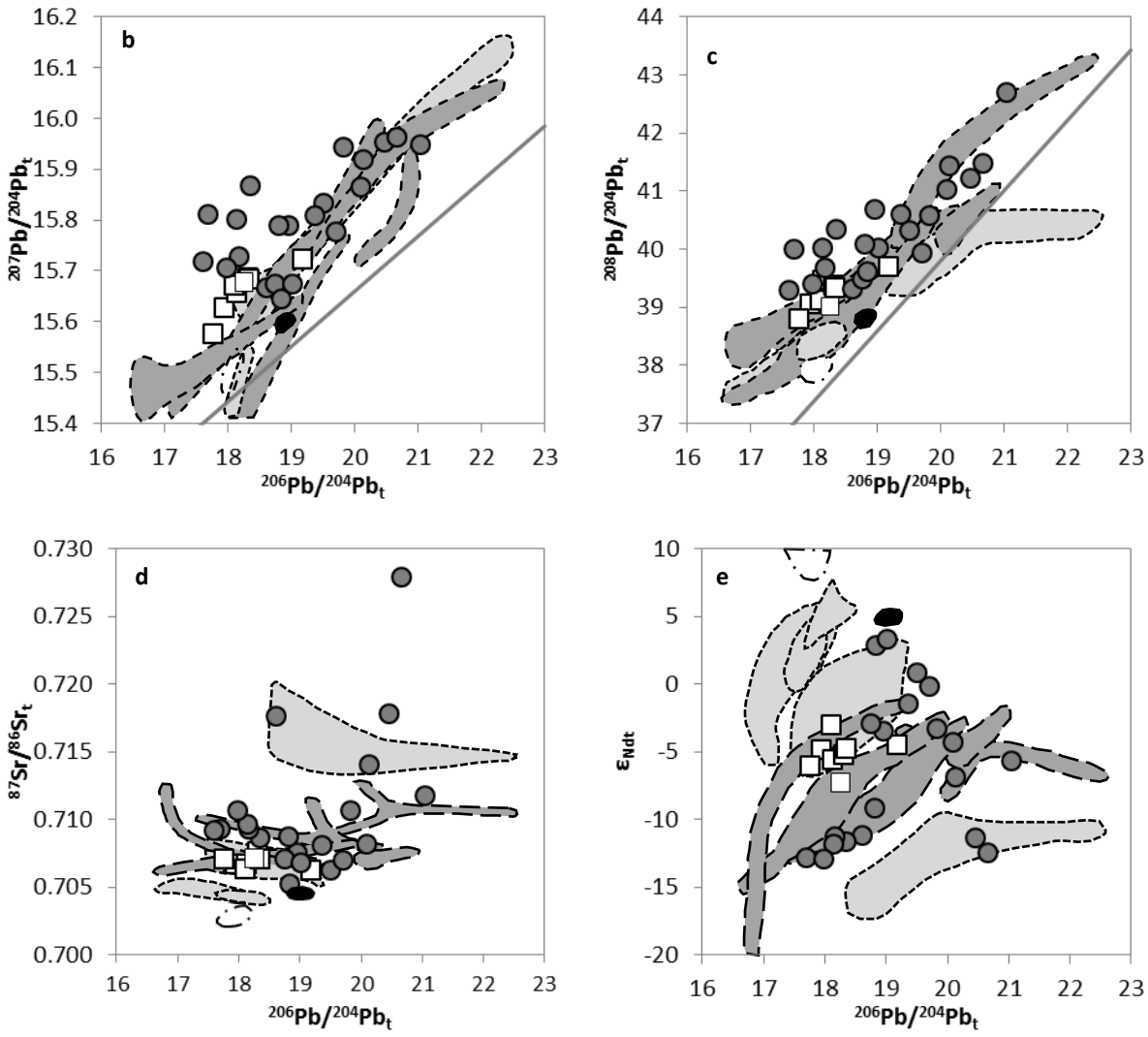

Fig. 6.11 a-e. Comparison between isotopic compositions of Narmada samples and Deccan lava formations. Dark grey fields: lower formations; light grey field: upper formations; black field: Reunion Island; white field: CIR (Central Indian Ridge). Deccan fields from Peng et al. (1994) and Lightfoot (1985), Reunion field from Fisk et al. (1988), CIR field from Mahoney et al. (1989.)

6.4.3. Trace elements – alkaline samples

The degree of enrichment and slope of trace element patterns of Narmada alkaline rocks and those of other areas in the Deccan Province is similar. They share the Ba spike, and negative K and Pb anomalies, though the latter in less marked in the Narmada rocks. On average they have lower Ti content with no positive anomaly. The La/Yb_N ratio of Narmada alkaline rocks (19-40) is comparable to that of Kutch basanites (12-30). High Nb/La (ca. 1.2) and Zr/Hf displayed by Narmada alkaline rocks and and Kutch basanites may be indicative of carbonatite metasomatism (Karmalkar et al., 2005).

Major variability in trace element contents is displayed by alkaline rocks from the Mumbai region, with the lamprophyre samples reaching the highest degree of enrichment, which is also

shown by the Narmada lamprophyre PL36, having a very similar pattern. On the contrary Mumbai melanephelinites and nephelineites are characterized by distinctively lower Nb, La, Ce, Nd, Zr, and Ti.

Other feature shared by all the alkaline rocks, are the high values of Ce/Pb and Rb/Sr ratios, which indicate that crustal contamination did not significantly affect these rocks.

Other alkaline rocks in India, though not associated with the Deccan Volcanic Province, and they are associated with carbonatitic complexes, such as in Tamil Nadu region (800Ma, Schleicher et al.,1998) and in Sung Valley (107-115Ma, Srivastava et al. 2005). On average, carbonatites have much more enriched patterns (more than 31000 times PM values), and are characterized by strong negative Rb, K, and Ti anomalies. Similar features are displayed also by the Deccan-age Amba Dongar carbonatite, that also display a strongly fractionated REE pattern.

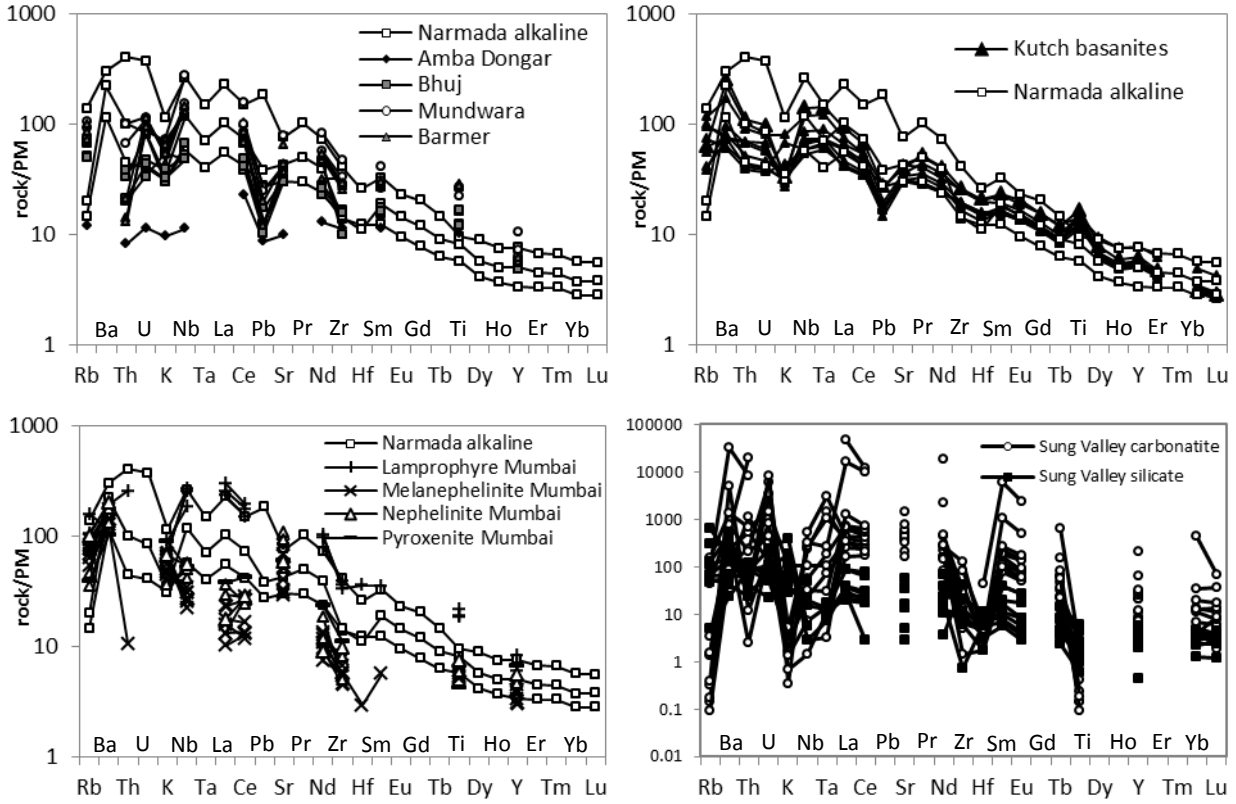

Fig. 6.12. PM normalized trace element contents of the most primitive alkaline samples compared to those of northern Deccan complexes (a); Kutch basanites (b); Murud alkaline rocks (c); Sung valley carbonatites (d).

6.4.4. Isotopes – alkaline samples

Narmada rocks have a more enriched isotopic composition with respect to all other alkaline rocks, with the exception of the nephelinites and melilite-nephelinites from the Mumbai area, which have much lower Nd isotopic composition. Rocks described by Simonetti et al., and lamprophyre from Mumbai area, have quite homogeneous composition, ranging between

0.51286 and 0.51270 in $^{143}Nd/^{144}Nd$, and between 0.70357 and 0.70570 in $^{87}Sr/^{86}Sr$; whereas the more enriched isotopic composition of the Narmada rocks plot between the EMI and EMII isotopic fields (of Zindler and Hart, 1986). Only the silicate samples associated with the carbonatite in the Sung Valley present more enriched composition, pointing towards the EMII end-member, whereas the carbonatites are slightly more enriched than the Narmada alkaline rocks (e.g., $^{143}Nd/^{144}Nd$ reaching a value of 0.51254).

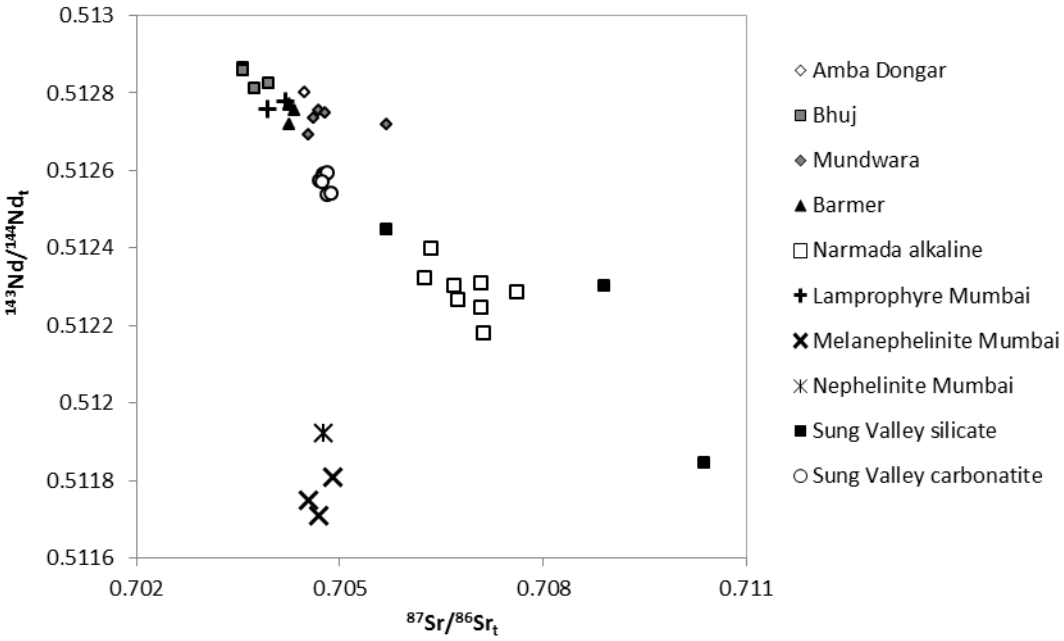

Fig. 6.13. comparison between isotopic compositions of Narmada alkaline rocks and other alkaline rocks in the Deccan province.

CHAPTER 7.
MINERAL COMPOSITIONS

Mineralogical compositions were measured at the IGG-CNR of Padua, by means of the electron microprobe CAMECA SX50, through core-rime traverses, in order to define the processes that led to the crystallization of the sampled rocks. Olivine, plagioclase, pyroxene, and amphibole crystals have been analyzed.

7.1. Plagioclase

Analytical traverses have been carried out on plagioclase crystals of 11 samples, whereas on 3 samples (PL48, PL31, PL56), due to the lack of large fresh zones, only single spots have been analyzed. These three samples are characterized by the presence of Na-K feldspars, with minor An component (fig. 7.1): PL31 feldspars are mainly sodic, with Ab=74.8-78%, and Or=25.2-21.2%; PL48 contains both Na-K feldspars (Ab=41.5-50.8%; Or=52.8-43.7%), and sodic plagioclase (Ab=63.1-64.4%; An=35.1-33.3%). PL56 presents two different kinds of feldspars, one Na-rich (Ab=73.3-78.7%, Or=19.5-18.5), and the other more potassic (Ab=30.9-29.1%; Or=65.3-67.6%).

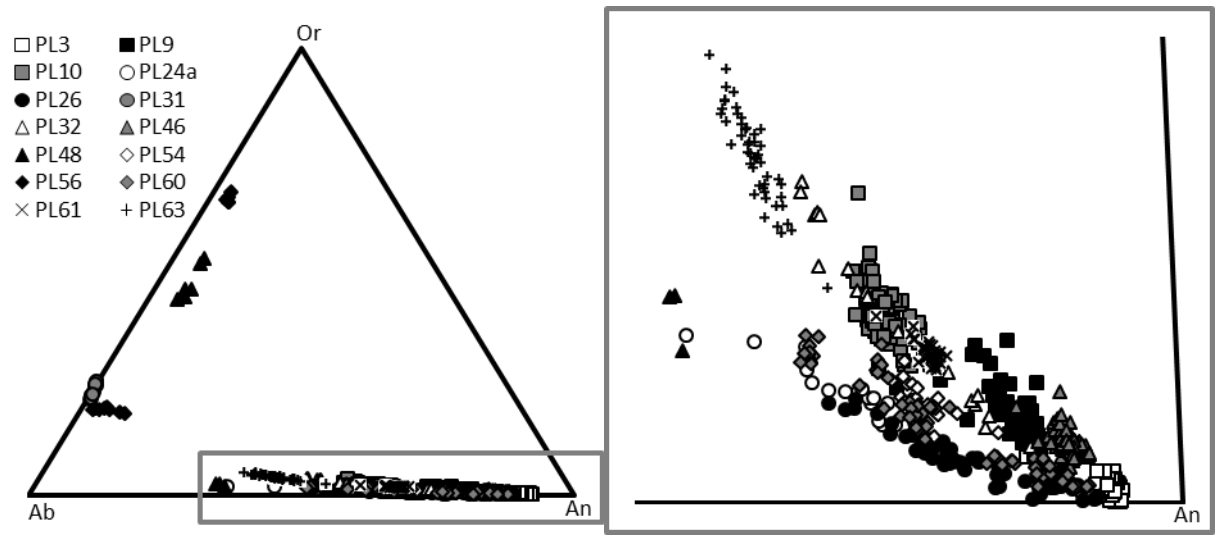

Fig. 7.1. Composition of the feldspars plotted in the Na-Ca-K ternary diagram. Ab: albite; An: anorthite; Or: orthoclase.

All other plagioclases have An content comprised between 35.5 and 92.2%, and are in rocks from all the sampled areas. Gabbros from Phenai Mata (PL3, PL9, PL10) are characterized by very different An contents, possibly representing different stages in the evolution of the intrusive complex. Plagioclase in PL3 are the most Ca-rich with core composition ranging from An_{92} to An_{87}, slightly decreasing towards the rim (minimum An_{80}), with little fluctuations along the traverses. PL10 has the lowest An content, PL9 has intermediate composition, and both present

plagioclase with marked zoning; in PL9, the two analyzed plagioclase crystals show cores of An_{81-77} and An_{77-71} rims; both of them present a steep drop at the rim, down to An_{65}. PL 10 plagioclases, as a whole, have compositions between An_{67} and $An_{56.5}$; the three plagioclases present marked fluctuations, respectively normal zonation in plg3 and reverse zonation in plg1 and plg3 (slightly rimward increasing An).

The analyzed plagioclase crystals from the Amba Dongar sector (samples PL24a and PL26) are euhedral and about 200-400µm in size. PL24a contains normally zoned plagioclases with An_{65-59} cores and An_{51--36} rims. In PL26, plagioclases have variable composition and are in general more Ca-rich than in PL24a, ranging between An_{89} and An_{54}. Two crystals (plg2 and plg3) show reverse zoning near the rim, whereas plg1 and plg4 show a reverse zoning within the core region.

Plagioclases are essentially the only phenocrysts in PL32 and reach 400µm in size. They show highly different core compositions and An contents increasing form the core to the rim ($An_{66.3-64.7}$, $An_{52-62.6}$, $An_{49.3-51.9}$, for plg2, plg4, plg3, respectively).

Plagioclases in sample PL46 have almost identical composition comprised between An_{88} and An_{81}, and all of them are characterized by frequent compositional oscillations throughout all the traverse.

Two plagioclases have been analyzed in PL54, and they show opposite behavior, i.e. normal zoning in plg1 (An_{76}-$An_{63.6}$), and reverse zoning in plg2 An (An65 to An68).

PL60 contains about 50 vol% of plagioclase crystals, which can vary from 1.3 mm to 300µm in size. Again, normal (Plg3 and plg2: An_{88-76} and An_{83-65}, respectively) , reverse zoning (plg1: An_{60-65}) and flat core-rim profiles (plg4: $An_{52.5-50.2}$) are observed.

PL61 and PL63 are the picrite and rhyolite glass, respectively, sampled at Mount Pavagadh, and as expected have very different plagioclase composition. Plg in PL61 range between An_{69} (core) and An_{60} (rim). In PL63 An is comprised between 53 and 37% with reverse zoning occurring in plg4 and normal zoning in plg1, while plg5a displays compositional oscillation in the traverse.

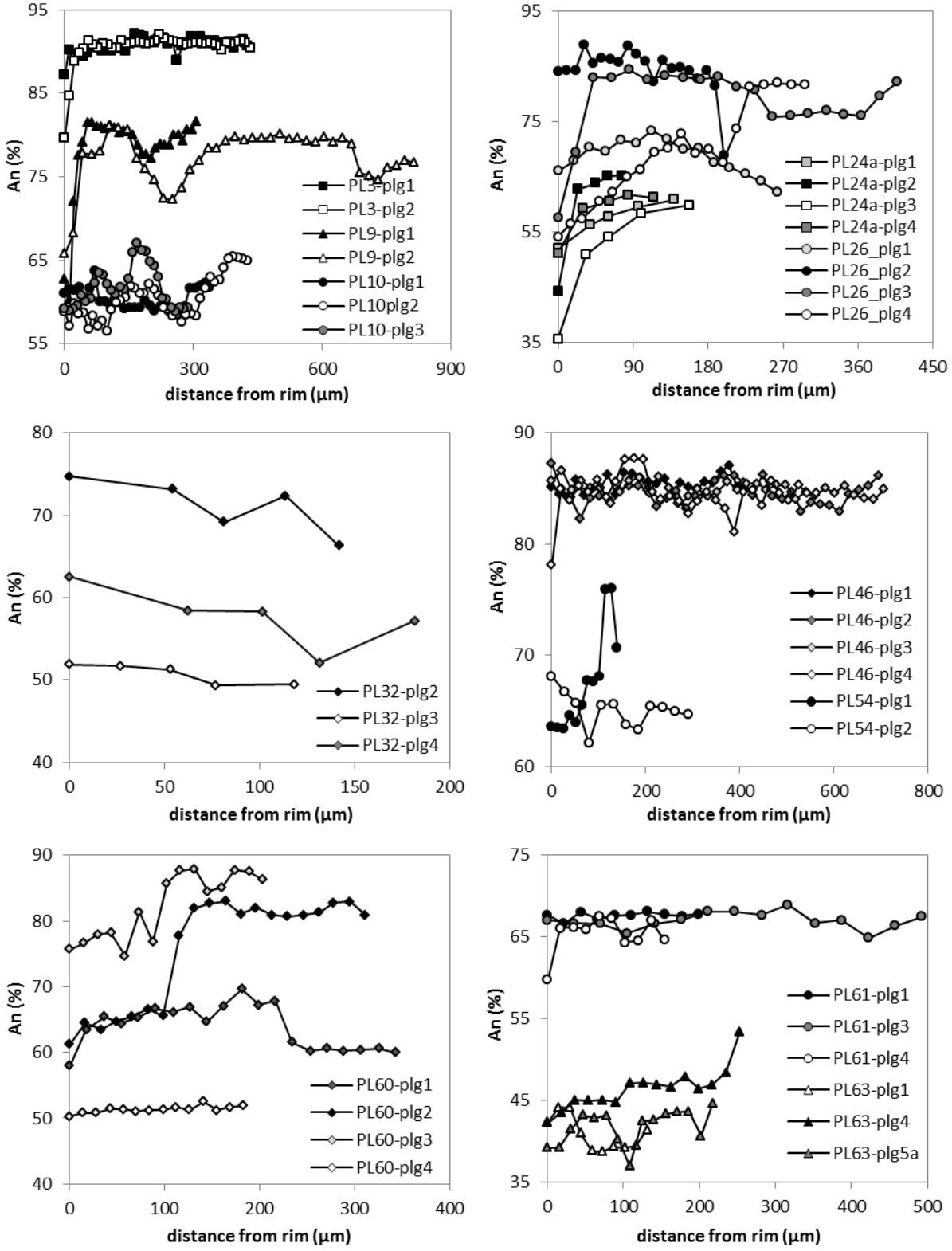

Fig. 7.2. Variation of the compositions (An%) in plagioclases along core-rim traverses formed by analytical points (symbols).

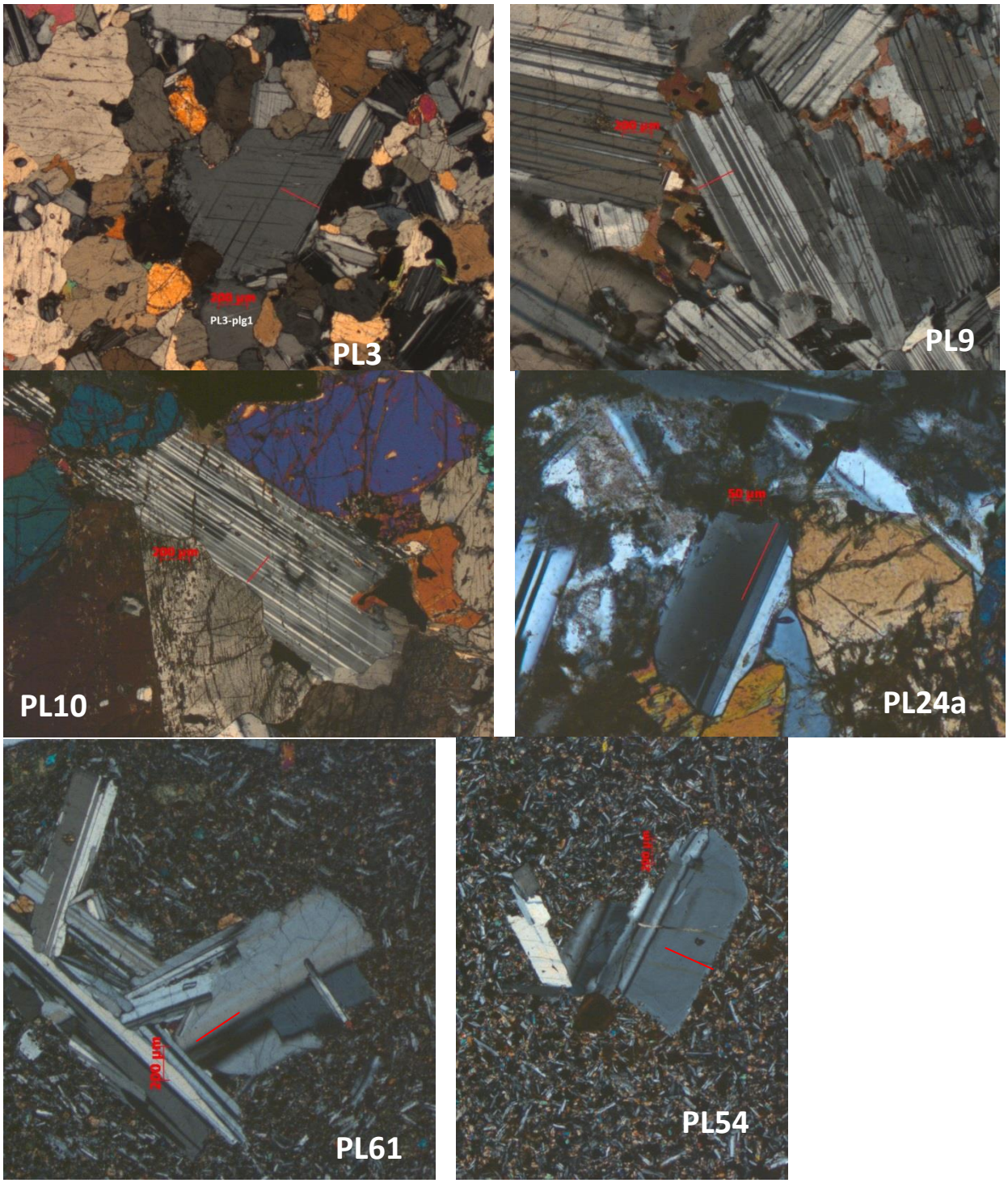

Fig. 7.3. Microphotographs of plagioclase. Red lines represent the analytical traverses.

7.2. Olivine

Olivine have been analyzed from the Phenai Mata gabbros. In PL9, PL10 the crystals can be up to 1mm in length and constitute about 12 and 40 vol%, respectively, while olivine in PL3 occurs as rare (vol%) small crystals of about 200µm in size. Olivine crystals occur also inthe picrite PL59 (Phulmahal-Bakatghar sector) as rare phenocrysts of up to 1mm in size.

Olivine in Phenai Mata gabbros PL3, PL9 and PL10 are poorly zoned and low in forsterite (Fo_{63-72}). PL59 shows both normally (Fo87 in the core to Fo_{75} at the rim) and reverse zoned crystals (from Fo_{74} to Fo_{80} within the crystal center and then Fo_{76} at the rim).

Ni is generally low in all crystals (maximum = 2005ppm in PL59, ol1) and is correlated with Fo contents.

According to the Rhodes diagram (fig. 7.4), and comparing olivine Fo content with the respective whole rock Mg#, only ol1 in PL59 results to be in equilibrium with the whole rock composition, suggesting possible accumulation of mafic minerals for Phenai Mata gabbros.

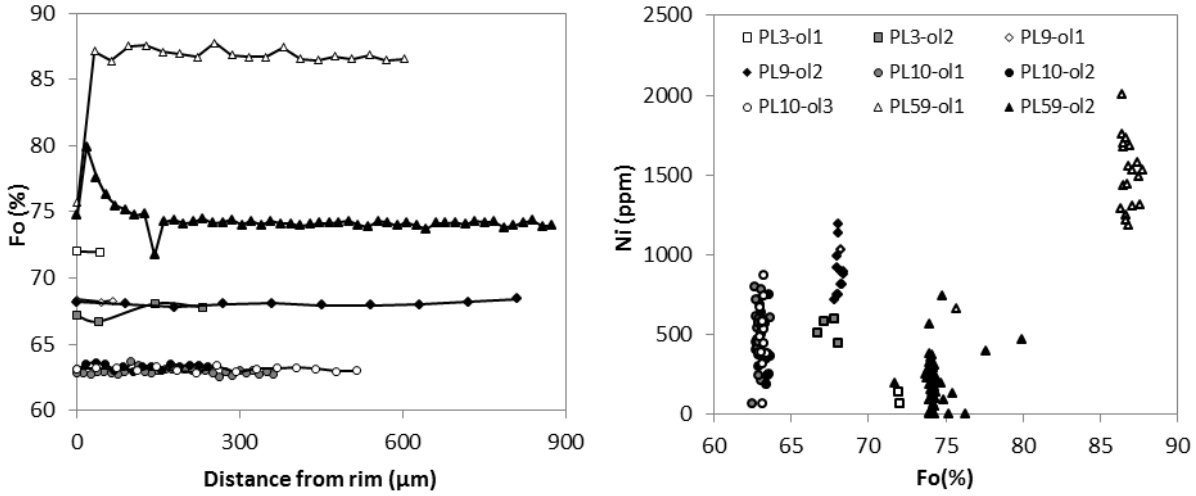

Fig. 7.4. a) Variation of the compositions (Fo%) in olivines along core-rim traverses formed by analytical points (symbols). b) Ni concentration (ppm) plotted vs. Fo content.

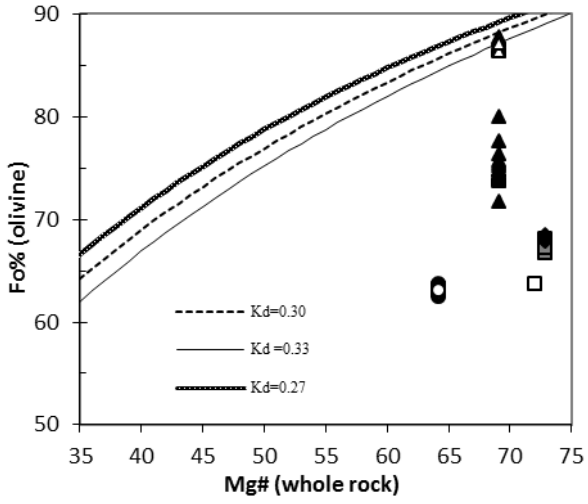

Fig. 7.5. Rhodes diagram for analyzed olivines. Curves represent $kd_{Fe/Mg}$, i.e. the ratio between Fe/Mg in olivine and Fe/Mg in the magma; values of 0.30±0.03 have been used.

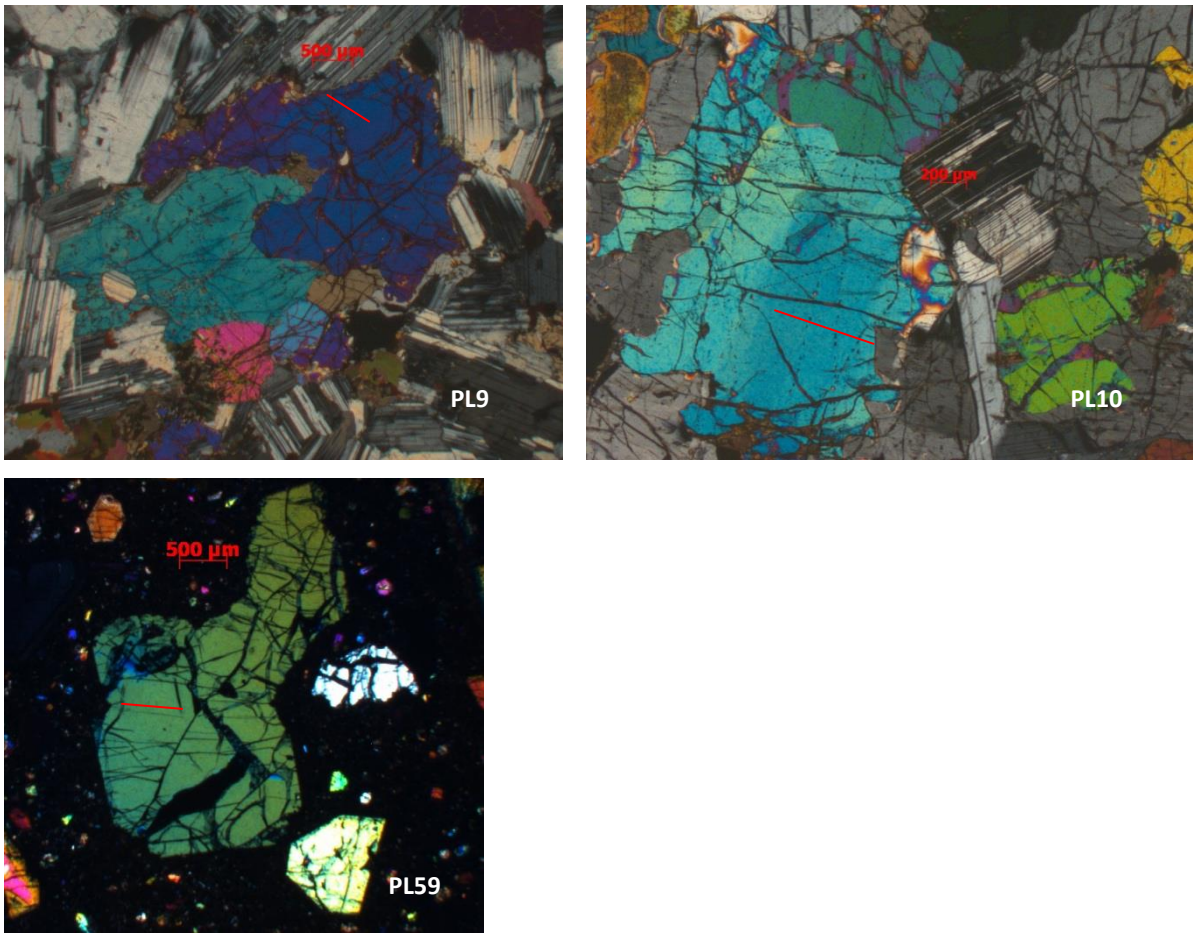

Fig. 7.6. Microphotographs of olivine. Red lines represent the analytical traverses.

7.3. Pyroxenes

Pyroxenes have been analyzed in the same samples where olivine was analyzed and in two tephri-phonolites (PL48 and PL56) from the north-eastern part of Phenai Mata.

Almost all the analyzed crystals are clinopyroxenes, with augitic compositions (fig. 7.4). PL10 only contains low-Ca clinopyroxenes and low-Mg orthopyroxene (Enstatite =..) .

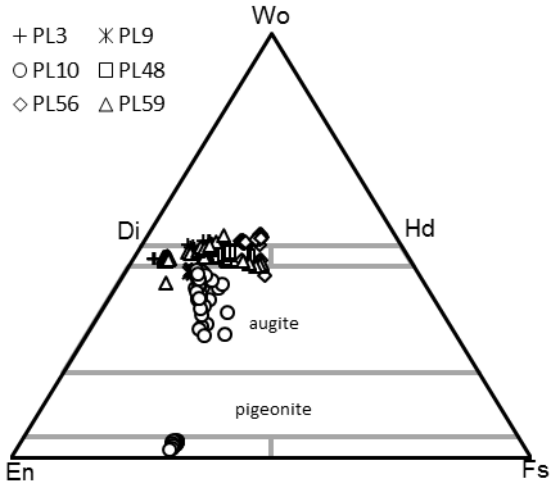

Fig. 7.7. Composition of the pyroxenes plotted in the Mg-Fe-Ca ternary diagram. Wo: wollastonite; En: enstatite; Fs: ferrosilite; Di: diopside; Hd: hedembergite.

The gabbro PL3 contains about 70 vol% clinopyroxene (100µm to 2mm in size). Many of these clinopyroxenes are normally zoned and the analyzed cpx1 presents an Mg-rich core (Mg#=98, with CaO=23.7 wt%) and a slightly more evolved rim with Mg#=89 and CaO=22.9wt%.

PL9 and PL10 contain normally oned clinopyroxenes (Mg# 82-79 in the cores, 78-62 at the rims).

Clinopyroxenes, together with amphiboles, constitute the phenocrysts of PL48; they are euhedral and distinctly zoned. Some crystals (e.g., cpx1 and cpx1a) are reverse zoned ((Mg# in the cores 70-74, and up to 84 at the rims). On the contrary, PL56 yields normally zoned clinopyroxenes (Mg# from 81 to 75).

Similarly to what has been observed in the case of olivine, clinopyroxenes in PL59, which are the most abundant phenocrysts and can reach several millimeters in size, present highly variable compositions, with marked zoning. Cpx1 has the highest Mg# (98 in the center and 86 at the rims). On the contrary, cpx2 shows reverse zoning (Mg#=63 in the core to 89 at the rims). Cpx4 has intermediate composition, with Mg#=91 at the core of the crystal, the central part of the traverse present Mg# of 86, which, towards the rim, it increases up to 93.5.

Comparing Mg# of the cpx with the one of whole rock, it can be noticed that cpx in PL9, PL10, PL48 and PL56 are not in equilibrium, having lower (PL9 and PL10) and higher (PL48 and PL56) Mg# than the predicted equilibrium values. Cpx in PL3 and PL59 are in general equilibrium with the whole rock, with the exception of the core of PL59-cpx2 and cpx1 which show, respectively, very low and high Mg# with respect to the equilibrium value (fig. 7.6).

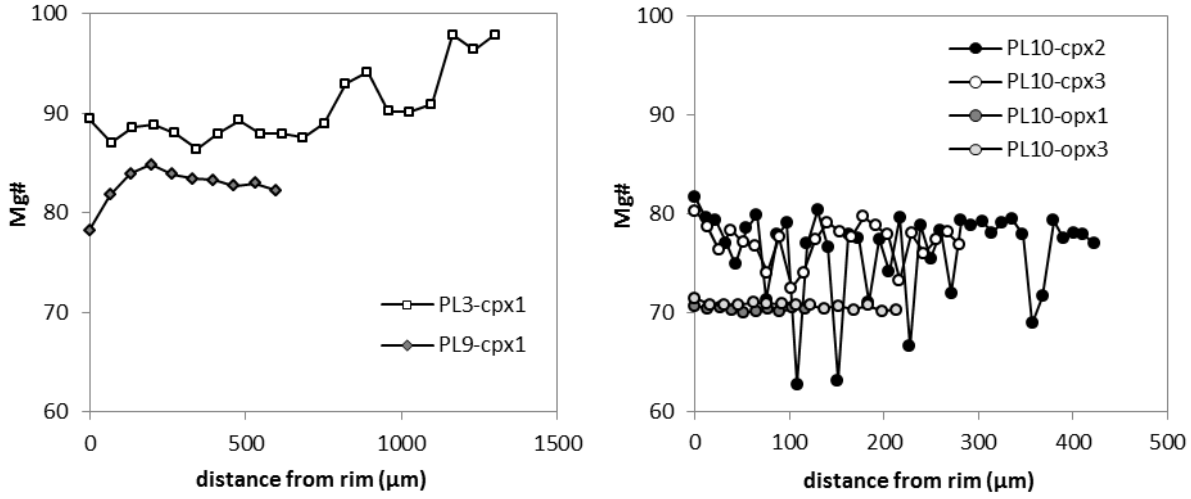

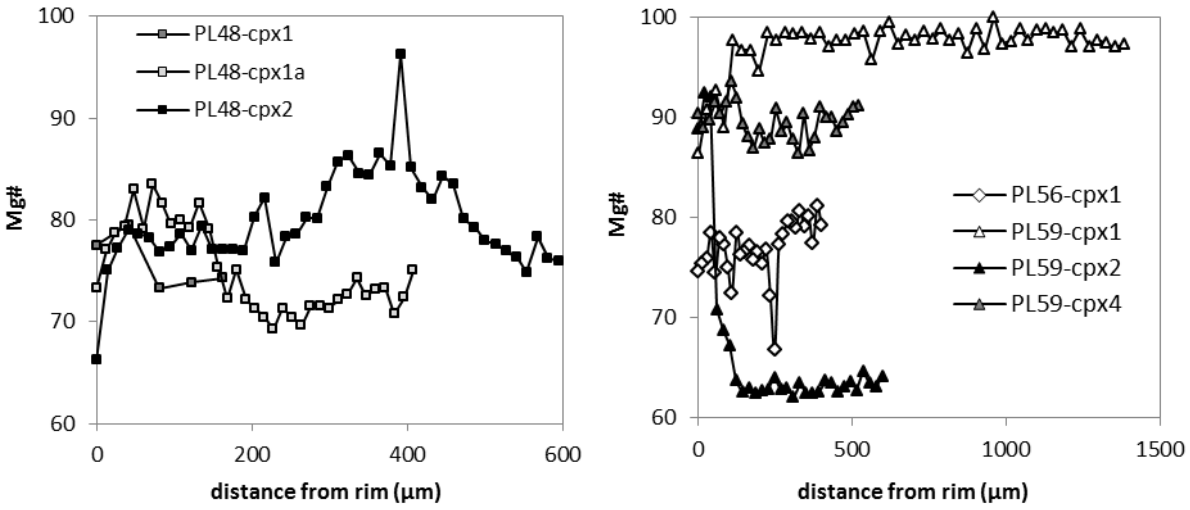

Fig. 7.8. Variation of the compositions (Mg#) in pyroxenes along core-rim traverses formed by analytical points (symbols).

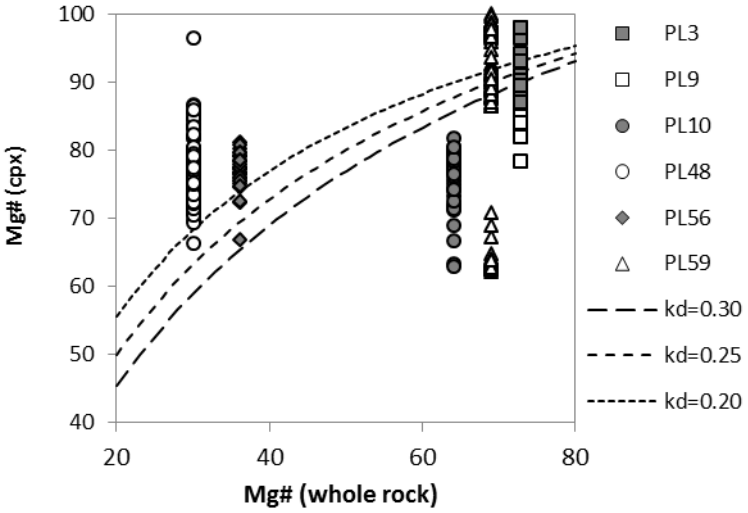

Fig. 7.9. Rhodes diagram for analyzed clinopyroxene. Curves represent $kd_{Fe/Mg}$, i.e. the ratio between Fe/Mg in cpx and Fe/Mg in the magma; values of 0.25±0.05 have been used.

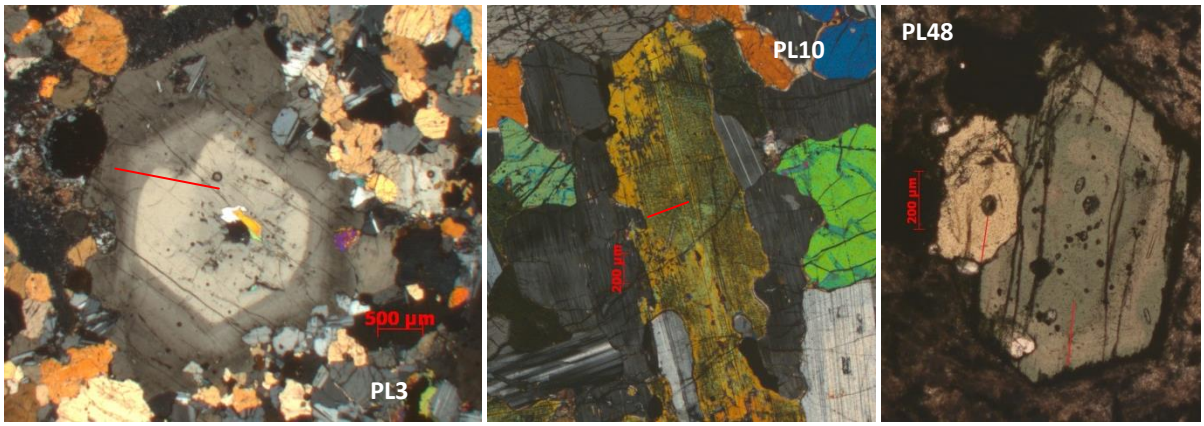

Fig. 7.10. Microphotographs of pyroxene. Red lines represent the analytical traverses.

7.4. Amphibole

Among the collected samples, only the syenite from Phenai Mata PL1, PL2 and the tephri-phonolite PL48 contain amphibole. Crystals from PL2 and PL48 have been analyzed and can be classified as pargasite and Fe-pargasite, since their Si (pfu) content ranges between 5.7 and 6.4 (with the exception of two data points), and Mg# varies from 6 and 67 (fig. 7.11a); moreover they can be further classified as potassian, having K in site A comprised between 0.25 and 0.5, titanian (Ti in site C comprised between 0.25 and 0.5), and calcic, having Ca+Na≥1 in site B, with Na<0.5.

Core-rim transect show that the crystals are zoned. Amph2 in PL2 presents core with higher Mg# (30.6), and it drops down to 5.5 at the rim. Amph1 in PL48 present a similar zoning, but with higher Mg#: 64.7 at the core and 45 at the rim; the zoning in PL48-amph2 is less marked, having the core with Mg#=46, it slightly increases up to 47.8, and decreases with two steps, the first at Mg#=42 and the second at Mg#=39.4.

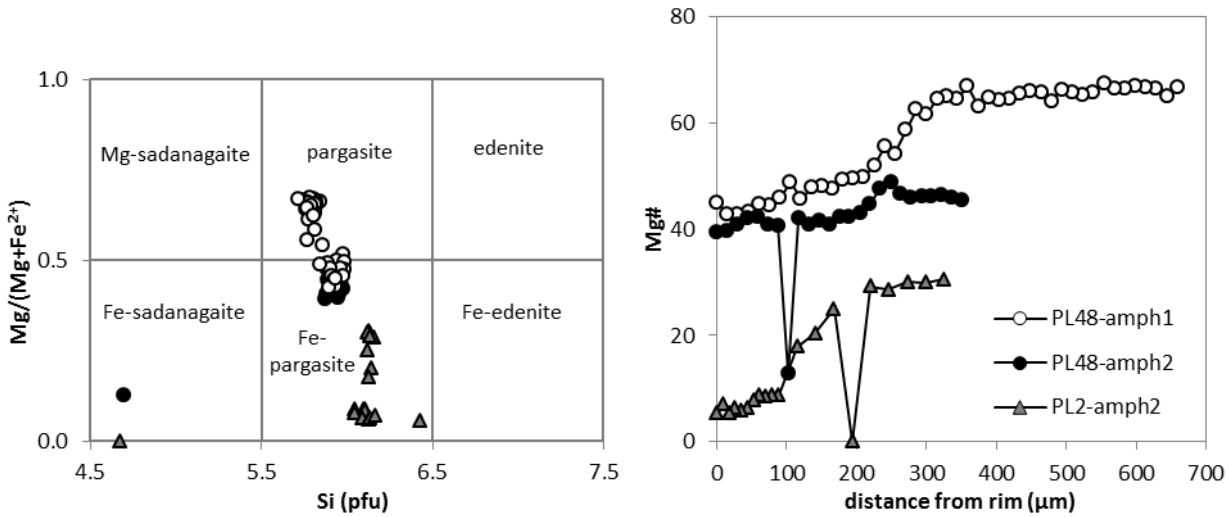

Fig. 7.11. a) Classification of amphibole based on Si and Mg#/100; b) Variation of the compositions (Mg#) in amphiboles along core-rim traverses formed by analytical points (symbols).

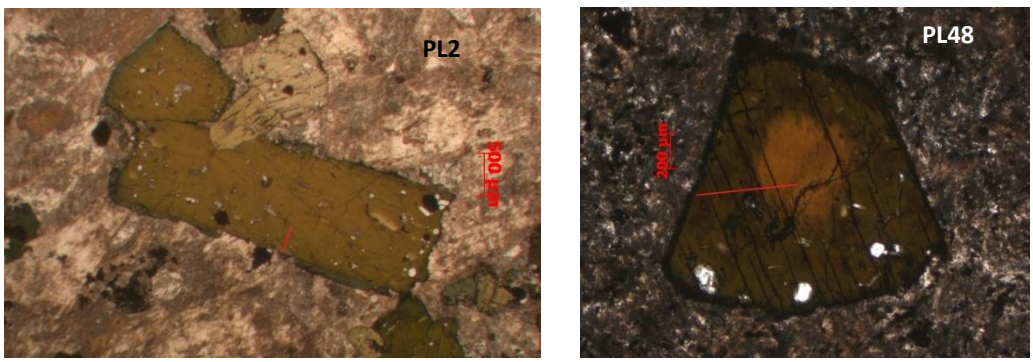

Fig. 7.10. Microphotographs of amphibole. Red lines represent the analytical traverses.

7.5. Geothermobarometry

P-T conditions of crystallization have been determined starting from the composition of the clinopyroxene; however, in order to obtain reliable conditions, only cpx in equilibrium with whole rock can be used, and at this purpose, and referring to the Rhode diagram in fig. 7.6, equilibrium compositions from PL3, PL48, PL56 and PL59 have been used as input compositions in the geothermobarometer of Putirka (2008). In general, the P and T values provided by the model are quite high, being comprised between 5.7 and 14 Kbar, and between 1030 and 1347 °C (fig. 7.13a).

Composition of PL3 yielded T of about 1250°C and P of 5.7-8.6 Kbar; cpx in equilibrium with PL59 have very different compositions, thus providing very different P-T conditions, cpx1 with the lowest T (1250-1270°C) and P (5.7-7.2 Kbar), and cpx4 reaching the highest values of 1347°C and 14 Kbar, in agreement with what is shown by the analyses of olivine and cpx, and addressing to different time in the crystallization and therefore different depth.

Though only one and two data points are equilibrium compositions, and probably not enough to be representative for, respectively, PL48 and PL56, they show the lowest T values of 1030 and 1111-1130°C, with P values comparable to those of PL59.

P conditions have been also determined by means of the geobarometer of Schmidt (1992), which correlates Al in amphiboles with P of crystallization. PL48 yielded P of 9 Kbar (on average), which is comparable with the value obtained from cpx compositions; PL2 yielded slightly lower P, being comprised between 6.7 and 7.5 Kbar (with two data points at 8.2 and 9.9 kbar).

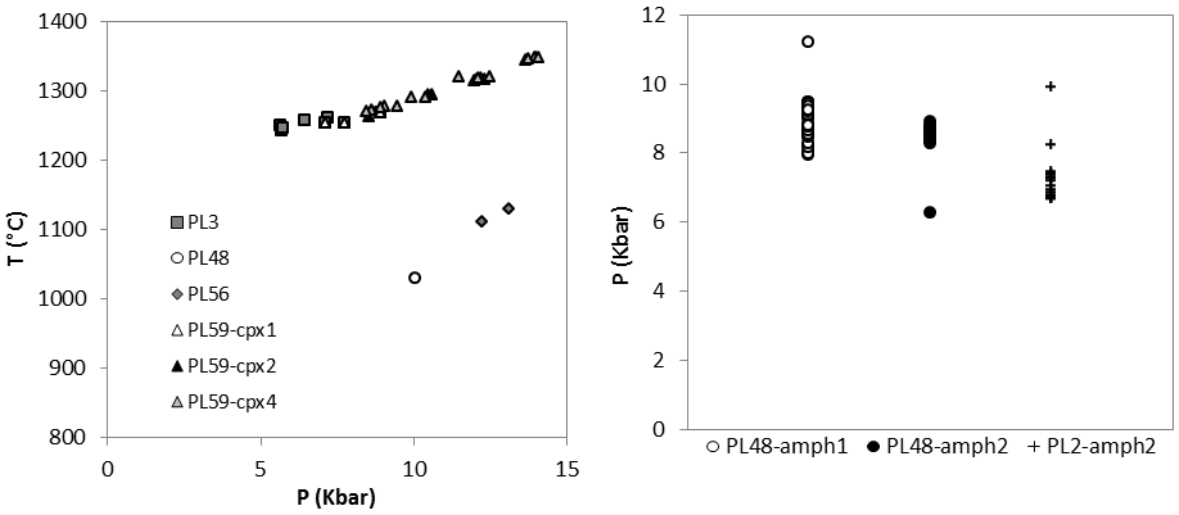

Fig. 7.13. a) P-T conditions obtained with the geothermobarometer of Putirka (2008), for cpx in equilibrium with whole rock; b) P conditions obtained from the barometer of Schmidt (1992), for amphiboles of PL48 and PL2.

CHAPTER 8.
CRUSTAL CONTAMINATION

The variability in isotopic compositions and the high $^{87}Sr/^{86}Sr_t$ values displayed by Indian samples, suggest crustal involvement in their generation. Crustal contamination, especially for the trend with higher $^{87}Sr/^{86}Sr_t$ (trend 2), is also suggested and supported by the correlation existing between Sr isotopic composition and elements or element ratios which are typically good proxies for such process: fig.8.1 shows the positive correlation between $^{87}Sr/^{86}Sr_t$, which is sensitive to crustal contamination, and SiO_2, K_2O/TiO_2 and K/Nb; the correlation is marked for tholeiitic samples which also reach the highest $^{87}Sr/^{86}Sr_t$ value, while alkaline rocks show near constant isotopic composition at increasing SiO_2 and K/Ti. Therefore, it is likely that the alkaline did not undergo significant crustal contamination, even if it may be possible that in this case the assimilation did not progressively augment during differentiation from SiO_2-poor to SiO_2-rich magmas (as expected in an AFC-type assimilation), yet it affected principally the less evolved magmas (as predicted for example in an ATA, assimilation during turbulent ascent differentiation model; Kerr, 1995).

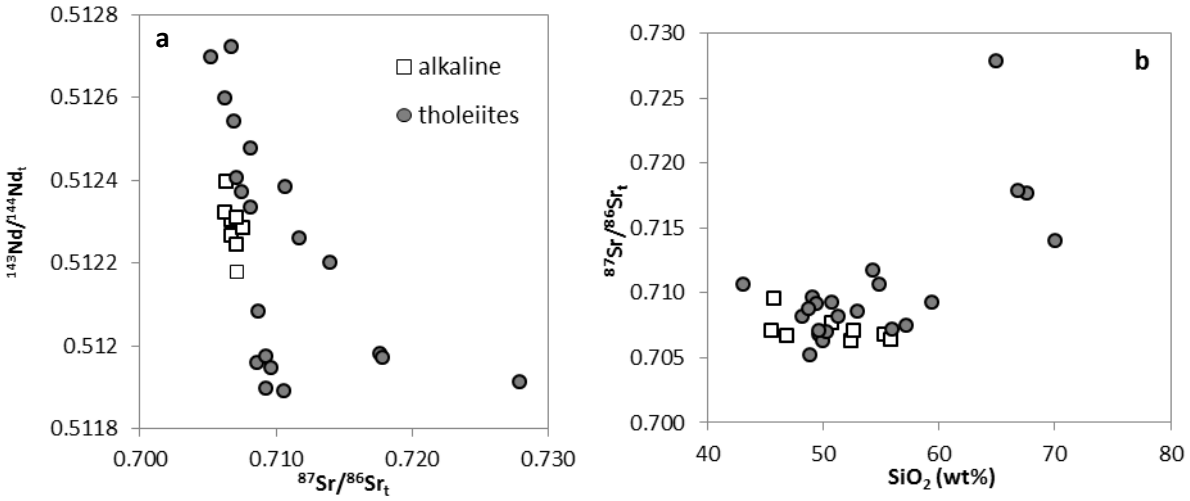

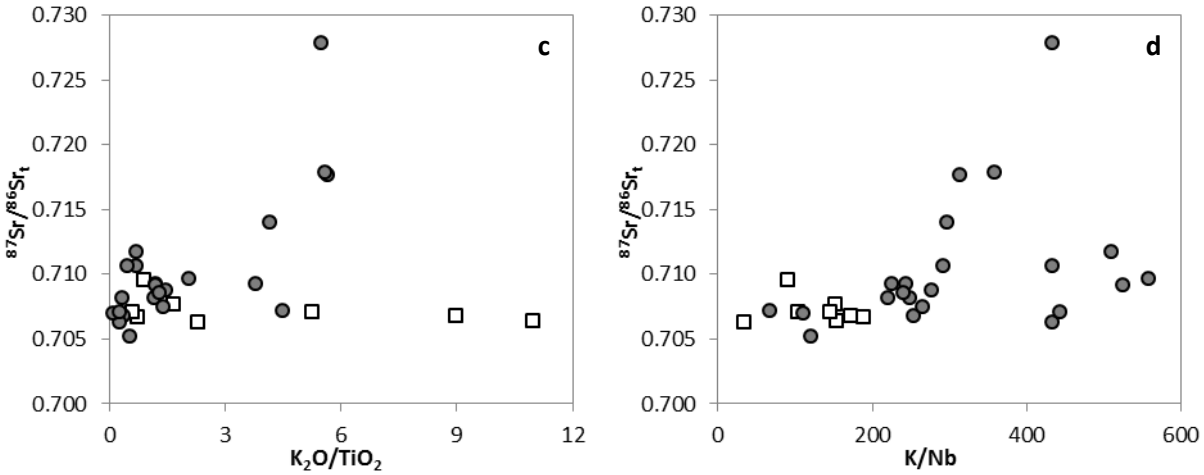

Fig. 8.1. Bivariate diagrams showing correlation between isotopic compositions (a), $^{87}Sr/^{86}Sr_t$ vs. element content (b), and element ratios (c and d) which can be considered as proxies for crustal contamination.

The crustal contamination has been characterized by means of the Assimilation and Fractional Crystallization model (AFC, De Paolo, 1981) and the Energy Constrained-AFC model (EC-AFC) which provides a thermochemical constrain of the process (Bohrson and Spera, 2001).

The modeling requires the definition of the parental magma which underwent contamination, the crust responsible for it, and the partition coefficients for the initial magma and the contaminant (the latter is required only in EC-AFC model). In table 1 are reported the compositions used in AFC, calculated at 66Ma.

	Initial magma	contaminant			
	Réunion	Dharwar		Aravalli	SIGT
	RE476	BH26a	BH31	RAJ-30	6617
Sr (ppm)	305	217	226	167.7	664
kd_{Sr}	0.93	2.4	2.4	2.4	2.4
$^{87}Sr/^{86}Sr$	0.70408	0.77456	0.78320	0.78292	0.71354
Nd (ppm)	20	63	45	98.19	37.62
kd_{Nd}	0.1	0.9	0.9	0.9	0.5
$^{143}Nd/^{144}Nd$	0.51275	0.51116	0.51058	0.51149	0.51048
	Fisk, 1988	Jayananda et al., 2000		Tobisch et al., 1994	Peucat et al., 1989
Pb (ppm)	1.5	15	15		
KdPb	0.23	0.7	0.7		
$^{206}Pb/^{204}Pb$	18.56	22.27	22.60		
$^{207}Pb/^{204}Pb$	15.59	16.15	16.21		
$^{208}Pb/^{204}Pb$	38.65	45.05	45.07		
	Tatsumi, 1990	Taylor,1983			

Table1. Isotopic and elemental compositions of Réunion samples, used as starting magma, and contaminants from Dharwar and Aravalli cratons, and from the Southern Indian Granulite Terrain.

In the assumption that the Deccan magmatism is due to the Réunion mantle plume (Richards et al., 1989, Campbell et al. 1990), compositions of olivine basalt from Réunion Island have been chosen as starting magma (Fisk, 1988; Tatsumi et al., 1990). Notably, the isotopic composition of Réunion basalts is slightly more depleted (higher Nd, lower Sr isotopic ratios) than those of the alkaline and of some transitional and tholeiitic Narmada rocks. The crustal contaminant can be chosen among the different lithologies that constitute the Indian Shield. The cratons bordering the Deccan Traps are the Aravalli craton, the Bastar craton, and the Dharwar craton; Fig 2a shows the available isotopic compositions for the cratons, and allows to exclude the rocks of the Bastar Craton as contaminant, since they present isotopic compositions comparable to those of PL samples, having isotopic composition ranging from 0.512447 to 0.511539 in $^{143}Nd/^{144}Nd$, and from 0.71765 to 0.74789 in $^{87}Sr/^{86}Sr$, thus implying unlikely amounts of crustal contamination. Moreover, in order to model crustal contamination also with a lower crust composition, samples of the Southern Indian Granulite Terrain have been used.

From the available cratonic compositions, only samples with evolved isotopic values (i.e. $^{87}Sr/^{86}Sr_t > 0.7106$ and $^{143}Nd/^{144}Nd_t < 0.5116$) have been considered, since only these could exert a strong effect as assimilates on the magmatic compositions (fig. 8.2b).

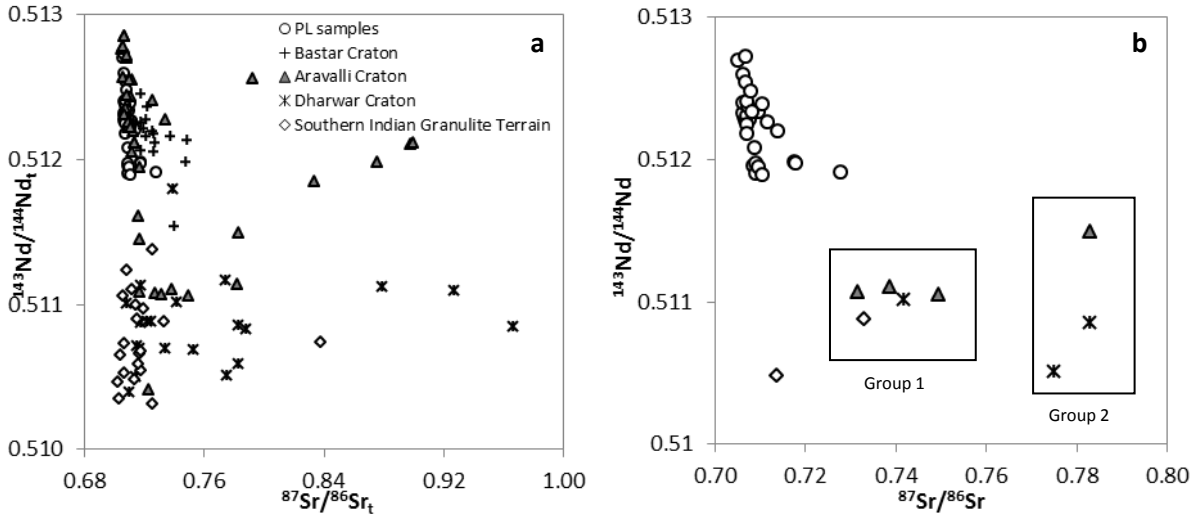

Fig. 8.2. a) Published isotopic compositions of the cratons bordering the Deccan Traps; b) selected isotopic compositions for crustal contamination modeling.

AFC has been modeled with an r value ranging from 0.1 to 0.5, being r the ratio between the mass assimilation rate and the fractional crystallization rate, and an F value (relative mass of magma remaining) from 1 to 0.5(De Paolo, 1981).

The isotopic trend with lower $^{87}Sr/^{86}Sr_t$ (trend 1) can be reproduced with a granulitic composition of the Southern Indian Granulitic Terrain (Peucat et al., 1989) and requires (for r = 0.5) up to

40% assimilation to reach compositions of Phenai Mata tholeiites (fig. 8.3), for example $^{87}Sr/^{86}Sr$ = 0.710612, $^{143}Nd/^{144}Nd$ = 0.51189. There are two groups of cratonic rocks from the Aravalli and the Dharwar cratons (Gopalan et al., 1990; Tobisch et al., 1994; Jayananda et al., 2000; fig. 8.2b) that could be used in modeling the contamination of trend 2: the first group is characterized by almost constant $^{143}Nd/^{144}Nd$ (0.51110-0.51087) and variable $^{87}Sr/^{86}Sr$ (0.73188-0.75042), whereas the second group has higher $^{87}Sr/^{86}Sr$ (0.77687-0.78583) and variable $^{143}Nd/^{144}Nd$ (0.51149-0.51051). The contamination with the rocks of group 1 would require values of F lower than 0.5 and therefore high amounts of assimilation (>50%), whereas, using the contaminants of the second group with more enriched composition, the contamination of RE476 with the gneiss RAJ-30 (Aravalli craton, cfr. Table 1) requires a maximum of 50% assimilation (r=0.5) to reach the isotopic composition of PL41, and slightly lower amounts of assimilation (30 to 42%, r=0.5) are required using the granites from the Dharwar craton as contaminants (fig. 8.3).

It can also be noticed that the behavior of Sr during the contamination is not completely reproduced by the model in the case of trend 2, and samples with higher Sr (up to 930ppm) of trend 1are not reached. Moreover, the AFC model cannot describe the behavior of Nd vs. $^{143}Nd/^{144}Nd$

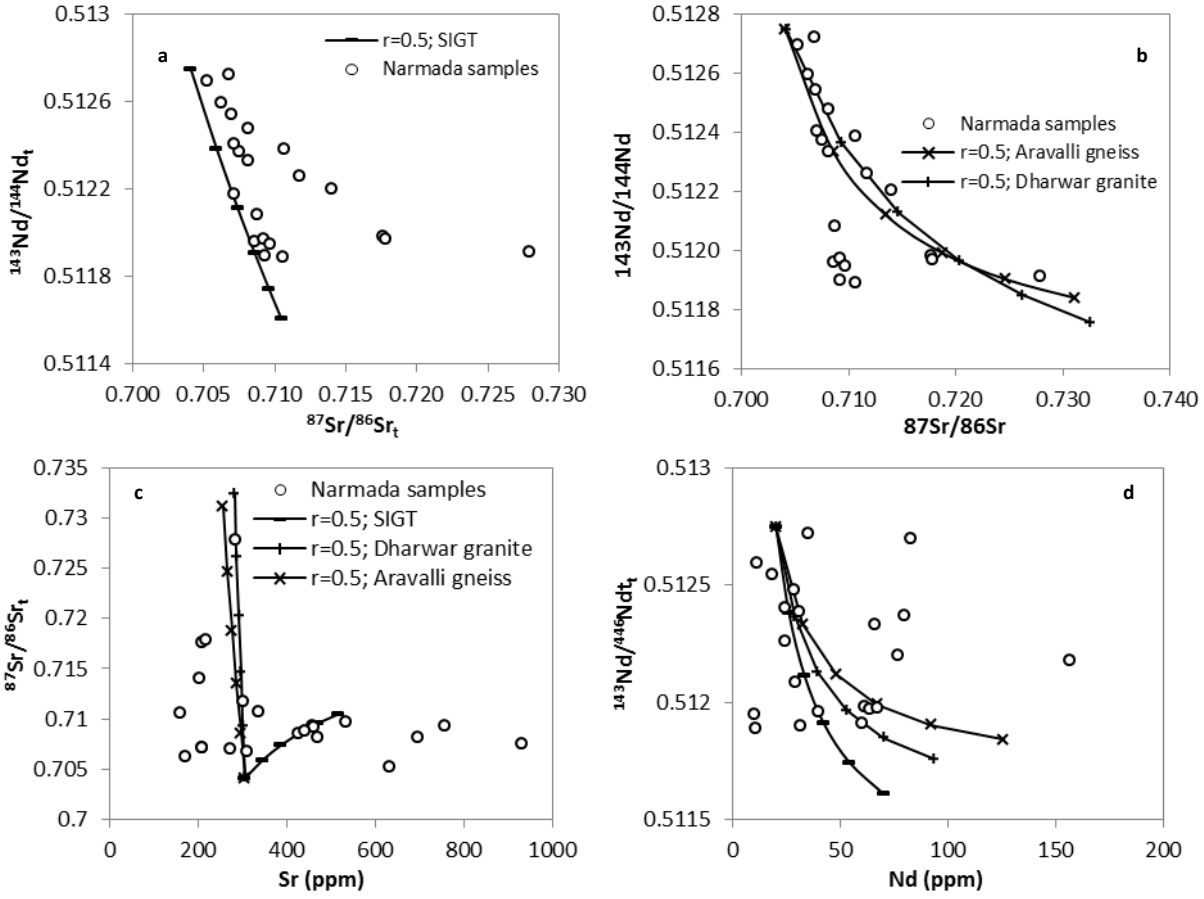

Fig. 8.3. AFC modeling using Réunion-type magma as starting composition and granulite from SIGT to reproduce isotopic compositions of trend1 (a), rocks from Aravalli and Dharwar cratons to reproduce

isotopic compositions of trend 2 (b); (c) and (d) show the modeling of the trace elements vs. isotopic compositions (in d same symbols as c).

Though the fraction of assimilation required is quite high, the composition with higher $^{87}Sr/^{86}Sr$ rocks have been used as contaminants to model EC-AFC, in order to further constrain the process (the thermal parameter are shown in table 2; Bohrson and Spera, 2001).

Indeed, with the EC-AFC model both trends can be reproduced with the same contaminants used in the AFC model, i.e. Southern Indian Granulite Terrain for trend 1, and Aravalli and Dharwar Cratons for trend 2; the two models differ in the amounts of assimilation yielded to reproduce the trends, which are lower in the case of trend1 (18%), and similar or slightly higher in the case of trend2 (35-41%). However, the EC-AFC model fails to reproduce the variation of Sr (ppm) for the trend1 (fig. 8.4 a and b).

		Initial magma	contaminant
upper crust	T_l (°C)	1280	1000
	T_i (°C)	1280	300
	T_s (°C)	900	
	T_{eq} (°C)	980	
	Δh_{cry} (J/Kg)	396000	
	$C_{p,m}$ (J/Kg K)	1484	
	Δh_{fus} (J/Kg)	270000	
	$C_{p,a}$ (J/Kg K)		1370
lower crust	T_l (°C)	1320	1100
	T_i (°C)	1320	600
	T_s (°C)	950	
	T_{eq} (°C)	980	
	Δh_{cry} (J/Kg)	396000	
	$C_{p,m}$ (J/Kg K)	1484	
	Δh_{fus} (J/Kg)	354000	
	$C_{p,a}$ (J/Kg K)		1388

Table 2. Thermal parameters used for EC-AFC modeling. Δh_{cry} = crystallization enthalpy; $C_{p,m}$ = isobaric specific heat of magma; Δh_{fus} = fusion enthalpy; $C_{p,a}$ = isobaric specific heat of assimilant; T_l = liquidus temperature; T_i = initial temperature; T_s = solidus temperature; T_{eq} = equilibration temperature.

Indeed, with the EC-AFC model both trends can be reproduced with the same contaminants used in the AFC model, i.e. Southern Indian Granulite Terrain for trend 1, and Aravalli and Dharwar Cratons for trend 2; the two models differ in the amounts of assimilation yielded to reproduce the trends, which are lower in the case of trend1 (18%), and similar or slightly higher in the case of trend2 (35-41%). However, the EC-AFC model fails to reproduce the variation of Sr (ppm) for the trend1 (fig. 8.4 a and b).

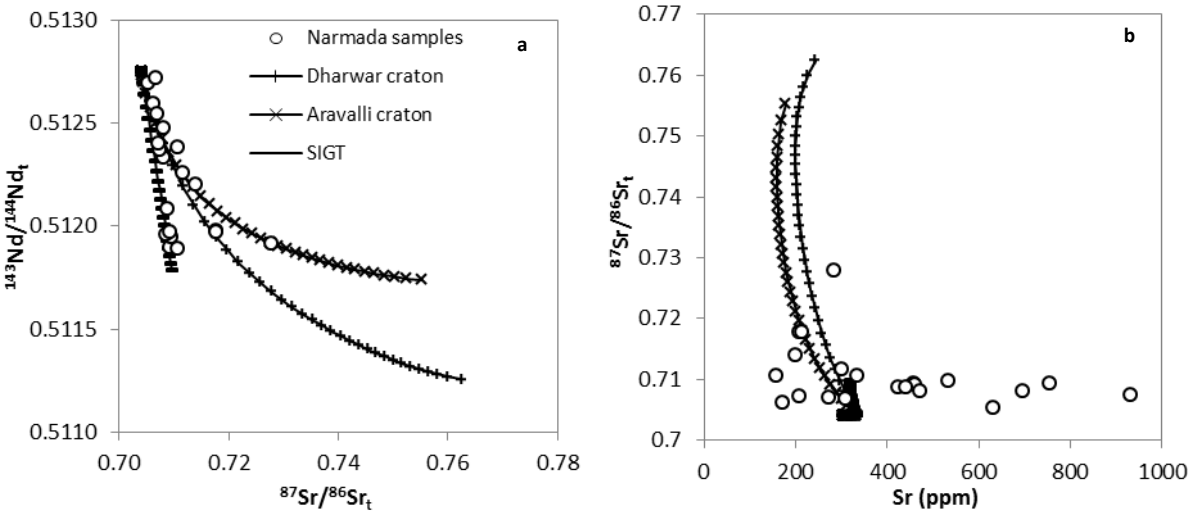

Fig. 8.4. EC-AFC modeling using Réunion-type magma as starting composition and contaminant from SIGT and Aravalli and Dharwar cratons to reproduce isotopic compositions of trend1 and trend2, respectively (a), (b) show the modeling of the trace elements vs. isotopic compositions.

A further constrain on the reliability of this model comes from the modeling of Pb isotopic compositions. It hasn't been possible to use the same sample of Indian cratons as contaminants because of the lack of a complete database with all isotopic compositions. Therefore, sample of the same lithology and similar age have been used (fig. 8.5a).

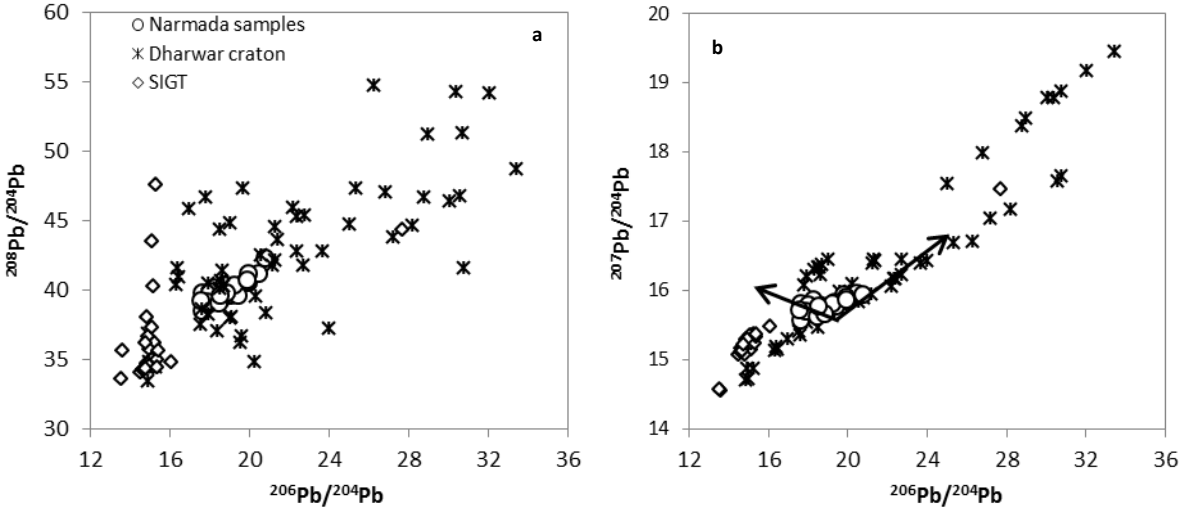

Fig. 8.5. Published Pb isotopic compositions of the Dharwar craton and of SIGT.

As described in chapter 6, departing from Réunion isotopic compositions, PL samples define two isotopic trends in Pb/Pb isotopic fields (fig. 8.5b). Modeling Pb isotopic compositions, both AFC and EC-AFC allow to reproduce trend 2 through the assimilation of granitic crust of the Dharwar Cratons with about 9-12% assimilation, significantly lower values than those required to reproduce Sr-Nd compositions. Moreover, after modeling Sr-Nd and Pb isotopic compositions

separately, the different isotopic systems have been compared by plotting the data on Pb vs. Sr and Nd diagrams where trend2 can be only partially reproduced (fig. 8.6), since the modeling can't reach the samples of the trend with lower $^{206}Pb/^{204}Pb$.

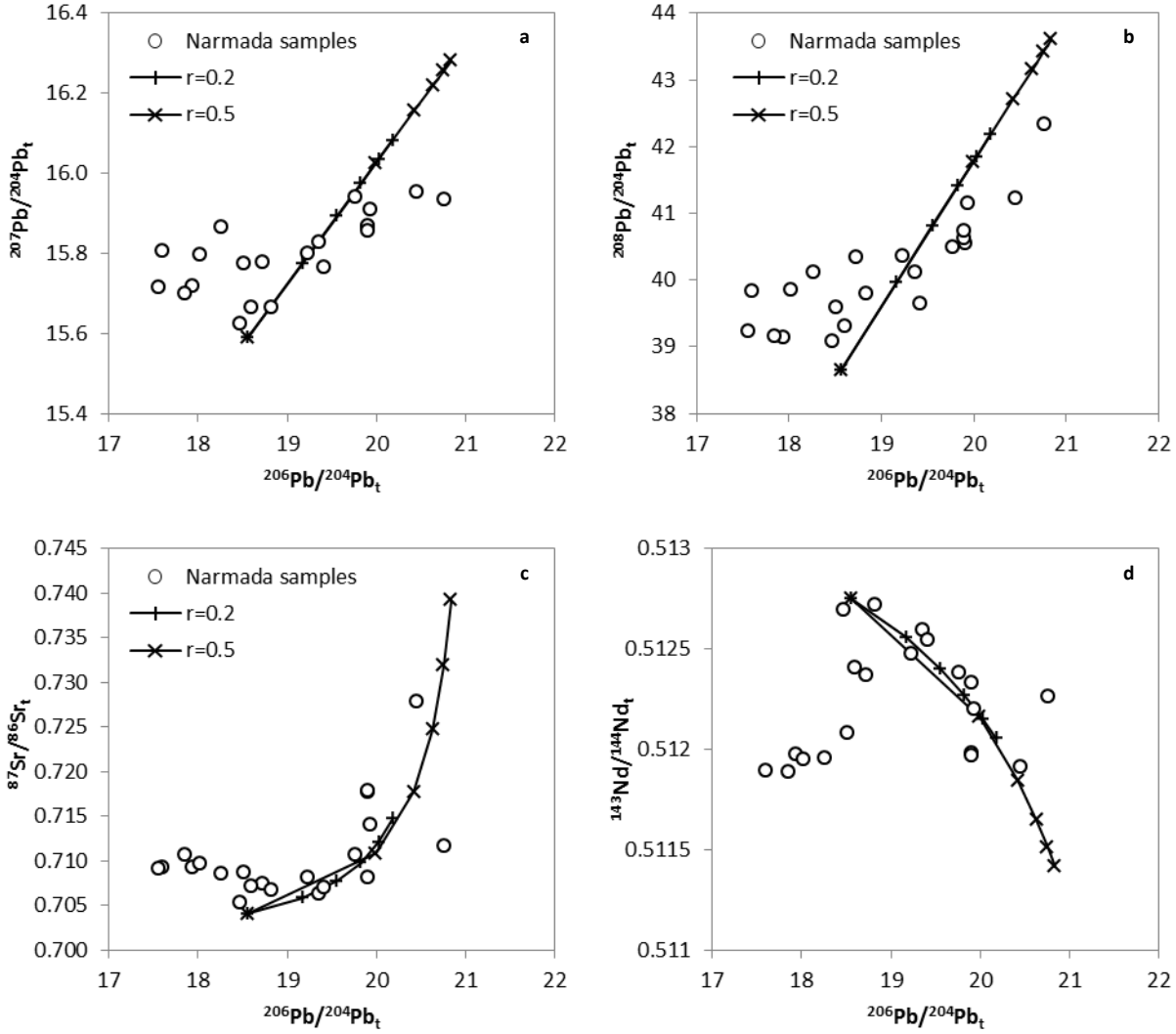

Fig. 8.6. AFC modeling using Réunion-type magma as starting composition and rocks from Dharwar craton as contaminant to reproduce isotopic compositions of trend 2; the r value shown in the plots are the minimum and maximum values required to reproduce the data.

A major problem arises when trying to model trend 1 which, for Nd and Sr isotopic compositions, is reproduced by the contamination with granulitic compositions: it is characterized by very radiogenic Pb compositions ($^{207}Pb/^{204}Pb$ and $^{208}Pb/^{204}Pb$). Therefore it would require an even more radiogenic crust as contaminant, with high $^{207}Pb/^{204}Pb$ and $^{208}Pb/^{204}Pb$ and low $^{206}Pb/^{204}Pb$. However, Pb isotopic compositions from the Southern Indian Granulitic Terrain are characterized by low $^{206}Pb/^{204}Pb$ and $^{207}Pb/^{204}Pb$ and can be excluded as contaminant; moreover among the other rocks from Indian cratons, isotopic compositions with

high $^{208}Pb/^{204}Pb$ at relatively low $^{206}Pb/^{204}Pb$ (i.e. at high Δ8/4) can be found, but compositions with high $^{207}Pb/^{204}Pb$ at low $^{206}Pb/^{204}Pb$ (and high Δ7/4) are not reported (fig. 8.5).

One solution to this problem can reside in the fact that the starting magma is different from a Réunion-type magma, and the trend-1 described by the Narmada samples is not departing from a $^{206}Pb/^{204}Pb$ composition of about 18.7 (as Réunion rocks), but from a composition characterized by lower $^{206}Pb/^{204}Pb$. The isotopic compositions described for the Central Indian Ridge basalts satisfy these criteria, being, on average, more depleted than those of Réunion. Therefore crustal contamination with an Indian Ridge-type MORB magma as starting composition has been attempted.

In this case, the contaminants of group2 allow to reproduce the trend 2 by 18-20% assimilation (r=0.3-0.5; Aravalli Craton) and by maximum 15% assimilation (r=0.2; 0.5) for the Dharwar Craton. After excluding SIGT as contaminant to reproduce trend-1, this can be reproduced only in its most enriched part ($^{87}Sr/^{86}Sr$ = 0.70713-0.71061; $^{143}Nd/^{144}Nd$ = 0.51218-0.51189) by 10-20% assimilation (r =0.1 to 0.5) of a Bangalore granite from the Dharwar Craton.

	Initial magma	contaminant			
	CIR MORB	Dharwar			Aravalli
		Bangalore granite		Hoskote-Kolar granite	BGC
Sr (ppm)	99	206	199	260	167.7
kd_{Sr}	0.93	2.4	2.4	2.4	2.4
$^{87}Sr/^{86}Sr$	0.70302	0.77487	0.72413	0.78272	0.78929
Nd (ppm)	9	48	63	89	98.19
kd_{Nd}	0.1	0.9	0.9	0.9	0.9
$^{143}Nd/^{144}Nd$	0.51295	0.51051	0.51088	0.51085	0.51149
	Price et al., 1986	Jayananda 2000			Tobisch et al., 1994
Pb (ppm)	0.56	14.3	8.5	15	
kd_{Pb}	0.23	0.7	0.7	0.7	
$^{206}Pb/^{204}Pb$	17.245	18.48	18.27	22.60	
$^{207}Pb/^{204}Pb$	15.528	16.22	16.33	16.21	
$^{208}Pb/^{204}Pb$	37.193	41.12	43.94	45.07	
	Price et al., 1986	Meen et al., 1992		Taylor,1983	

Table 3. Elemental and isotopic compositions of Indian Ridge MORB and contaminants from the Dharwar and Aravalli Craton used for AFC and EC-AFC modeling.

In order to reproduce all the Pb isotopic compositions of the Narmada rocks, at least two compositions from the Indian Shield with Pb more radiogenic than the MORB ones are needed: one to reproduce samples pointing towards the highest $^{208}Pb/^{204}Pb$ (42.33), and a second one to

explain the composition of the samples characterized by high Δ7/4. Contamination with compositions like those of the Chitradurga Granite ($^{206}Pb/^{204}Pb$ = 22.60; $^{207}Pb/^{204}Pb$ = 16.21; $^{208}Pb/^{204}Pb$ = 45.07; Taylor et al., 1983) can reproduce samples with the most radiogenic $^{208}Pb/^{204}Pb$ through a maximum of 10% assimilation (r = 0.5), whereas samples with high Δ7/4 can be modeled through the contamination of CIR-MORB magma by either trondhjemite ($^{206}Pb/^{204}Pb$ = 18.27; $^{207}Pb/^{204}Pb$ = 16.33; $^{208}Pb/^{204}Pb$ = 43.94) or the Arsikere granite ($^{206}Pb/^{204}Pb$ = 18.48; $^{207}Pb/^{204}Pb$ = 16.21; $^{208}Pb/^{204}Pb$ = 41.12) from the Dharwar Craton (Meen et al., 1992) with respectively maximum of 8 and 20% assimilation (r=0.5).

In $^{206}Pb/^{204}Pb$ vs. $^{87}Sr/^{86}Sr$ plot, it can be observed that samples that describe trend1 starting from Réunion composition, in the case of CIR-type starting composition constitute less defined trend, and can be almost entirely reproduced with the same contamination of trend2 samples (Chitradurga granite); differently, in $^{206}Pb/^{204}Pb$ vs. $^{143}Nd/^{144}Nd$ space they define a separate cluster and are partially reproduced by the contaminants with lower $^{206}Pb/^{204}Pb$ (trondhjemite or Arsikere granite).

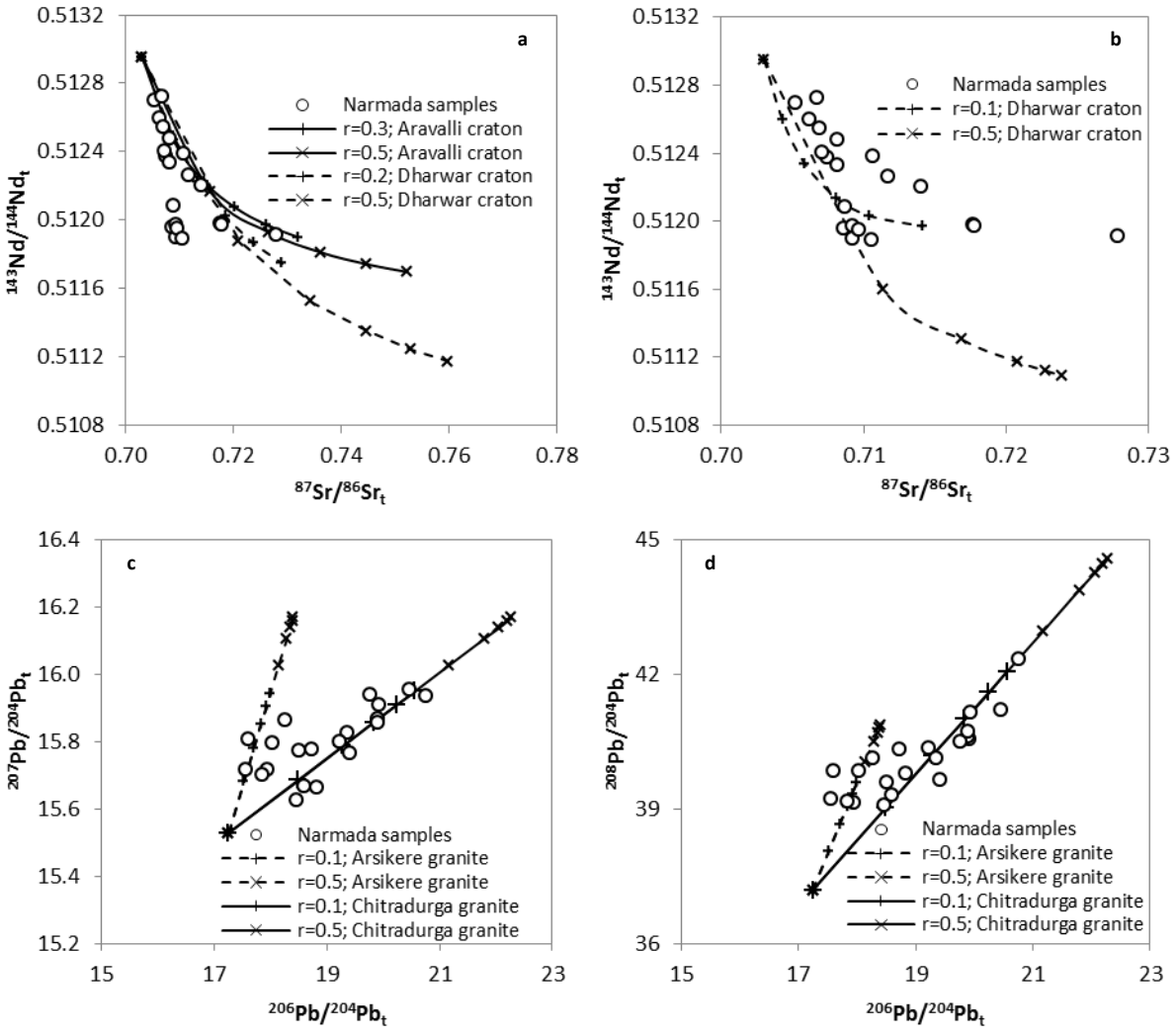

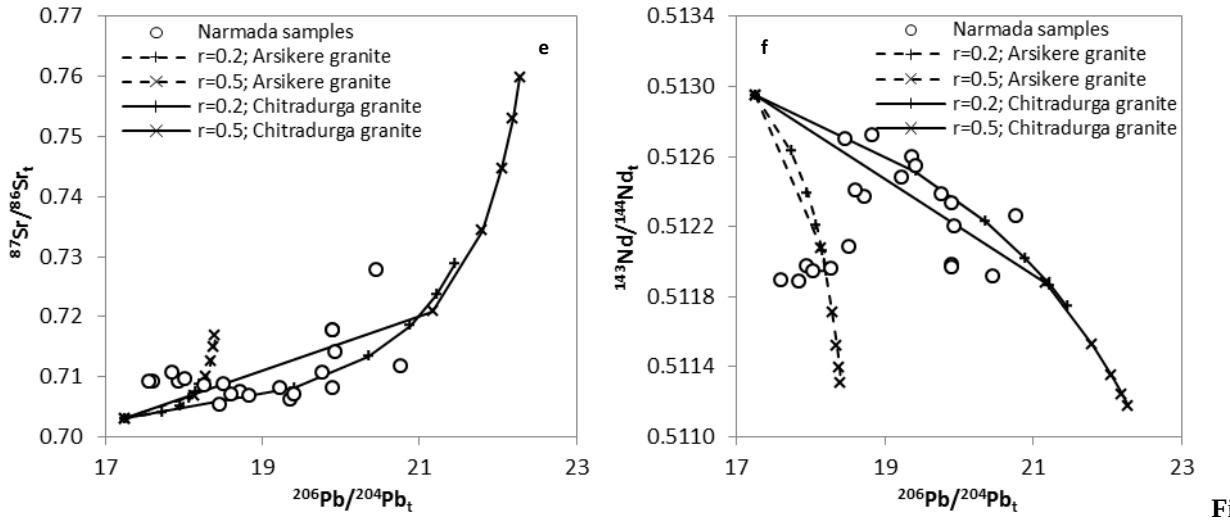

Fig. 8.7. AFC modeling using CIR-type magma as starting composition, and rocks from Dharwar and Aravalli cratons to reproduce Sr-Nd isotopic compositions of trend2 (a); rocks from Dharwar craton to reproduce Sr-Nd isotopic compositions of trend1 (b); Arsikere granite and Chitradurga granite (Dharwar cratons) as contaminants to reproduce Pb isotopic compositions of trend 1 and 2, respectively (c-f).

Similarly to what has been observed in the case where the Réunion magma was considered as initial composition, modeling crustal contamination by means of EC-AFC with Indian Ridge MORB as starting composition, yielded, on average, similar or slightly higher amounts of assimilation than AFC in reproducing Sr-Nd isotopic compositions, and lower amounts of assimilation in reproducing Pb isotopic compositions. In particular, using the contaminants from the second group, trend 2 is completely reproduced by either 20% assimilation of Banded Gneissic complex (Aravalli Craton), or 12% assimilation of Hoskote Kolar granite from the Dharwar Craton. Trend1can be modeled by 16% assimilation of the less enriched granite of the Dharwar Craton (Bangalore granite).

The modeling of Pb isotopic compositions requires lower amounts of assimilation: about 5% assimilation is required to reproduce PL compositions with high $^{208}Pb/^{204}Pb$ by contamination with the Chitradurga granite; whereas samples with high Δ7/4 can be reached with about 3% assimilation of trondhjemite or Arsikere granite of the Dharwar Craton (fig. 8.8b). In the comparison of Pb-Sr-Nd isotopic systems, the model doesn't reproduce samples of trend2 with lower $^{206}Pb/^{204}Pb$.

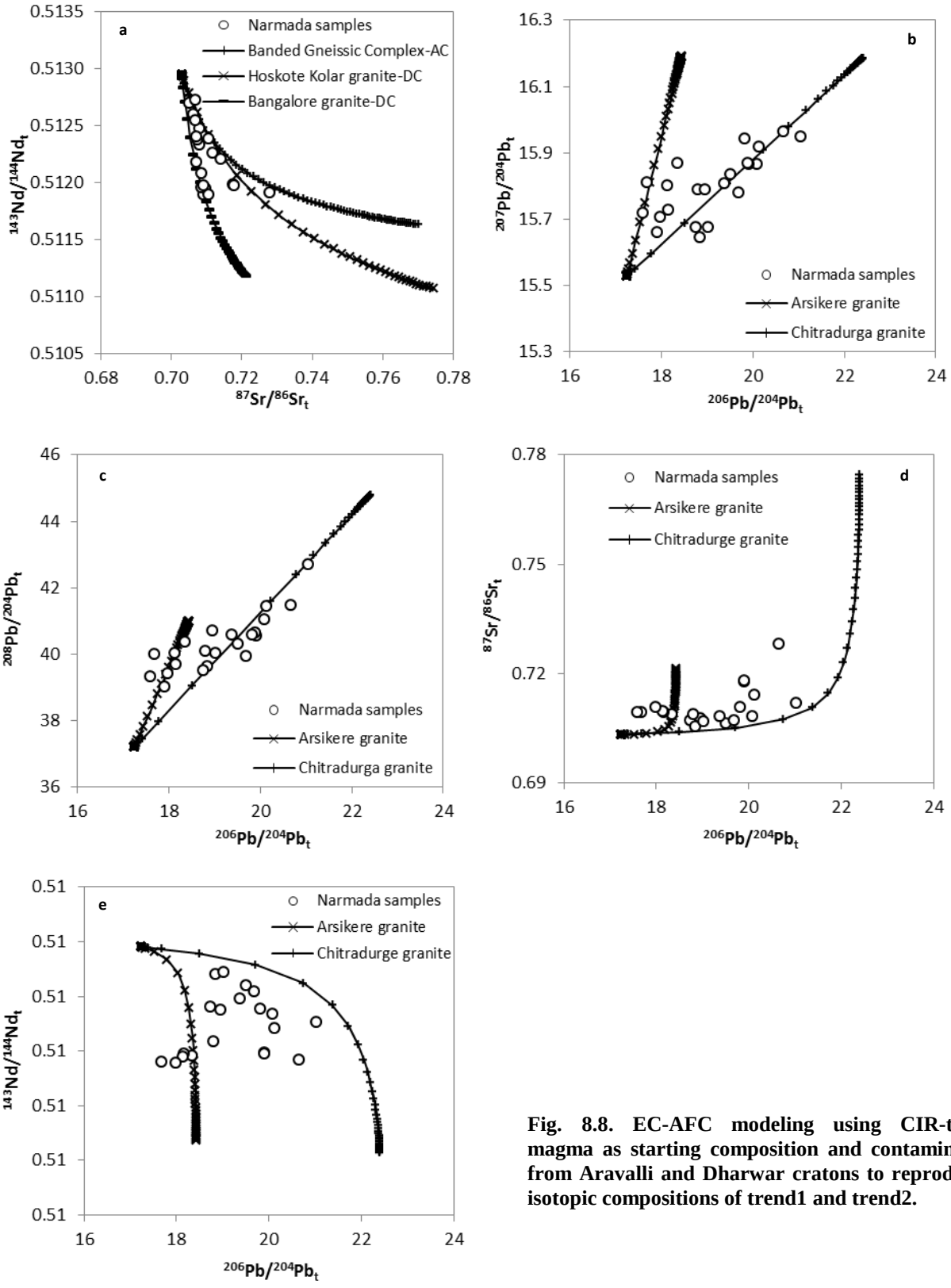

Fig. 8.8. EC-AFC modeling using CIR-type magma as starting composition and contaminant from Aravalli and Dharwar cratons to reproduce isotopic compositions of trend1 and trend2.

Crustal contamination can't completely describe the isotopic variability of the Narmada rocks.

An involvement of lower crust represented by the Southern Indian Granulite Terrain can be excluded, since it fails in reproducing Pb isotopic composition of trend1 both using Réunion-type starting magma and CIR composition.

When Réunion-type magma is considerd as starting composition, similar results have been obtained in modeling trend2 with AFC and EC-AFC, which yielded very different amounts of assimilation in reproducing Sr/Nd and Pb isotopic compositions. This difference suggests that crustal contamination can't account for the composition of trend2, at least with Réunion-like starting composition. However, it has to be considered that the the lack of agreement among different isotopic systems can be due to inappropriate choice of pairs of contaminants to model Sr-Nd and Pb isotopic. On the other hand, if CIR-like magma is taken as parental magma in the modeling of trend2, the different isotopic systems, even with different contaminants, yielded similar, albeit not identical, amounts of assimilation, more similar in AFC model (10% vs. 12%, if lower and more likely r values are considered), slightly more different in the case of EC-AFC model, but still comparable (12% vs. 6%). Conversely, the amounts of assimilation required to reproduce Sr/Nd isotopic compositions of trend1 are much higher (16%) than those required for Pb (3%).

Therefore the modeling suggests that crustal contamination can account for the isotopic composition of trend2 as a result of contamination of CIR-like parental magma with a granitic contaminant from the Dharwar Craton, which yielded lower amount of assimilation than those given by the contamination with Banded Gneissic complex of the Aravalli Craton.

CHAPTER 9.
MANTLE SOURCE

Given the discrepancy among the different isotopic systems in modeling crustal contamination, this process cannot account for the enriched character of the trend1 samples (Phenai Mata mafic tholeiites) that present low $^{143}Nd/^{144}Nd_t$ and high $^{207}Pb/^{204}Pb_t$ and $^{208}Pb/^{204}Pb_t$ at a given $^{206}Pb/^{204}Pb_t$. Therefore, these compositions are likely to be due to the mantle source of such samples. Mantle components which are typically characterized by enriched isotopic compositions are Enriched Mantle I and II (EMI and EMII; Zindler and Hart, 1986). We therefore used these mantle poles as end-member compositions in a pseudo-binary mixing modeling (Douglass and Schilling, 2000). Since the definition of the EM-II and in particular EM-I mantle components is not univocal/very constrained, the most enriched compositions reported so far (Zindler and Hart, 1986; Stracke et al., 2012) have been used in the modeling for the Narmada samples. Besides these enriched end-members, the third pole may be represented either by a Reunion-like composition, i.e. a mantle-plume component, or by a DMM, i.e. upper mantle component (table 1). However, the modeling with such components fails to reproduce the observed data. In particular, while an involvement of EMI and EMII could be consistent with the Sr and Nd isotopic compositions, these components are not enriched enough (in $^{207}Pb/^{204}Pb$ and $^{208}Pb/^{204}Pb$) to explain the observed Pb isotopic compositions (fig. 9.1).

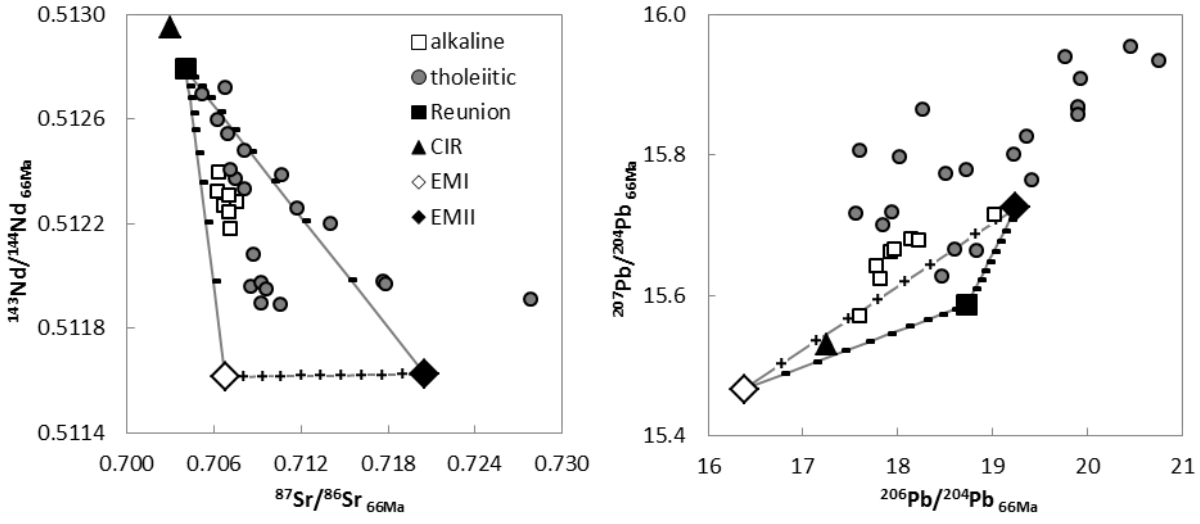

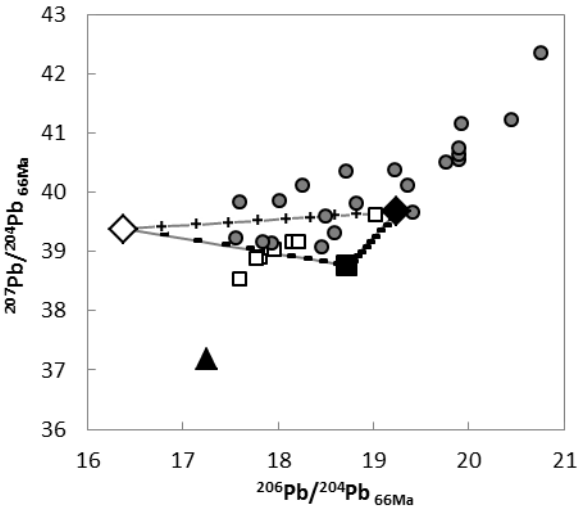

Fig. 9.1. Plot of $^{87}Sr/^{86}Sr$ vs. $^{143}Nd/^{144}Nd$, and $^{206}Pb/^{204}Pb$ vs. $^{207}Pb/^{204}Pb$, and $^{208}Pb/^{204}Pb$, showing the pseudo-binary mixing line resulting from the modeling with Reunion (Fisk et al., 1988), EMI and EMII as end-member compositions.

Table1.

	$^{87}Sr/^{86}Sr_t$	Sr	$^{143}Nd/^{144}Nd_t$	Nd	$^{206}Pb/^{204}Pb_t$	$^{207}Pb/^{204}Pb_t$	$^{208}Pb/^{204}Pb_t$	Pb
Reunion	0.704046	89	0.512793	8	18.73	15.57	38.76	0.135
DMM-ClR	0.70302	7.7	0.51295	0.6	17.25	15.53	37.19	0.02
EMI	0.706752	23.88	0.511614	2	16.38	7	39.38	0.072
EMII	0.72054	21.89	0.511625	2	19.25	15.73	39.67	0.105

Trace elements and isotopic composition used for pseudo-binary mixing. Trace elements are expressed in ppm, and from Willbold and Stracke (2010), Workmann and Hart (2005), and Stracke et al. (2003); isotopic compositions are corrected at 66Ma, and from Zindler and Hart (1986), Stracke et al. (2012), Fisk et al. (1988), and Price et al. (1986).

The isotopic composition displayed by EMI and EMII has been explained by Stracke (2012) as the result of interaction between recycled oceanic lithosphere and lower and upper continental crust, respectively. The author showed that about 20% of each crust is required to reproduce the compositions of Pitcairn and Samoa islands which are representative of EMI and EMII end-members, respectively. Therefore, a stronger contribution of the continental crusts in the mantle could result in even more enriched mantle components and account for the observed high Δ7/4 and Δ8/4. We therefore calculated the isotopic composition of upper and lower crustal rocks (UC and LC, respectively) of ca. 2.5 Ga, corresponding to the age of the Indian cratons. This composition was calculated assuming that the crust formed from a primitive mantle (recalculated to 2.5 Ga) and successively evolved by radioactive decay until 66 Ma. These UC and LC compositions have then been used as new poles in the pseudo-binary mixing model. In the Sr-Nd isotopic space, the compositions of the samples can be explained with the involvement of lower and upper crust, but again the obtained Pb isotopic composition are not enriched enough, especially in the case of $^{208}Pb/^{204}Pb_t$ (fig. 9.2). I.e. the calculated UC and LC compositions are apparently too low in Th.

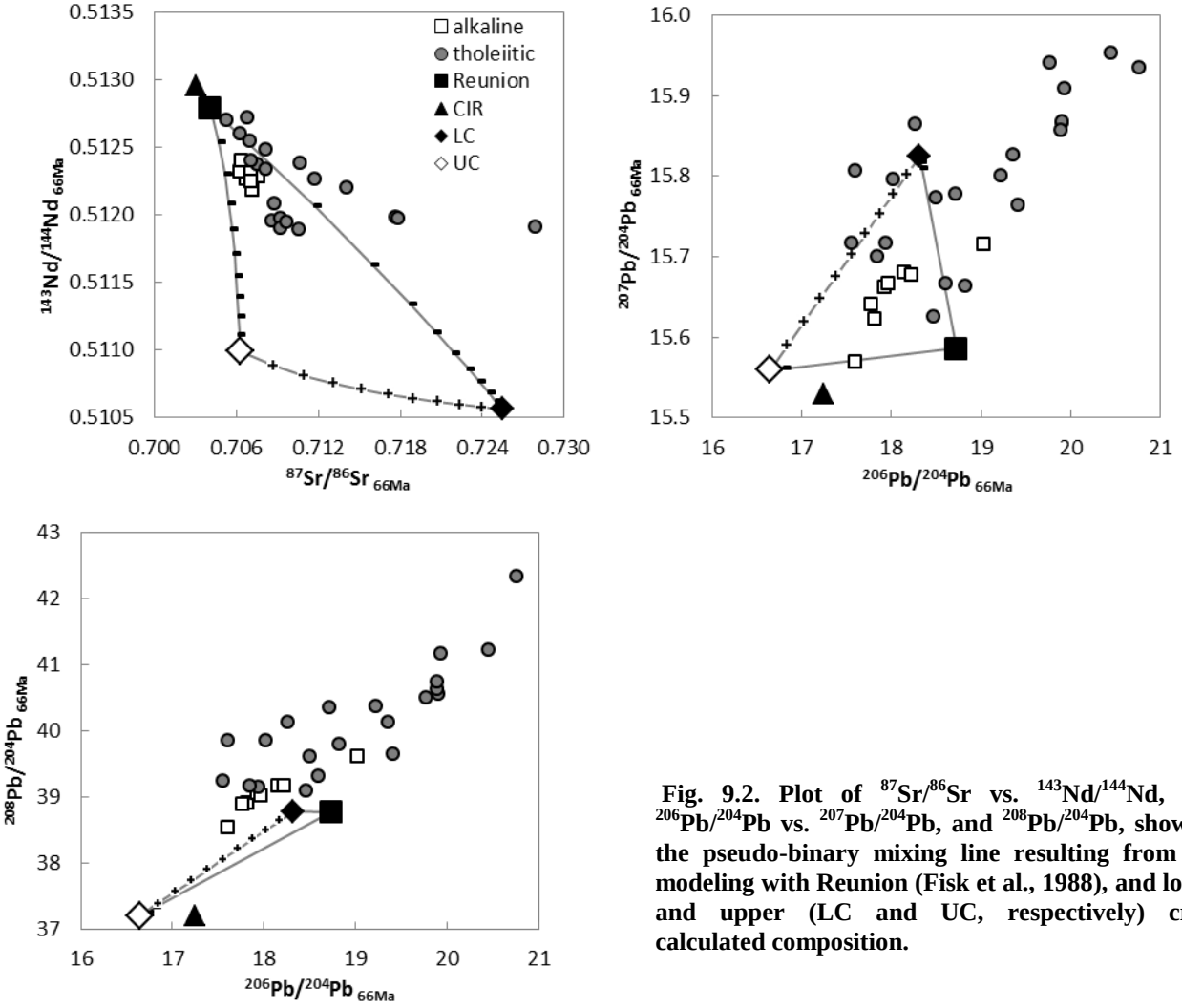

Fig. 9.2. Plot of $^{87}Sr/^{86}Sr$ vs. $^{143}Nd/^{144}Nd$, and $^{206}Pb/^{204}Pb$ vs. $^{207}Pb/^{204}Pb$, and $^{208}Pb/^{204}Pb$, showing the pseudo-binary mixing line resulting from the modeling with Reunion (Fisk et al., 1988), and lower and upper (LC and UC, respectively) crust calculated composition.

Walvis Ridge basalts have been considered to represent the EMI component end-member, together with Pitcairn island (Salters et al., 2010). Salters et al. (2013) proposed a three stage model active during the early stages of Earth evolution for the formation of Walvis Ridge mantle source. However, even these calculated compositions (e.g., $^{206}Pb/^{204}Pb_t$ = 16.69, $^{207}Pb/^{204}Pb_t$ =15.75, and $^{208}Pb/^{204}Pb_t$ =36.98) fail to reproduce of the Pb isotopic composition of Phenai Mata rocks, even considering the most extreme combination of age and μ. Once again, the major problem with this model resides in the $^{208}Pb/^{204}Pb_t$ ratio which is much more depleted than that observed in Phenai Mata mafic rocks.

The close association of the Phenai Mata tholeiites with alkaline rocks outcropping in the same complex, can suggest a genetic relationship between them. If the alkaline rocks are interpreted as product of interaction of the plume with the subcontinental lithospheric mantle (SCLM), the isotopic composition of the Phenai Mata rocks, which are more enriched than the

alkaline ones, should point to a greater contribution of the SCLM. But also in this case, Phenai mata sub-alakaline rocks yield isotopic compositions that are much more enriched than other SCLM-derived alkaline rocks from India, and worldwide (fig. 9.3).

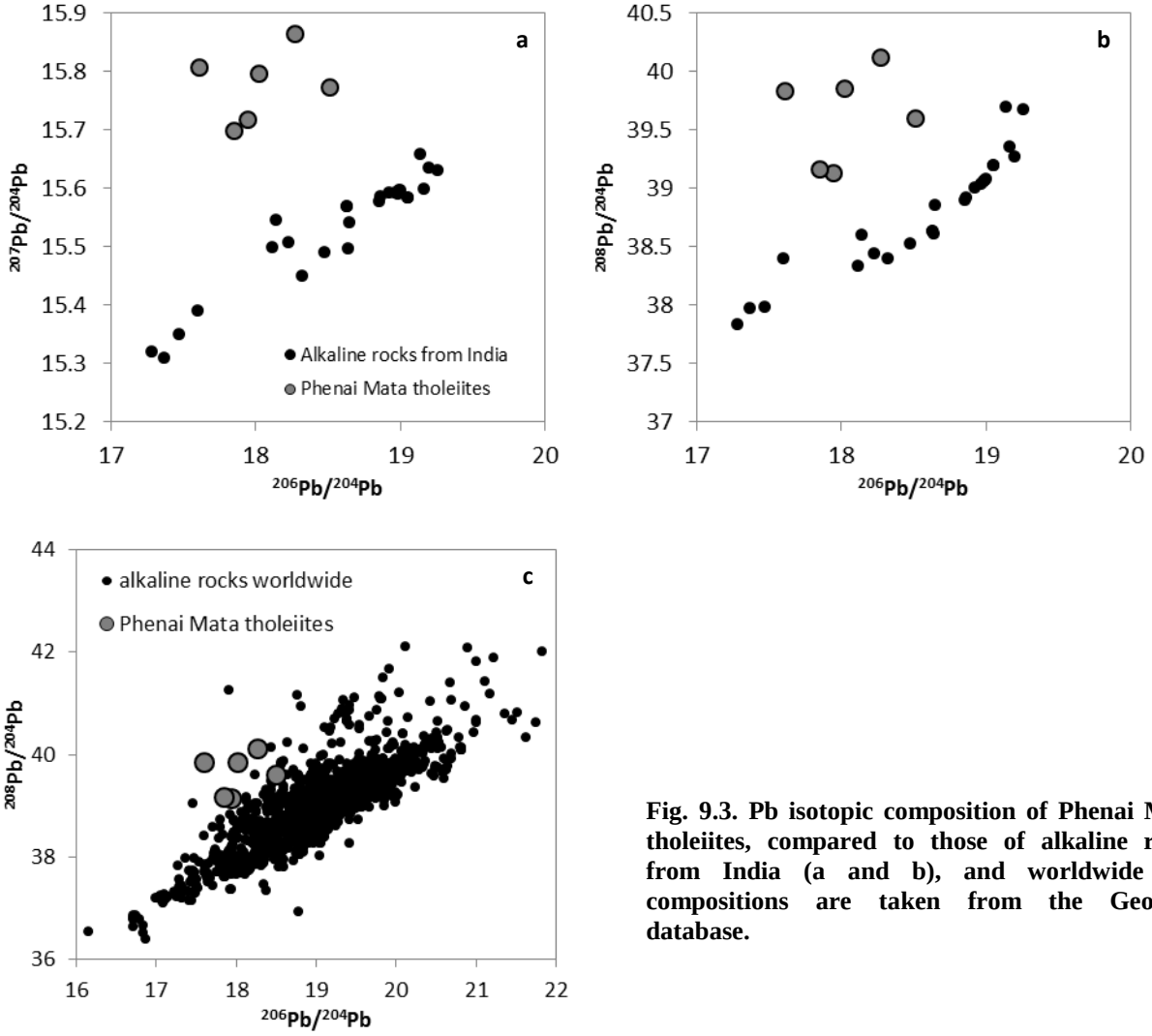

Fig. 9.3. Pb isotopic composition of Phenai Mata tholeiites, compared to those of alkaline rocks from India (a and b), and worldwide (c); compositions are taken from the Georock database.

Basalts form the Elan Bank (central Kerguelen Plateau), are tholeiitic rocks which show enriched Pb isotopic composition (even if not as enriched as those of Phenai Mata rocks), and for which magma contamination by continental crust has been suggested as an AFC process (Weis et al., 2001; Ingle et al., 2002). While an AFC-type assimilation of the local continental crust does not reproduce the Phenai Mata data (cf. chapter 8), the Kerguelen data point still to a crustal component to explain high Δ7/4 and Δ8/4 values. Unlike the calculated compositions of Salters et al. (2013), this crustal component needs high Th concentration, in order to achieve high time-integrated $^{208}Pb/^{204}Pb$ compositions. It has been recognized that sediments are rich in Th, and

particularly high contents are observed in mature, weathered rocks where U is preferentially leached relative to Th (Plank et al., 1998). The recycling of sediments from an ancient basin (2-2.5Ga), with a reasonable Th content of 20 ppm (Rudnick and Fountain, 1995) would be develop sufficiently high $^{208}Pb/^{204}Pb$ and constitute the enriched component to account for the peculiar isotopic composition of the Phenai Mata tholeiites.

CHAPTER 10.
CONCLUSIONS

A comprehensive study of both tholeiitic and alkaline rocks from the northern region of the Deccan Traps (Narmada) allowed to recognize the different processes responsible for their formation, and to recognize the (isotopically) most enriched compositions reported so far.

Through $^{40}Ar/^{39}Ar$ dating on mineral separates, two different pulses have been distinguished for the Narmada magmatism, one at ca. 66.5 Ma and the second at ca. 65.2 Ma. A alkaline rocks in particular belong to both pulses, thus indicating that they also formed during the main peak of Deccan volcanism (66Ma) and not only before and after it, as previously indicated. Moreover, these data strongly suggest a clear overlap in time (and thus a possible causal link) between the emplacement of the province and the Cretaceous/Paleogene mass extinction, with implication on the role played by the alkaline rocks which can be defined with further investigations.

The Narmada alkaline rocks present trace element patterns comparable to those of other alkaline complexes in the north (Bhuj, Mundwara), and in the south (Murud) of the province, as well as to carbonatite complexes of Amba Dongar, and Sung Valley (northeast India). Conversely they present slightly different isotopic compositions, more enriched with respect to all other Deccan-related alkaline complexes. The enrichment in incompatible element and isotopic compositions point toward the interaction between a mantle plume and an enriched lithospheric mantle, with dominant contribution of the latter in the generation of the Narmada alkaline rocks.

For the generation of the subalkaline rocks, two different processes have been proposed. The most enriched (and most evolved, mostly acid) samples are the result of crustal contamination with granitic contaminant from the Dharwar craton. Mafic subalkaline rocks, notably those from the Phenai Mata intrusion, displaying lower Sr isotopic composition, are characterized by very high $^{207}Pb/^{204}Pb$ and $^{208}Pb/^{204}Pb$which would require the involvement in the mantle source of a contribution of recycled sediments, since any other component cannot explain the extreme enriched composition. However, further Os isotopic analyses on such samples are in progress and will help to better constrain the mantle source vs crustal contamination processes.

References.

ALBAREDE, F., LUAIS, B., FITTON, G., SEMET, M., KAMINSKI, E., UPTON, B. G. J., BACHELERY, P., CHEMINEE, J. L., 1997. The geochemical regimes of Piton de la Fournaise Volcano (Reunion) during the last 530000 years. *Journal of Petrology*, 38, 171-201.

ALLEGRE, C.J., BIRCK, J.L., CAPMAS, F., COURTILLOT, V., 1999. Age of the Deccan traps using ^{187}Re–^{187}Os systematics. *Earth and Planetary Science Letters*, 170, 197–204.

AZMI, R.J., JOSHI, D., TEWARI, B.N., JOSHI, M.N., SRIVASTAVA, S.S., 2008. A synoptic view on the current discordant geo- and biochronological ages of the Vindhyan Supergroup, central India. *Journal of Himalayan Geology*, 29, 177–191.

BAKSI, A.K., 2013. The Deccan Trap – Cretaceous–Paleogene boundary connection; new $^{40}Ar/^{39}Ar$ ages and critical assessment of existing argon data pertinent to this hypothesis. *Journal of Asian Earth Sciences*, http://dx.doi.org/10.1016/j.jseaes.2013.08.021.

BAKSI, A.K., ARCHIBALD, D.A,. FARM, E., 1996. Intercalibration of $^{40}Ar/^{39}Ar$ dating standards. *Chemical Geology*, 129, 307-324.

BAKSI, A.K., 1994. Geochronological studies on whole-rock basalts, Deccan Traps, India: evaluation of the timing of volcanism relative to the K-T boundary. *Earth and Planetary Science Letters*, 121, 43-56.

BAKSI, A.K., 1987. Critical evaluation of the age of the Deccan Traps, India: Implications for flood-basalt volcanism and faunal extinctions. *Geology*, 15,147-150.

BALAKRISHNAN, S., HANSON, G.N., RAJAMANI, V., 1990. Pb and Nd isotope constraints on the origin of high Mg and tholeiitic amphibolites, Kolar Schist Belt, South India. *Contribution to Mineralogy and Petrology*, 107, 279-292.

BANDOPADHYAY, P.C., SENGUPTA, S., 2004. The Paleoproterozoic supracrustal Kolhan Group in Singhbhum Craton, India and the Indo-African supercontinent. *Gondwana Research, Japan*, 7, 1228–1235.

BANDYOPADHYAY, B. K., CHATTOPADHYAY, A., KAHN A. S., HUIN, A. K., 2001. Assembly of the Rodinia Supercontinent: evidence from the Sakoli and Sausar Belts in Central India. *Gondwana Research*, 4, 569-570.

BASU, A., PATRANABIS-DEB, S., SCHIEBER, J., DHANG, P.C., 2008. Stratigraphic position of the 1000 Ma Sukhda Tuff (Chattisgarh Supergroup, India) and the 500 Ma question. *Precambrian Research*, 167, 383–388.

BASU, A. R., RENNE, P. R., DASGUPTA, D.K., TEICHMANN F., POREDA, R.J., 1993. Early and late alkali igneous pulses and a high-^{3}He plume origin for the Deccan flood basalts. *Science*, 261, 902-906.

BAXTER, A. N., 1990. Major and trace element variations in basalts from Leg 115. In: Duncan, R. A., Backman, J., Peterson, L. C., et al. (eds) *Proceedings of the Ocean Drilling Program, Scientific Results*, 115. College Station, TX: Ocean Drilling Program, pp. 11–21.

BEANE, J.E., TURNER, C.A., HOOPER, P.R., SUBBARAO, K.V., WALSH, J.N., 1986. Stratigraphy, composition and form of the Deccan Basalts, Western Ghats, India. *Bulletin of Volcanology*, 48, 61-83.

BELL, K., SIMONETTI, A., 1996. Carbonatite magmatism and plume activity: implications from the Nd, Pb and Sr isotope systematics of Oldoinyo Lengai. *Journal of Petrology*, 37, 1321–1339.

BERNARD-GRIFFITHS, J., JAHN, B.M., SEN, S.M., 1987. Sm–Nd isotopes and REE geochemistry of Madras granulites: an introductory statement. *Precambrian Research*, 37, 343–355.

BHATTACHARYA, S., CHAUDHARY, A. K.,. SAW, A. K, DAS, P., CHATTERJEE, D., 2012. Mafic granulite xenoliths in the Chilka Lake suite, Eastern Ghats Belt, India: evidence of deep-subduction of residual oceanic crust. *Solid Earth Discussions*, 4, 1379–1410.

BHATTACHARYYA, P. K., BHATTACHARYA, H. N., MUKHERJEE, A. D., 1988. The Chitradurga greenstone succession in south India and evolution of the late Archaean basin. *Geological Magazine*, 125, 5 507-519.

BOHRSON, W. A., SPERA, F. J., 2001. Energy-constrained open-system magmatic processes II: application of Energy-Constrained Assimilation and Fractional Crystallization (EC-AFC) model to magmatic systems. *Journal of Petrology*, 42, 1019-1041.

BOSCH, D., BLICHERT-TOFT, J., MOYNIER, F., NELSON, B.K., TELOUK, P.H., GILLOT, P.Y., ALBAREDE, F., 2008. Pb, Hf and Nd isotope compositions of the two Reunion volcanoes (Indian Ocean): a tale of two smallscale mantle ‘‘blobs’’? *Earth and Planetary Science Letters*, 265, 748–768.

BRAUN, I., CENKI-TOK, B., PAQUETTE, J.L., TIEPOLO, L., 2007. Petrology and U–Th–Pb geochronology of the sapphirine–quartz-bearing metapelites from Rajapalayam, Madurai Block, southern India: evidence for polyphase Neoproterozoic highgrade metamorphism. *Chemical Geology*, 241, 129–147.

BUICK, I.S., ALLEN, C., PANDIT, M., RUBATTO, D., HERMANN, J., 2006. The Proterozoic magmatic and metamorphic history of the banded gneiss complex, central Rajasthan, India; LA-ICP-MS U/Pb zircon constraints. *Precambrian Research*, 151, 119–142.

CANDE, S. C., KENT, D. V., 1992. A New Geomagnetic Polarity Time Scale for the Late Cretaceous and Cenozoic. *Journal of Geophysical Research*, 97, 13917-13951.

CANDE, S. C., KENT, D. V., 1995. Revised calibration of the geomagnetic polarity timescale for the Late Cretaceous and Cenozoic. *Journal of Geophysical Research*, 100, 6093-6095.

CARLSON, R.W., IRVING, A.J., 1994. Depletion and enrichment history of subcontinental lithospheric mantle: an Os, Sr, Nd, and Pb isotopic study of ultramafic xenolith from the northwestern Wyoming Craton. *Earth and Planetary Science Letters*, 126, 457-472.

CHALAPATHI RAO, N. V., GIBSON, S. A., PYLE D.M., DICKIN, A. P., 2004. Petrogenesis of Proterozoic Lamproites and Kimberlites from the Cuddapah Basin and Dharwar Craton, Southern India. *Journal of Petrology*, 45, 907-948.

CHANDRASEKHARAM, D., MAHONEY, J.J., SHETH, H.C., DUNCAN, R.A., 1999. Elemental and Nd-Sr-Pb isotope geochemistry of flows and dikes from the Tapi rift, Deccan flood basalt province, India. *Journal of Volcanology and Geothermal Research*, 93, 111-123.

CHATTERJEE, N., BHATTACHARJI, S., 2001. Petrology, geochemistry and tectonic settings of the mafic dykes and sills associated with the evolution of the Proterozoic Cuddapah basin of south India. *Proceedings of the Indian Academy of Sciences. Earth and Planetary Science*, 110, 433–453.

CHAUDHURI, A.K., 2003. Stratigraphy and paleogeography of the Godavari Supergroup in the south-central Pranhita-Godavari Valley, south India. *Journal of Asian Earth Sciences*, 21, 595–611.

CHAUDHURI, A.K., SAHA, D., DEB, G.K., DEB, S.P., MUKHERJEE, M.K., GHOSH, G., 2002. The Purana basins of southern cratonic province of India; a case for Mesoproterozoic fossil rifts. *Gondwana Research*, 5, 23–33.

CHENET, A. L., COURTILLOT, V., FLUTEAU, F., GERARD, M., QUIDELLEUR, X., KHADRI, S. F. R., SUBBARAO, K.V., THORDARSON, T., 2009. Determination of rapid Deccan eruptions across the Cretaceous-Tertiary boundary using paleomagnetic secular variation: 2. Constraints from analysis of eight new sections and synthesis for a 3500-m-thick composite section. *Journal of Geophysical Research*, 114, B06103, doi:10.1029/2008JB005644.

CHENET, A. L., FLUTEAU, F., COURTILLOT, V., GERARD, M., SUBBARAO, K.V., 2008. Determination of rapid Deccan eruptions across the Cretaceous-Tertiary boundary using paleomagnetic secular variation: Results from a 1200-m-thick section in the Mahabaleshwar escarpment. *Journal of Geophysical Research*, 113, B04101, doi:10.1029/2006JB004635.

CHENET, A. L., QUIDELLEUR, X., FLUTEAU, F., COURTILLOT, V., BAJPAI, S., 2007. ^{40}K–^{40}Ar dating of the Main Deccan large igneous province: Further evidence of KTB age and short duration. *Earth and Planetary Science Letters*, 263, 1–15.

CHOUDHARY, A.K., GOPALAN, K., SASTRY, C.A., 1984. Present status of the geochronology of the Precambrian rocks of Rajasthan. *Tectonophysics*, 105, 131–140.

CLARK, C., COLLINS, A.S., TIMMS, N.E., KINNY, P.D., CHETTY, T.R.K., SANTOSH, M., 2009. SHRIMP U–Pb age constraints on magmatism and high-grade metamorphism in the Salem Block, southern India. *Gondwana Research*, 16, 27–36.

COLLIER, J.S., SANSOM, V., ISHIZUKA, O., TAYLOR, R.N., MINSHULL, T.A., WHITMARSH, R.B., 2008. Age of Seychelles–India break-up. *Earth and Planetary Science Letters*, 272, 264-277.

COLLINS, A.S., SANTOSH, M., BRAUN, I., CLARK, C., 2007. Age and sedimentary provenance of the southern granulites, S. India: U–Th–Pb SHRIMP secondary ion mass spectrometry. *Precambrian Research*, 155, 125–138.COURTILLOT, V., RENNE, P. R., 2003. On the ages of flood basalt events. *Comptes Rendus Geoscience*, 335, 113–140.

COURTILLOT, V., GALLET, Y., ROCCHIA, R., FERAUD, G., ROBIN, E., HOFMANN, C., BHANDARI, N., GHEVARIYA Z.G., 2000. Cosmic markers, $^{40}Ar/^{39}Ar$ dating and paleomagnetism of the KT sections in the Anjar Area of the Deccan large igneous province. *Earth and Planetary Science Letters*, 182, 137-156.

COURTILLOT, V., FERAUD, G., MALUSKI, H., VANDAMME, D., MOREAU, M.G., BESSE, J., 1988. Deccan flood basalts and the Cretaceous/Tertiary boundary. *Nature*, 333, 843-846.

COURTLLLOT, V., BESSE, J., VANDAMME, D., MONTIGNY, R., JAEGER, J.-J., CAPPETTA, H., 1986. Deccan flood basalts at the Cretaceous/Tertiary boundary? *Earth and Planetary Science Letters*, 80, 361-374.

COX, K. G., HAWKESWORTH, C. J., 1984. Relative Contribution of Crust and Mantle to Flood Basalt Magmatism, Mahabaleshwar Area, Deccan Traps. *Phil. Trans. R. Soc. Lond. A,* 310, 627-641.

COX, K. G., HAWKESWORTH, C. J., 1985. Geochemical Stratigraphy of the Deccan Traps at Mahabaleshwar, Western Ghats, India, with Implications for Open System Magmatic Processes. *Journal of petrolgy*, 24. Part 2, 355-377.

DAS, K., YOKOYAMA, K., CHAKRABORTY, P.P., SARKAR, A., 2009. Basal tuffs and contemporaneity of the Chattisgarh and Khariar basins based on new dates and geochemistry. *Journal of Geology*, 117, 88–102.

DEB, S.P., 2004. Lithostratigraphy of the Neoproterozoic Chhattisgarh sequence: its bearing on the tectonics and paleogeography. *Gondwana Research*, 7, 323–337.

DEB, M., THORPE, R.I., KRSTIC, D., CORFU, F., DAVIS, D.W., 2001. Zircon U–Pb and galena Pb isotopic evidence for an approximate 1.0 Ga terrane constituting the western margin of the Aravalli-Delhi orogenic belt, northwestern India. *Precambrian Research*, 108, 195–213.DE PAOLO, D. J., 1981. Trace elements and isotopic effects of combined wallrock assimilation and fractional crystallization. *Earth and Planetary Science Letters*, 53, 189-202.

DESSAI, A. G., DOWNES, H., LOPEZ-MORO, F.-J., LOPEZ-PLAZA, M., 2008. Lower crustal contamination of Deccan Traps magmas: evidence from tholeiitic dykes and granulite xenoliths from western India. *Mineral. Petrol.*, 93, 243-272.

Dessai, A.G., Markwick, A., Vaselli, O., Downes, H., 2004. Granulite and pyroxenite xenoliths from the Deccan Trap: insight into the nature and composition of the lower lithosphere beneath cratonic India. *Lithos*, 74, 263-290.

DESSAI, A. G., VASELLI, O., 1999. Petrology and geochemistry of xenoliths in lamprophyres from the Deccan Traps: implications for the nature of the deep crust boundary in western India. *Mineralogical Magazine*, 63, 703-722.

DEVEY, C. W., and STEPHENS, W. E., 1992. Deccan-related magmatism west of the Seychelles-India rift. *Geological Society, London, Special Publications*, 68, 271-291.

DEVEY, C.W., and COX, K.G., 1987. Relationships between crustal contamination and crystallization in continental flood basalt magmas with special reference to the Deccan Traps of the Western Ghats, India. *Earth and Planetary Science Letters*, 84, 59-68.

DE WIT, M.J., GHOSH, J.G., BOWRING, S., ASHWAL, L.D., 1998. Late Neoproterozoic shear zones in Madagascar, and India: Gondwana ‘‘life-lines”. *Journal of African Earth Sciences*, 27, 58–67.

DEY, S., PANDEY, U.K., RAI, A.K., CHAKI, A., 2012. Geochemical and Nd isotope constraints on petrogenesis of granitoids from NW part of the eastern Dharwar craton: Possible implications for late Archaean crustal accretion. *Journal of Asian Earth Sciences*, 45, 40–56.

DEY, S., RAI, A.K., CHAKI, A., 2009. Palaeoweathering, composition and tectonics of provenance of the Proterozoic intracratonic Kaladgi–Badami basin, Karnataka, southern India: evidence from sandstone petrography and geochemistry. *Journal of Asian Earth Sciences*, 34, 703–715.

DOUGLASS, J., SCHILLING, J.-G., 2000. Systematics of three-component, pseudo-binary mixing lines in 2D isotope ratio space representations and implications for mantle plume-ridge interaction. *Chemical Geology*, 163, 1-23.

DUNCAN, R. A., 1990. The volcanic record of the Reunion hotspot. In: Duncan, R. A., Backman, J., Peterson, L. C., (eds) et al. *Proceedings of the Ocean Drilling Program, Scientific Results*, 115. College Station, TX: Ocean Drilling Program, pp. 3–10.

DUNCAN, R.A., PYLE, D.G., 1988. Rapid eruption of the Deccan flood basalts at the Cretaceous/Tertiary boundary. *Nature*, 333, 841-833.

ELDHOM, O. AND COFFIN, M.F. (2000). In: *Large igneous provinces and plate tectonics*. American Geophysical Union, Washington D.C.. 121: 5-6. doi: 10.1029/GM121p0309.

ERIKSSON, P.G., MAZUMDER, R., CATUNEANU, O., BUMBY, A.J., ILONDO, B.O., 2006. Precambrian continental freeboard and geological evolution: a time perspective. *Earth-Science Reviews*, 79, 165–204.

FISK, M. R., UPTON, B. G. J., FORD, C. E., WHITE, W. M., 1988. Geochemical and experimental study of the genesis of magmas of Reunion Island, Indian Ocean. *Journal of Geophysical Research*, 93, 4933–4950.

FRENCH, J.E., HEAMAN, L.M., CHACKO, T., RIVARD, B., 2008. 1891–1883 Ma southern Bastar craton-Cuddapah mafic igneous events, India: a newly recognized large igneous province. *Precambrian Research*, 160, 308–322.

FRIEND, C.R.L., NUTMAN, A.P., 1991. SHRIMP U–Pb Geochronology of the Closepet Granite and Peninsular Gneiss, Karnataka, South India. *Journal of the Geological Society of India*, 38, 357–368.

GOPALAN, K., MACDOUGALL, J.D., ROY, A.B., MURALI, A.V., 1990. Sm-Nd evidence for 3.3 Ga old rocks in Rajasthan, northwestern India. *Precambrian Research*, 48, 287-297.

GREENOUGH, J. D., HARI, K. R., CHATTERJEE, A. C., SANTOSH, M., 1998. Mildly alkaline basalts from Pavagadh Hill, India: Deccan flood basalts with an asthenospheric origin. *Mineralogy and Petrology*, 62, 223-245.

GREGORY, L.C., MEERT, J.G., PRADHAN, V., PANDIT, M.K., TAMRAT, E., MALONE, S.J., 2006. A paleomagnetic and geochronologic study of the Majhgawan Kimberlite, India: implications for the age of the Vindhyan Supergroup. *Precambrian Research*, 149, 65–75.

GWALANI, L.G., ROCK, N.M.S., CHANG, W.-J., FERNANDEZ, S., ALLEGRE, C.J., PRINZHOFER, A. 1993. Alkaline rocks and carbonatites of Amba Dongar and adjacent areas, Deccan igneous province, Gujarat, India: 1. Geology, petrography and petrochemistry. *Mineralogy and Petrology* 47, 219-253.

HAGGERTY, S. E., BIRKETT, T., 2004. Geological setting and chemistry of kimberlite clan rocks in the Dharwar Craton, India. *Lithos*, 76, 535-549.

HARI, K. R., CHALAPATHI RAO, N. V., SWARNKAR, V., 2011. Petrogenesis of Gabbro and Orthopyroxene Gabbro from the Phenai Mata Igneous Complex, Deccan Volcanic Province: Products of Concurrent Assimilation and Fractional Crystallization. *Journal of Geological Society of India*, 78, 501-509.

HARRIS, N.B.W., SANTOSH, M., TAYLOR, P.N., 1994. Crustal evolution in southern India: constraints from Nd isotopes. *Journal of Geology*, 102, 139–150.

HILDEBRAND, A.R., PENFIELD, G.T., KRING, D.A., PILKINGTON, M., CAMARGO, A., JACOBSEN, S.B., BOYNTON, W.V., 1991. Chicxulub crater: a possible Cretaceous/Tertiary boundary impact crater on the Yucatan Peninsula, Mexico. *Geology*, 19, 867–871.

HOFMANN, C., FERAUD, G., COURTILLOT, V., 2000. $^{40}Ar/^{39}Ar$ dating of mineral separates and whole rocks from the Western Ghats lava pile: further constraints on duration and age of the Deccan traps. *Earth and Planetary Science Letters*, 180, 13-27.

HOOPER, P., WIDDOWSON, M., KELLEY, S., 2010. Tectonic setting and timing of the final Deccan flood basalt eruptions. *Geology*, 38, 839-842.

HOOPER, P.R. (I 990). The timing of crustal extension and the eruption of continental flood basalts. *Nature*, 345, 246-249.

HUSSAIN, M.F., MONDALL, M.E.A., AHMAD, T., 2004. Petrological and Geochemical Characteristics of Archean Gneisses and Granitoids from Bastar Craton, Central India - Implication for Subduction Related Magmatism. *Gondwana Research*, 7, 531 -537.

INGLE, S., WEIS, D., FREY, F. A., 2002. Indian continental crust recovered from Elan Bank, Kerguelen plateau (ODP Leg 183, Site 1137). *Journal of Petrology*, 43, 1241-1257.

INGLE, S., WEIS, D., FREY, F. A., J. S., SCOATES, FREY, F. A., 2002. Relationship between the early Kerguelen plume and continental flood basalts of the paleo-Eastern Gondwanan margins. *Earth and Planetary Science Letter*, 197, 35-50.

JAYANANDA, M., CHARDON, D., PEUCAT, J.-J., CAPDEVILA, R., 2006. 2.61 Ga potassic granites and crustal reworking in the western Dharwar craton, southern India: Tectonic, geochronologic and geochemical constraints. *Precambrian Research*, 150, 1-26.

JAYANANDA, M., MOYEN, J.-F., MARTIN, H., PEUCAT, J.-J., AUVRAY, B., MAHABALESWAR, B., 2000. Late Archaean (2550-2520 Ma) juvenile magmatism in the Eastern Dharwar craton, southern India: constraints from geochronology, Nd-Sr isotopes and whole rock geochemistry. *Precambrian Research*, 99, 225-254.

JAYANANDA, M., MARTIN, H., J.J., PEUCAT, MAHABALESHWAR, B., 1995. Late Archean crust-mantle interactions: geochemistry of LREE-enriched mantle derived magmas. Example of the Closepeth Batholith, southern India. *Contribution to Mineralogy and Petrology*,119, 314-329.

JOURDAN, F., RENNE, P. R., 2007. Age calibration of the Fish Canyon sanidine $^{40}Ar/^{39}Ar$ dating standard using primary K–Ar standards. *Geochimica et Cosmochimica Acta*, 71, 387–402.

KANEOKA, I., 1980. $^{40}Ar/^{39}Ar$ dating on volcanic rocks of the Deccan Traps, India. *Earth and Planetary Science Letters*, 46, 233-243.

KARMALKAR, N.R., REGE S., GRIFFIN, W.L., O'REILLY, S. Y., 2005. Alkaline magmatism from Kutch, NW India: Implications for plume-lithosphere interaction. *Lithos*, 81, 101- 119.

KAUR, P., CHAUDHARI, N., RACZEK, I., KRÖNER, A., HOFMANN, A.W., 2007. Geochemistry, zircon ages and whole-rock Nd isotopic systematic for Paleoproterozoic A-type granitoids in the northern part of the Delhi belt, Rajasthan, NW India: implications for late Paleoproterozoic crustal evolution of the Aravalli craton. *Geological Magazine*, 144, 361–378.

KELLER, G., BHOWMICK, P.K., UPADHYAY, H., DAVE, A., REDDY, A.N., JAIPRAKASH, B.C., ADATTE, T., 2011. Deccan Volcanism linked to the Cretaceous-Tertiary Boundary mass extinction: new evidence from ONGC wells in the Krishna-Godavari Basin. *Journal Geological Society of India*, 78, 399-428.

KELLER, G., ADATTE, T., BAJPAI, S., MOHABEY, D.M., WIDDOWSON, M., KHOSLA, A,. SHARMA, R., KHOSLA, S.C., GERTSCH, B., FLEITMANN, D., SAHN, A., 2009. K–T transition in Deccan Traps of central India marks major marine seaway across India. *Earth and Planetary Science Letters*, 282, 10-23.

KELLER, G., ADATTE, T., GARDIN , S., BARTOLINI, A., BAJPAI, S., 2008. Main Deccan volcanism phase ends near the K–T boundary: Evidence from the Krishna–Godavari Basin, SE India. *Earth and Planetary Science Letters*, 268, 293-311.

KERR, A. C., KEMPTON, P. D., THOMPSON, R. N., 1995. Crustal assimilation during turbulent magma ascent (ATA); new isotopic evidence from the Mull Tertiary lava succession, N. W. Scotland. *Contribution to Mineralogy and Petrology*, 119, 142-154.

KNIGHT, K. B., RENNE, P. R., HALKETT, A., WHITE, N., 2003. $^{40}Ar/^{39}Ar$ dating of the Rajahmundry Traps, Eastern India and their relationship to the Deccan Traps. *Earth and Planetary Science Letters*, 208, 85-99.

KRISHNAMURTY, P., COX, K.J. 1980. A potassium-rich alkali suite from the Deccan Traps, Rajpipla, India. *Contribution to mineralogy and Petrology*, 73, 179-189.

KROGSTAD, E. J., HANSON, G. N., RAJAMANI, V., 1995. Sources of continental magmatism adjacent to the late Archean Kolar Suture Zone, south India: distinct isotopic and elemental signatures of two late Archean magmatic series. *Contribution to mineralogy and Petrology*, 122, 159-173.

KUMAR, A., HEAMAN, L.M., MANIKYAMBA, C., 2007. Mesoproterozoic kimberlites in south India: a possible link to 1.1 Ga global magmatism. *Precambrian Research*, 154, 192–204.

LI, L., KELLER, G., 1998. Maastrichtian climate, productivity and faunal turnovers in planktic foraminifera in South Atlantic DSDP sites 525A and 21. *Marine Micropaleontology*, 33, 55-86.

LIGHTFOOT, P. C., HAWKESWORTH, C. J., DEVEY, C. W., ROGERS, N. W., VAN CALSTEREN, P. W. C., 1990. Source and Differentiation of Deccan Trap Lavas: Implications of Geochemical and Mineral Chemical Variations. *Journal of Petrology*, 31, 1165-1200.

LIGHTFOOT, P., HAWKESWORTH, C., 1988. Origin of Deccan Traps lavas: evidence from combined trace elements and Sr-, Nd- and Pb-isotope studies. *Earth and Planetary Science Letters*, 91, 89-104.

LIGHTFOOT, P., HAWKESWORTH, C., SETHNA, S.F., 1987. Petrogenesis of rhyolites and trachytes from the Deccan Trap: Sr, Nd and Pb isotope and trace element evidence. *Contribution to Mineralogy and Petrology*, 95, 44-54.

MAHESHWARI, A., SIAL, A.N., GUHEY, R., FERREIRA, V.P., 2005. C-isotope composition of carbonates from the Indravati Basin, India: implications for regional stratigraphic correlation. *Gondwana Research*, 8, 603–610.MAHONEY, J.J., DUNCAN, R.A., KHAN, W., GNOS, E.,

MCCORMICK, G.R., 2002. Cretaceous volcanic rocks of the South Tethyan suture zone, Pakistan: implications for the Réunion hotspot and Deccan Traps. *Earth and Planetary Science Letters*, 203, 295-310.

MAHONEY J.J., DUNCAN, R.A., KHAN, W., GNOS, E., MCCORMICK, G.R., 2002. Cretaceous volcanic rocks of the South Tethyan suture zone, Pakistan: implications for the Re¤union hotspot and Deccan Traps. *Earth and Planetary Science Letters*, 203, 295-310.

MAHONEY; J. J., SHETH, H. C., CHANDRASEKHARAM, D., PENG, Z. X., 2000. Geochemistry of Flood Basalts of the Toranmal Section, Northern Deccan Traps, India: Implications for Regional Deccan Stratigraphy. *Journal of Petrology*, 41, 1099-1120.

MAHONEY, J.J. 1988. Deccan Traps. 151-194. *In*: J.D. MACDOUGALL (ed.). *Continental Flood Basalt.* Kluwer Academic Publishers.

MAHONEY, J. J., MACDOUGALL, J.D., LUGMAIR,G.W., GOPALAN, K., KRISHNAMURTHY, P., 1985. Origin of contemporaneous tholeiitic and K-rich alkalic lavas: case study from the northern Deccan Plateau, India. *Earth and Planetary Science Letters*, 72, 39-53.

MAHONEY, J. J., MACDOUGALL, J.D., LUGMAIR,G.W., MURALI, A.V., SANKAR DAS, M., GOPALAN, K., 1982. Origin of the Deccan Trap flows at Mahabaleshwar inferred from Nd and Sr isotopic and chemical evidence. *Earth and Planetary Science Letters*, 60, 41-60.

MALONE, S.J., MEERT, J.G., BANERJEE, D.M., PANDIT, M.K., TAMRAT, E., KAMENOV, G.D., PRADHAN, V.R., SOHL, L.E., 2008. Paleomagnetism and detrital zircon geochronology of the Upper Vindhyan sequence, Son Valley and Rajasthan, India: a ca. 1000 Ma closure age for the Purana basins? *Precambrian Research*, 164, 137–159.MAZUMDER, R., 2005. Proterozoic sedimentation and volcanism in the Singhbhum crustal province, India and their implications; sedimentary systems and sequence stratigraphy related to Precambrian sea level change; a special issue dedicated to Pradip K. Bose. *Sedimentary Geology*. 176, 167–193.

MARATHE, S.S., KULKARUI, S.R., KARMANKAR, B.M., GUPTE, R.B., 1981. Variation in the nature of Deccan Trap volcanicity of western Maharashtra in time and space. *Memoir Geological Society of India*, 3, 117-127.

MCDONOUGH, W.F., SUN, S.-S, 1995. The composition of the Earth. *Chemical Geology*, 120, 223-253.

MEEN, J. K., ROGERS, J. J.W., FULLAGAR, P. D., 1992. Lead isotopic compositions of the Western Dharwar Craton, southern India: Evidence for distinct Middle Archean terranes in a Late Archean craton. *Geochimica et Cosmochimica Acta*,56, 2455-2470.

MEERT, J. G., PANDIT, M. K., PRADHAN, V. R., BANKS, J., SIRIANNI, R., STROUD, M., NEWSTEAD, B., GIFFORD, J., 2010. Precambrian crustal evolution of Peninsular India: A 3.0 billion year odyssey. *Journal of Asian Earth Sciences*, 39 483–515.

MELLUSO, L., MAHONEY, J. J., DALLAI, L., 2006. Mantle sources and crustal input as recorded in high-Mg Deccan Traps basalts of Gujarat (India). *Lithos*, 89, 259-274.

MELLUSO, L., SETHNA, S.F., D'ANTONIO, M., JAVERI, P., BENNIO, L., 2002. Geochemistry and petrogenesis of sodic and potassic mafic alkaline rocks in the Deccan volcanic province, Mumbai area (India). *Mineralogy and Petrology*, 74, 323-342.

MELLUSO, L., BECCALUVA, L., BROTZU, P., GRENANIN, A., GUPTA, A.K., MORBIDELLI, L., TRAVERSA, G., 1995. Constraints on the mantle sources of the Deccan Traps from the petrology and geochemistry of the basalts of Gujarat State (Western India). *Journal of Petrology*, 36, 1393-1432.

MILLER, K. G., KOMINZ, M. A., BROWNING, J. V., WRIGHT, J. D., MOUNTAIN, G. S., KATZ, M. E., SUGARMAN, P.J., CRAMER, B. S., CHRISTIE-BLICK, N., PEKA, S.F., 2005. The Phanerozoic Record of Global Sea-Level Change. *Science*, 310, 1293-1298.

MIN, K., MUNDIL, R., RENNE, P. R., LUDWIG, K.R., 2000. A test for systematic errors in $^{40}Ar/^{39}Ar$ geochronology through comparison with U/Pb analysis of a 1.1 Ga rhyolite. *Geochimica et Cosmochimica Acta*, 64, 73–98.

MISRA, S., 2006. Precambrian chronostratigraphic growth of Singhbhum-Orissa craton, Eastern Indian shield: an alternative model. *Journal of the Geological Society of India*, 67, 356–378.

MITCHELL, C., and WIDDOWSON, M., 1991. A geological map of the southern Deccan Traps, India and its structural implications. *Journal of the Geological Society, London*, 148, 495-505.

MOLINA, E., ALEGRET, L., ARENILLAS, I., ARZ, J.A., GALLALA, N., HARDENBOL, J., VON SALIS, K., STEURBAUT, E., VANDENBERGHE, N., ZAGHBIB-TURKI, D., 2006. The global boundary stratotype and point for the base of the Dania Stage (Paleocene, Paleogene, "Tertiary", Cenozoic) at El Kef, Tunisia- Original definition and revision. Episode, 29, 263-273.

MONDAL, M.E.A., GOSWAMI, J.N., DEOMURARI, M.P., SHARMA, K.K., 2002. Ion microprobe $^{207}Pb/^{206}Pb$ ages of zircons from the Bundelkhand Massif, northern India: implications for crustal evolution of the Bundelkhand–Aravalli supercontinent. *Precambrian Research*, 117, 85–100.

MONDAL, S.K., FREI, R., RIPLEY, E.M., 2007. Os isotope systematics of mesoarchean chromitite-PGE deposits in the Singhbhum Craton (India): implications for the evolution of lithospheric mantle. *Chemical Geology*, 244, 391–408.

MORGAN, W.J., 1981. Hotspot Tracks and the opening of the Atlantic and Indian Oceans. In: C.Emiliani (Ed) The Sea, v.7, Wiley, New York, pp.443-487.

MURTHY, Y.G.K., 1995. Proterozoic mafic dykes in southern Peninsular India; a review. *Memoir Geological Society of India*, 33, 81–98.

NAGANJANEYULU, K., SANTOSH, M., 2010. The Cambrian collisional suture of Gondwana in southern India: a geophysical approach. *Journal of Geodynamics*.doi:10.1016/j.jog.2009.12.01.

NAQVI, S.M., MANIKYAMBA, C., GNANESHWAR, R.T., SUBBA-RAO, D.V., RAM MOHAN, M., SRINIVASA SARMA, D., 2002. Geochemical and isotopic constraints of late Archaean fossil plume for the evolution of the volcanic rocks of the Sandur Greenstone belt. *Journal of the Geological Society of India*, 60, 27–56.

NAQVI, S.M., ROGERS, J.J.W., 1987. Precambrian Geology of India. Oxford University Press Inc.. 223 p.

NOBRE SILVA, I. G., WEIS, D., SCOATES, J. S., BARLING, J., The Ninetyeast Ridge and its Relation to the Kerguelen, Amsterdam and St. Paul Hotspots in the Indian Ocean. *Journal of Petrology*, 54, 1177-1210.

NOHDA, S., KANEOKA, I., HANYU, T., XU, S., UTO, K., 2005. Systematic Variation of Sr-, Nd- and Pb-Isotopes with Time in Lavas of Mauritius, Reunion Hotspot. *Journal of Petrology*, 46, 505-522.

NUTMAN, A.P., EHLERS, K., 1998. Evidence for multiple Palaeoproterozoic thermal events and magmatism adjacent to the Broken Hill Pb–Zn–Ag orebody, Australia. *Precambrian Research*, 90, 203–238.

NUTMAN, A.P., CHADWICK, B., KRISHNA RAO, B., VASUDEV, V.N., 1996. SHRIMP U/Pb zircon ages of acid volcanic rocks in the Chitradurga and Sandur groups, and granites adjacent to the Sandur schist belt, Karnataka. *Journal of the Geological Society of India*, 47, 153–164.

PANDE, K., PATTANAYAK, S.K., SUBBARAO, K.V., NAVANEETHAKRISHNAN, P., VENKATESAN, T. R., 2004. $^{40}Ar/^{39}Ar$ age of a lava flow from the Bhimashankar Formation, Giravali Ghat, Deccan Traps. *Proceedings of the Indian academy of Sciences (Earth and Planetary Sciences)*, 113, 755-758.

PANDE, K., 2002. Age and duration of the Deccan Traps, India: a review of radiometricand paleomagnetic constraints. *Proceedings of the Indian academy of Sciences (Earth and Planetary Sciences)*, 111, 115-123.

PANDIT, M.K., CARTER, L.M., ASHWAL, L.D., TUCKER, R.D., TORSVIK, T.H., JAMTVEIT, B., BHUSHAN, S.K., 2003. Age, petrogenesis and significance of 1 Ga granitoids and related rocks from the Sendra area, Aravalli Craton, NW India. *Journal of Asian Earth Sciences*, 22, 363–381.

PARANTHAMAN, S., 2005. Geology and geochemistry of Archaean Ghattihosahalli mafic–ultramafic complex, Chitradurga, Karnataka. *Journal of the Geological Society of India*, 66, 653–657.

PATRANABIS-DEB, S., BICKFORD, M.E., HILL, B., CHAUDHARI, A.K., BASU, A., 2007. SHRIMP ages of zircon in the uppermost tuff in Chattisgarh Basin in central India require up to 500 Ma adjustments in Indian Proterozoic stratigraphy. *Journal of Geology*, 115, 407–416.

PAUL, D. K., RAY, A., DAS, B., PATIL, S. K., BISWAS, S.K., 2008. Petrology, geochemistry and paleomagnetism of the earliest magmatic rocks of Deccan Volcanic Province, Kutch, Northwest India. *Lithos*, 102, 237–259.

PENG, Z. X., MAHONEY, J. J., HOOPER, P. R., MACDOUGALL, J.D., KRISHNAMURTY, P., 1998. Basalts of the northeastern Deccan Traps, India: Isotopic and elemental geochemistry and relation to southwestern Deccan stratigraphy. *Journal of Geophysical Research*, 103, 29843-29865.

PENG, Z. X., MAHONEY, J. J., 1995. Drillhole lavas from the northwestern Deccan Traps, and the evolution of Réunion hotspot mantle. *Earth and Planetary Science Letters*, 134, 169-185.

PENG, Z. X., MAHONEY, J. J., HOOPER, P., HARRIS, C., BEANE, J. 1994. A role for lower continental crust in flood basalt genesis? Isotopic and incompatible element study of the lower six formations of the western Deccan Traps. *Geochimica e Cosmochimica Acta*, 58, 267-288.

PEUCAT, J.J., JAYANANDA, M., CHARDONC, D., CAPDEVILA, R., FANNING, C. M., PAQUETTE, L.S, 2013. The lower crust of the Dharwar Craton, Southern India: Patchwork of Archean granulitic domains. *Precambrian Research*, 227, 4–28.

PEUCAT, J. J., VIDAL, P., BERNARD-GRIFFITHS, J., CONDIE, K. C., 1989. Sr, Nd, and Pb Isotopic Systematics in the Archean Low- to High-Grade Transition Zone of Southern India: Syn-Accretion vs. Post-Accretion Granulites. *Journal of Geology*, 97, 537-549.

PLANK, T., LANGMUIR, C. H., 1998. The chemical composition of subducting sediment and its consequences for the crust and mantle. *Chemical Geology*, 145, 325–394.

PLANK, T., 2005. Constraints from Th/La on sediment recycling at subduction zones and the evolution of the continents. *Journal of Petrology*, 46, 921-944.

PRADHAN, V.R., PANDIT, M.K., MEERT, J.G., 2008. A cautionary note of the age of the paleomagnetic pole obtained from the Harohalli dyke swarms, Dharwar craton, southern India. In: Srivastava, R.K., Sivaji, Ch., Chalapati Rao, N.V. (Eds.), *Indian Dykes: Geochemistry, Geophysics, and Geochronology*. Narosa Publishing Ltd., New Delhi, India, pp. 339–352.

PRICE, R.C., KENNEDY, A.K., SNEERINGER, M.R., FREY, F.A., 1986. Geochemistry of basalts from the West Indian Triple Junction: implication for the generation and evolution of Indian Ocean Ridge basalts. *Earth and Planetary Science Letters*, 78, 379-396.

RAITH, M.M., SRIKANTAPPA, C., BUHL, D., KOEHLER, H., 1999. The Nilgiri enderbites, South India; nature and age constraints on protolith formation, high-grade metamorphism and cooling history. *Precambrian Research*, 98, 129–150.

RAIA RAO C., S., SAHASRABUNDHE, Y.S., DESHMUKH, S.S., RAMAN, R., 1978. Distribution, structure and petrography of the Deccan Trap, India. *Rep. Geol. Survey Ind*., 43 pp.

RAMAKRISHNAN, M., VAIDYANADHAN, R., 2008. Geology of India: volume 1. Geological Society of India, 994 p.

RAO, V.V., PRASAD, R.B., 2006. Structure and evolution of the Cauvery Shear Zone system, southern Granulite Terrain, India: evidence from deep seismic and other geophysical studies. *Gondwana Research*, 10, 29–40.

RAO, J.M., 2004. The wide-spread 2 Ga dyke activity in the Indian shield-evidences from Bundelkhand mafic dyke swarm, Central India and their tectonic implications. *Gondwana Research*, 7, 1219–1228.

RAVIZZA, G., PEUCKER-EHRENBRINK, B., 2003. Chemostratigraphic evidence of Deccan volcanism from the marine Osmium isotope record. *Science*, 302, 1392-1395.

RAY, R., SHUKLA, A. D., SHETH, H. C., RAY, J. S., DURAISWAMI, R. A., VANDERKLUYSEN, L., RAUTELA, C. S., MALLIK, J., 2008. Highly heterogeneous Precambrian basement under the central Deccan Traps, India: Direct evidence from xenoliths in dykes. *Gondwana Research*, 13, 375-385.

RAY, J. S., SHUKLA, P. N., 2004. Trace element geochemistry of Amba Dongar carbonatite complex, India: Evidence for fractional crystallization and silicate-carbonate melt immiscibility. *Proceedings of the Indian academy of Sciences (Earth and Planetary Sciences)*, 113, 519–531.

RENNE, P. R., DEINO, A. L., HILGEN, F. J., KUIPER, K. F., MARK, D. F., MITCHELL, W. S., MORGAN, L. E., MUNDIL, R., SMIT, J., 2013. Time Scales of Critical Events Around the Cretaceous-Paleogene Boundary. *Science*, 339, 684-687.

RENNE, P. R., MUNDIL, R., BALCO, G., MIN, K., LUDWIG, K. R., 2011. Response to the comment by B. H. Shwarz et al. on "Joint determination of ^{40}K decay constants and ^{40}Ar*/^{40}K for the Fish Canyon Sanidine standard, and improved accuracy for ^{40}Ar/^{39}Ar geochronology" by P. R. Renne (2010). *Geochimica et Cosmochimica Acta*, 75, 5097–5100.

RENNE, P. R., MUNDIL, R., BALCO, G., MIN, K., LUDWIG, K. R., 2010. Joint determination of ^{40}K decay constants and ^{40}Ar*/^{40}K for the Fish Canyon Sanidine standard, and improved accuracy for ^{40}Ar/^{39}Ar geochronology. *Geochimica et Cosmochimica Acta*, 74, 5349–5367.

RENNE, P. R., SWISHER, C. C., DEINO, A. L., KARNER, D. B., OWENS, T. L., DEPAOLO, D. J., 1998. Intercalibration of standards, absolute ages and uncertainties in $^{40}Ar/^{39}Ar$ dating. *Chemical Geology*, 145, 117- 152.

ROY, A., KAGAMI, H., YOSHIDA, M., ROY, A., BANDYOPADHYAY, B.K., CHATTOPADHYAY, A., 2006. Rb/Sr and Sm/Nd dating of different metamorphic events from the Sausar mobile belt, central India; implications for Proterozoic crustal evolution. *Journal of Asian Earth Sciences*, 26, 61–76.

ROY, A.B., KRÖNER, A., BHATTACHARYA, P.K., RATHORE, S., 2005. Metamorphic evolution and zircon geochronology of early Proterozoic granulites in the Aravalli Mountains of northwestern India. *Geological Magazine*, 142, 287–302.

ROY, A.B., 2003. Geological and geophysical manifestations of the Reunion plume-indian lithosphere interactions - evidence from Northwest India. *Gondwana Research*, 6, 487-500.

RUDNICK, R., GAO, S., 2003. Composition of the continental crust. In: Carlson, R.W., Holland, H.D., Turekian, K.K. (Eds.), Treatise on Geochemistry: The Crust. Elsevier, pp. 1–64.

RUDNICK, R., FOUNTAIN, D. M. (1995). Nature and composition of the continental crust: a lower crustal perspective. *Reviews of Geophysics*, 33, 267–309.

SALTERS, V.J.M., SACHI-KOCHER, A., 2010. An ancient metasomatic source for the Walvis Ridge basalts. *Chemical Geology*, 273, 151-167.

SANO, T., FUJII, T., DESHMUKH, S.S., FUKUOKA, T., ARAMAKI, S., 2001. Differentiation processes of Deccan Trap basalts: contribution from geochemistry and experimental petrology. *Journal of Petrology*, 42, 2175-2195.

SANTOSH, M., COLLINS, A.S., TAMASHIRO, I., KOSHIMOTO, S., TSUTSUMI, Y., YOKOYAMA, K., 2006. The timing of ultrahigh-temperature metamorphism in southern India: U–Th–Pb electron microprobe ages from zircon and monazite in sapphirinebearing granulites. *Gondwana Research*, 10, 128–155.

SANTOSH, M., KATORI, R., YOSHIKURA, S., HIGASHI, S., SALIM, A.K., 2002. Pink sapphire from southern Kerala, S. India; implications on India–Madagascar correlation within Gondwana assembly. *Gondwana Research*, 5, 894–901.

SCHIANO, P., DAVID, K., VLASTELIC, I., GANNOUN, A., KLEIN, M., NAURET, F., BONNAND, P., 2012. Osmium isotope systematics of historical lavas from Piton de la Fournaise (Reunion Island, Indian Ocean). *Contribution to Mineralogy and Petrology*, DOI 10.1007/s00410-012-0774-0.

SCHULTE et al., 2010. The Chicxulub asteroid impact and mass extinction at the Cretaceous-Paleogene boundary. *Science*, 327, 1214-1218. DOI: 10.1126/science.1177265

SCHWARZ, W. H., KOSSERT, K., TRIELOFF, M., HOPP, J., 2011. Comment on the "Joint determination of 40K decay constants and $^{40}Ar^*/^{40}K$ for the Fish Canyon Sanidine standard, and improved accuracy for $^{40}Ar/^{39}Ar$ geochronology" by Paul R. Renne et al. (2010). *Geochimica et Cosmochimica Acta*, 75, 5094–5096.

SELF, S., WIDDOWSON, M., THORDARSON, T., JAY, A.E., 2006. Volatile fluxes during flood basalt eruptions and potential effects on the global environment: A Deccan perspective. *Earth and Planetary Science Letters*, 248, 518-532.

SELF, S., BLAKE, S., SHARMA, K., WIDDOWSON, M., SEPHTON, S. 2008. Sulfur and chlorine in late Cretaceous Deccan magmas and eruptive gas release. *Science* 319, 1654-1657.

SEN, G., BIZIMIS, M., DAS, R., PAUL D. K., RAY, A., BISWAS, S., 2009. Deccan plume, lithosphere rifting, and volcanism in Kutch, India. *Earth and Planetary Science Letters*, 277, 101–111.

SHETH, H.C., CHOUDHARY, A. K., BHATTACHARYYA, S., CUCCINIELLO C., LAISHRAM, R., GURAV, T., 2011. The Chogat-Chamardi subvolcanic complex, Saurashtra, northwestern Deccan Traps: geology, petrochemistry, and petrogenetic evolution. *Journal of Asian Earth Sciences*, 41, 307-324.

SHETH, H.C., MELLUSO, L. 2008. The Mount Pavagadh volcanic suite, Deccan Traps: geochemical stratigraphy and magmatic evolution. *Journal of Asian Earth Sciences* 32, 5-21.

SHETH, H.C., 2005. Were the Deccan Flood basalts derived in part from ancient oceanic crust within the Indian continental lithosphere? *Gondwana Research*, 8, 109-127.

SHETH, H.C., 2005b. From Deccan to Réunion: No trace of a mantle plume. *in* Foulger, G.R., Natland, J.H., Presnall, D.C., and Anderson, D.L., eds., Plates, plumes, and paradigms: Geological Society of America Special Paper, 388, 477–501.

SHETH, H.C., MAHONEY, J. J., CHANDRASEKHARAM, D., 2004. Geochemical stratigraphy of Deccan flood basalts of the Bijasan Ghat section, Satpura Range, India. *Journal of Asian Earth Sciences*, 23, 127–139.

SHETH, H.C., PANDE, K., BHUTANI, R., 2001. $^{40}Ar/^{39}Ar$ ages of Bombay trachytes: evidence for a Palaeocene phase of Deccan volcanism. *Geophysical Research Letters*, 28, 3513-3516.

SHETH, H.C., CHANDRASEKHARAM, D., 1997. Early alkaline magmatism in the Deccan traps: implications for plume incubation and lithospheric rifting. *Physics of the Earth and Planetary Interiors*, 104, 371-376.

SIMONETTI, A., BELL, K., VILADKAR, S.G. 1995. Isotopic data from the Amba Dongar Carbonatite Complex, west-central India: Evidence for an enriched mantle source. *Chemical Geology (Isotope Geoscience Section)* 122, 185-198.

SIMONETTI, A., GOLDSTEIN, S. L., SCHMIDBERGER, S. S., VILADKAR , S. G., 1998. Geochemical and Nd, Pb, and Sr Isotope Data from Deccan Alkaline Complexes— Inferences for Mantle Sources and Plume-Lithosphere Interaction, *Journal of petrolgy*, 39 (11-12), 1847-1864.

SPERA, F. J., BOHRSON, W. A., 2001. Energy-constrained open-system magmatic processes I: general model and Energy-Constrained Assimilation and Fractional Crystallization (EC-AFC) formulation. *Journal of Petrology*, 42, 999-1018.

SRIVASTAVA, R. K., ELLAM, R. M., GAUTAM, G. C.,2009. Sr–Nd isotope geochemistry of the early Precambrian sub-alkaline mafic igneous rocks from the southern Bastar craton, Central India. *Mineralogy and Petrology*, 96, 71-79.

SRIVASTAVA, R.K., HEAMAN, L. M., SINHA, A. K., SHIHUA, S., 2005. Emplacement age and isotope geochemistry of Sung Valley alkaline-carbonatite complex, Shillong plateau, northeastern India: implications for primary carbonate melt and genesis of the associated silicate rocks. *Lithos*, 81, 33- 54.

STEIGER, R.H., JAGER, E., 1977. Subcommission on geochronology: convention on the use of decay constants in geo- and cosmochronology. *Earth and Planetary Science Letters*, 36, 359-362.

STOREY, M., MAHONEY,J.J., SAUNDERS,A.D., DUNCAN,R.A., KELLEY, S.P., COFFIN, M.F., 1995. Timing of hot spot related volcanism and the breakup of Madagascar from India. *Science*, 267, 852-855.

STRACKE, S., BIZIMIS, M., SALTERS, V. J. M., 2003. Recycling oceanic crust: quantitative constraints. *Geochemistry Geophysics Geosystems*, 4, doi:10.1029/2001GC000223.

SUBBA RAO, D.V., NAQVI, S.M., 1999. Archaean komatiites from the older schist belt of Kalyadi in Western Dharwar Craton, Karnataka. *Journal of the Geological Society of India*, 53, 347–354.

SUBRAHMANYA, K.R., 1998. Tectono-magmatic evolution of the west coast of India. *Gondwana Research*, l, 319-327.

SUKHESWALA R.N., SETHNA S. F. 1973. Oversaturated and undersaturated differentiates in the tholeiitic igneous complex of Phenai Mata, Baroda District, Gujarat State, India. *N. Jb. Miner. Abh*. 118, 2, 159-176.

SUN, S.-S. & MCDONOUGH, W.F., 1989. Chemical and isotopic systematics of oceanic basalts: implications for mantle composition and processes. *Geological Society, London, Special Publications*, 42, 313-345.

TATSUMI, Y., NOHDA, S., 1990. Geochemical stratification in the upper mantle: evidence from Leg 115 basalts in the Indian Ocean. In: Duncan, R. A., Backman, J., Peterson, L. C., et al. (eds) *Proceedings of the Ocean Drilling Program, Scientific Results*, 115. College Station, TX: Ocean Drilling Program, pp. 63–69.

TAYLOR, P.N., CHADWICK, B., MOORBATH, S., RAMAKRISHNAN, M., VISWANATHA, M.N., 1984. Petrography, chemistry and isotopic ages of Peninsular Gneiss, Dharwar acid volcanic rocks amd the Chitradurga Granite with special reference to the late Archean Evolution of the Karnataka Craton, Southern India. *Precambrian Research*, 23, 349-375.

TOBISCH, O. T., COLLERSON, K.D., BHATTACHARYYA, T., MUKHOPADHYAY, D., 1994. Structural relationships and Sr-Nd isotope systematics of polymetamorphic granitic gneisses and granitic rocks from central Rajasthan, India: implications for the evolution of the Aravalli craton. *Precambrian Research*, 65, 19-339.

TODAL, A., EDHOLM, O., 1998. Continental margin off Western India and Deccan Large Igneous Province. *Marine Geophysical Researches*, 20, 273–291.

TORSVIK, T.H., CARTER, L.M., ASHWAL, L.D., BHUSHAN, S.K., PANDIT, M.K., JAMTVEIT, B., 2001. Rodinia refined or obscured: paleomagnetism of the Malani Igneous Suite (NW India). *Precambrian Research*, 108, 319–333.

VANDAMME, D., COURTILLOT, V., 1992. Paleomagnetic constraints on the structure of the Deccan traps. *Physics of the Earth and Planetary Interiors*, 74, 241-261.

VANDAMME, D., COURTILLOT, V., BESSE, J., MONTIGNY, R., 1991. Paleomagnetism and age determinations of the Deccan Traps (India): result for a Nagpur –Bombay traverse and review of earlier work. *Reviews of Geophysics*, 29, 159-190.

VANDERKLUYSEN, L., MAHONEY, J. J., HOOPER, P.R., SHETH, H.C., RAY, R., 2010. The Feeder System of the DeccanTraps (India): Insights from Dike Geochemistry. *Journal of Petrology*, 0, 1-29.

VENKATESAN, T. R., PANDE, K., GHEVARIYA, Z.G., 1996. $^{40}Ar/^{39}Ar$ ages of Anjar Traps, western Deccan province (India) and its relation to the Cretaceous-Tertiary Boundary events. *Current Science*, 70, 990-996.

VENKATESAN, T. R., PANDE, K., GOPALAN, K., 1993. Did Deccan volcanism pre-date the Cretaceous/Tertiary transition? *Earth and Planetary Science Letters*, 19, 181-189.

VILADKAR, S.G., and SCHIDLOWSKI, M., 2000. Carbon and Oxygen Isotope Geochemistry of the Amba Dongar Carbonatite Complex, Gujarat, India. *Gondwana Research*, 3, 415-424.

VOLPE, A.M, MACDOUGALL, J.D., 1990. Geochemistry and isotopic characteristics of mafic (Phulad Ophiolite) and related rocks in the Delhi Supergroup, Rajasthan, India: implications for riofting in the Proterozoic. Precambrian Research, 48. 167-191.

WEAVER, B. L., 1980. Rare-Earth Element Geochemistry of Madras Granulites. *Contribution to Mineralogy and Petrology*, 71, 271-279.

WEIS, D., INGLE, S., DAMASCENO, D., FREY, F. A., NICOLAYSEN, K.,BARLING, J., 2001. Leg 183 Shipboard Scientific PartyOrigin of continental components in Indian Ocean basalts: Evidence from Elan Bank (Kerguelen Plateau, ODP Leg183, Site 1137). *Geology*, 29,147-150.

WHITE, W. M., CHEATHAM, M. M., DUNCAN, R. A., 1990. Isotope geochemistry of Leg 115 basalts and inferences on the history of the Reunion mantle plume. In: Duncan, R. A., Backman, J., Peterson,
L. C., et al. (eds) *Proceedings of the Ocean Drilling Program, Scientific Results*, 115. College Station, TX: Ocean Drilling Program, pp. 53–61.

WIDDOWSON, M., PRINGLE, M.S., FERNANDEZ, O.A., 2000. A post K-T boundary (early Paleocene) age for Deccan-type feeder dykes, Goa, India. *Journal of Petrology*, 41, 1177-1194.

WIEDENBECK, M., GOSWAMI, J.N., ROY, A.B., 1996. Stabilization of the Aravalli Craton of northwestern India at 2.5 Ga: an ion microprobe zircon study. *Chemical Geology*, 129, 325–340.

WIGNALL, P.B., 2001. Large igneous provinces and mass extinctions. *Earth-Science Reviews*, 53, 1–33.

WILF, P., JOHNSON, K. R., HUBER, B.T., 2003. Correlated terrestrial and marine evidence for global climate changes before mass extinction at the Cretaceous–Paleogene boundary. *Proceedings of the National Academy of Sciences*, 100, 599–604.

WILLBOLD, M. and STRACKE, S., 2006. Trace element composition of mantle end-members: implications for recycling of oceanic and upper and lower continental crust. *Geochemistry Geophysics Geosystems*, 7, doi:10.1029/2005GC001005.

WILSON, G.P., 2005. Mammalian Faunal Dynamics During the Last 1.8 Million Years of the Cretaceous in Garfield County, Montana. *Journal of Mammalian Evolution*, 12, 53-76.

WINDLEY, B.F., RAZAFINIPARANY, A., RAZAKAMANANA, T., ACKERMAND, D., 1994. Tectonic framework of the Precambrian of Madagascar and its Gondwana connections: a review and reappraisal. *Geologisches Rundschau*, 83, 642–659.

WORKMAN, R. K., HART, S. R., 2005. Major and trace element composition of the depleted MORB mantle (DMM). *Earth and Planetary Science Letters*, 231, 53- 72.

ZACHARIAH, J.K., RAJAMANI, V., HANSON, G. N., 1997. Petrogenesis and source characteristics of metatholeiites from the Archean Ramagiri schist belt, eastern part of Dharwar craton, India. *Contribution to Mineralogy and Petrology*, 129, 87-104.

ZACHARIAH, J.K., HANSON, G.N., RAJAMANI, V., 1995. Postcrystallization disturbance in the neodymium and lead isotope systems of metabasalts from the Ramagiri schist belt, southern India. *Geochimica et Cosmochimica Acta*, 59, 3189–3203.

ZEGER, T., WHITE, S., DE KEIJZER, M., DIRKS, P., 1996. Extensional structures during deposition of the 3460 Ma Warrawoona Group in the eastern Pilbara Craton, Western Australia. *Precambrian Research*, 80, 89–105.

ZINDLER, A., HART, S., 1986. Chemical geodynamics. *Ann. Rev. Earth Planet. Sci*., 14, 493-571.